MIXING PROPERTIES AND SOLUBILITY OF ATOMIC AND MOLECULAR SPECIES IN CRYOSOLIDS

A Thesis Submitted to the

College of Graduate and Postdoctoral Studies

In Partial Fulfillment of the Requirements

For the Degree of Master of Science

In the Department of Physics and Engineering Physics

University of Saskatchewan

Saskatoon

By:
Momina Mateen

“All of physics is either impossible or trivial. It is impossible until you understand it, and then it becomes trivial.”
Ernest Rutherford

PERMISSION TO USE

In presenting this thesis in partial fulfillment of the requirements for a Postgraduate degree from the University of Saskatchewan, I agree that the Libraries of this University may make it freely available for inspection. I further agree that permission for copying of this thesis in any manner, in whole or in part, for scholarly purposes may be granted by the professor or professors who supervised my thesis/dissertation work or, in their absence, by the Head of the Department or the Dean of the College in which my thesis work was done. It is understood that any copying or publication or use of this thesis or parts thereof for financial gain shall not be allowed without my written permission. It is also understood that due recognition shall be given to me and to the University of Saskatchewan in any scholarly use which may be made of any material in my thesis/dissertation.

DISCLAIMER

The Mixing Properties and Solubility of Atomic and Molecular Species in Cryosolids was exclusively created to meet the thesis and/or exhibition requirements for the degree of Master of Science at the University of Saskatchewan. Reference in this thesis to any specific commercial products, process, or service by trade name, trademark, manufacturer, or otherwise, does not constitute or imply its endorsement, recommendation, or favoring by the University of Saskatchewan. The views and opinions of the author expressed herein do not state or reflect those of the University of Saskatchewan and shall not be used for advertising or product endorsement purposes.

Requests for permission to copy or to make other uses of materials in this thesis/dissertation in whole or part should be addressed to:

Head of the Department of Physics and Engineering Physics
116 Science Place
University of Saskatchewan
Saskatoon, Saskatchewan S7N 5E2 Canada

OR

Dean
College of Graduate and Postdoctoral Studies
University of Saskatchewan
116 Thorvaldson Building, 110 Science Place
Saskatoon, Saskatchewan S7N 5C9 Canada

ABSTRACT

Exoplanetary research has shown that there are compositions of nitrogen (N_2) and methane (CH_4) on some planet surfaces. The following thesis studies these compositions in a vacuum state to mimic the conditions of outer space. It can then serve as a reference for future astronomical research. The solubility of nitrogen in methane (or vice versa) at cryogenic temperatures has previously been studied in the 1980s and has created a framework for what structural changes can be expected for methane and nitrogen co-deposition. Additionally, data collected from pure N_2 and CH_4 allowed a quantitative assessment between the Hard X-ray Micro-Analysis (HXMA) and Brockhouse beamlines at the Canadian Light Source (CLS).

This was achieved by depositing CH_4 and N_2 at varying concentrations on a diamond substrate at cryogenic temperatures (10 K). X-rays penetrated through the sample and a unique diffraction pattern was obtained for each sample set in a time-resolved manner. Diffraction patterns were captured as each sample set was warmed to the melting point of the substances within it. Rietveld analysis was used to refine the diffraction patterns and calculate lattice parameters to model the crystal structure of each compound.

The results showed that while the Brockhouse beamline produced diffraction patterns with at higher scattering angles, the HXMA beamline produced better refinable data indicating better quality data. The type of leak valve for the gases that was used may have been a contributing factor in this research and so repeating the experiment is required and adjusting the flow rate of each valve to allow a fair comparison between the two. The analysis of the lattice parameters for both beamlines showed that the results from both the HXMA and Brockhouse beamline agreed with what has been previously observed validating the reliability of the results. Next, a new phase of methane was observed at 37 K, which is further analyzed and discussed. Finally, the co-deposition of methane and nitrogen showed that the expected deposition ratios did not correspond with the observed ratios. This could be due to the individual molecular properties, the surface-molecule tension, or the quantity of substance that was deposited.

ACKNOWLEDGEMENTS

The completion of this thesis would not have been possible without the continuous guidance, patience, and support from Dr. John Tse, my graduate supervisor. The Advisory Committee also played a significant role in the editing and presentation of this thesis. I would also like to thank Robert Bauer for his advice and technical support during the experimental set ups and analyses. Marj and Debbie, who are the physics administrative staff, remained strong pillars as I navigated the technicalities of completing this thesis – thank you for your continuous support.

DEDICATION

I dedicate this thesis to my mother and father. It is their continuous sacrifice and support that has allowed me to have access to opportunities that they never did.

TABLE OF CONTENTS

LIST OF TABLES

LIST OF FIGURES

CHAPTER 1: INTRODUCTION

There are three primary objectives of this research project. Firstly, the performance of the Hard X-ray Micro-Analysis (HXMA) and Brockhouse beamlines for powder diffraction will be compared at the Canadian Light Source (CLS) based in Saskatoon, Saskatchewan. This will be explored in terms of the differences of wavelength, monochromator, intensity, and resolution. This analysis will be completed by commissioning a low-temperature vapour deposition system and an in-situ powder diffraction instrument at the Brockhouse and HXMA beamlines. The second, and scientific goal, is to explore the properties and solubility of mixtures of nitrogen and methane at very low temperatures. The objective is to establish the solubility of nitrogen in methane or vice versa and study the changes in the structures of the cryosolid as functions of temperature and concentration as well as the changes in the lattice parameters of the solids formed. There will also be a brief discussion regarding the methodology of deposition and a comparison thereof. A tertiary objective from this deposition system will be to determine the relative concentrations of nitrogen and methane in the cryogenic system using powder diffraction. Projects presented in this study may have future applications in global energy storage systems. Since the properties of methane in the presence of other species at very low temperatures is being investigated, it will also have implications in astrophysics such as in exoplanetary research.

One example of relevant planetary research is by Trafton et al. in 2015[1], who explored the N_2:CH_4 solid solution composition on the planet Pluto and Triton. This study explored the planetary surface to assess the structure of the ice and attempted to isolate N_2:CH_4 mixtures on solid continent-sized areas. A quantitative investigation was also completed using compositional analysis to determine how much of the surface contained N_2 or CH_4. In the following study, the amount of deposition of methane and nitrogen onto a thin diamond plate was controlled to allow assessment of the molecular and crystal structures of these mixtures. This data has the potential to serve as a reference for further exoplanetary research.

In 1980, Connolley et al.[2] conducted a preliminary survey of the phase diagram of condensed nitrogen-methane mixtures. Their research primarily focused on whether the results produced by Barrett and Meyer[3], who studied the crystal structure properties between nitrogen and argon mixtures, which could be consistent with nitrogen and methane. The preliminary results of the Barrett and Meyer study showed that when nitrogen (in small amounts) was mixed with argon gas, it led to a hexagonal closest packed (hcp) lattice of 28 atoms. It also showed that "equal mixtures of the two molecules led to an hcp lattice at all temperatures". The premise that Connolley et al. used to extrapolate and then investigate this further was that since the molecular size of argon and methane molecules are similar, the mixture diagrams with nitrogen should be comparable. It was noted that the only difference between methane and argon was that methane has a quadrupole moment which interacts with weak orientational forces with nearby molecules. The primary objective of their research was to identify the face-center cubic (fcc) and hexagonal close packed (hcp) lattices of the co-condensed solid mixtures. The results are presented in Figure 1.1.

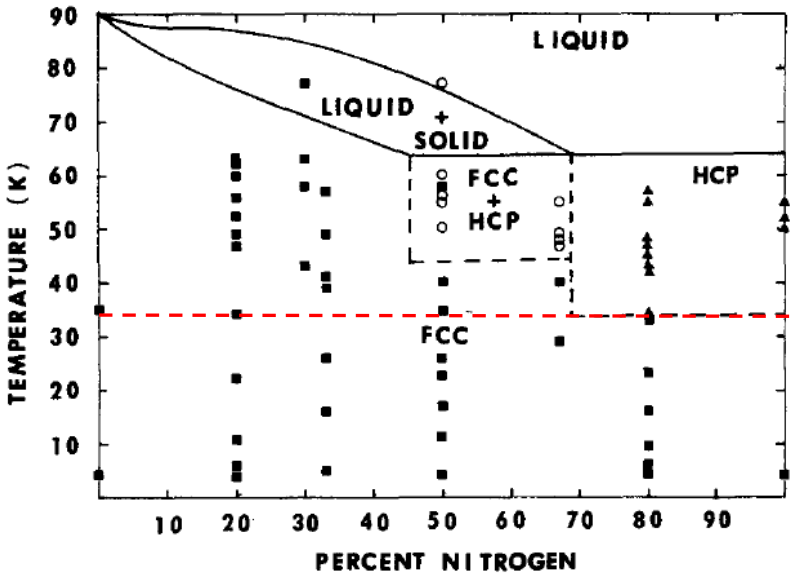

Figure 1.1. Preliminary results of N_2 and CH_4 mixtures obtained by x-ray diffraction by Connolley et al. The solid lines are used to indicate phase boundaries established from literature and dashed lines illustrate the preliminary phase boundaries. Reprinted with permission.

Connolley et al. were able to show that the crystal structure for all mixtures below 36 K had an fcc structure and noted 36 K (Figure 1.1 red dashed line) as the transition point between an fcc structure and an hcp structure. For nitrogen concentration mixtures between 70 % to 100%, the crystal structures took on an hcp structure up until the melting point of N_2 (63.15 K). Crystal

structures formed with N_2 concentrations between 50% and 70% and between 43 K and 63 K were a mixture of fcc and hcp. It is important to note that the paper quoted 77.3 K as the N_2 melting point, however, literature shows[4] that the N_2 melting point is 63.15 K.

One of the goals of this research project is to use the Rietveld refinement of the diffraction patterns to determine the lattice parameters and relative concentrations of methane (CH_4) and nitrogen (N_2) mixtures deposited under cryogenic conditions. Then, the results will be used to calibrate the precision of the relative amount extracted from the intensity ratio of the characteristic vibrational bands of CH_4 and N_2 from simultaneous in-situ Raman measurements, in conjunction with a separate project.

All the experiments for this study were performed at the Canadian Light Source (CLS). The CLS came into operation in 2005 and has since then changed the dynamics of Canadian research. It uses strong magnets to accelerate electrons to nearly the speed of light. When these electrons are bent, x-rays are emitted and then channeled down beamlines. At each beamline, the user can optimize which part of the spectrum would be ideal for their experiment. The CLS has 22 beamlines that each have a unique purpose allowing for a wide range of research opportunities. We used the HXMA and Brockhouse beamlines. The HXMA beamline allows the user to access a spectral range of 5 – 40 keV. The Brockhouse beamline with the High Energy Wiggler allows the user to access a spectral range of 20 – 94 keV. We conducted powder x-ray diffraction on both these beamlines for nitrogen, methane, and mixtures thereof.

Using these beamlines, two primary goals are outlined. Firstly, to evaluate the performance of HXMA and Brockhouse hard x-ray beamlines to obtain powder diffraction patterns for quantitative analysis. This was accomplished by depositing pure N_2 and pure CH_4 at each beamline on a diamond substrate. These samples were warmed, and time resolved diffraction patterns were collected. This data was refined used Rietveld analysis and the quality of the data was compared.

The second objective was to determine whether it is possible to deposit CH_4 and N_2 gas mixtures of different stoichiometry and analyze the relative concentrations after Rietveld analysis. Three sets of mixtures were deposited at each beamline. Using these sets of data, it was also determined

if CH_4 and N_2 maintain their independent structures or if there are interactions between the two substances that result in changes in the diffraction pattern and, therefore, structural changes.

CHAPTER 2: BACKGROUND

This section reviews the theory behind the instrumental and methodology for structural refinement techniques that were used in the analysis of the results at obtained at the HXMA and Brockhouse beamlines.

2.1 Cryogenics

Cryogenics is the study of material behaviour at low temperatures. In the laboratory, these temperatures are achieved by using 'cryogens', such as liquid helium, which has a boiling point of 4.22 K, or liquid nitrogen, which has a boiling point of 77.36 K. The sample is stored in an insulated flask known as a Dewar flask. The goal of the experimental set up was to mimic interstellar space (ISM) conditions, i.e., high vacuum and very low temperature. A recycled He cryostat, called a DISPLEX[5], was used that allowed the system to reach the desired temperature of approximately 10 K under 10^{-7}-10^{-8} torr. The gaseous species were deposited onto a thin diamond substrate attached to a copper block. The temperature was controlled by an automatic heater with a feedback loop. The set-up is illustrated in Figure 2.1 below:

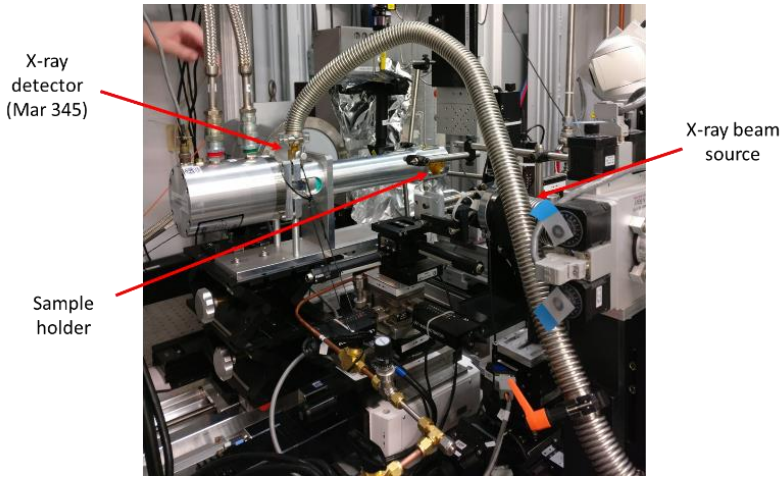

Figure 2.1. This experimental set up shows the sample holder at the distal end of the DISPLEX. It contains the copper block on to which the diamond substrate was deposited. The N2 and CH4 gases were leaked into this DISPLEX system for the experiments

2.2 X-rays

First discovered by Roentgen in 1895, x-rays are a penetrating type of electromagnetic radiation with a wavelength in the order of 10^{-10} meters. Laboratory x-rays are usually produced in cathode tubes under vacuum in which electrons are accelerated at the speed of light by a high voltage x-ray generator through a tungsten filament cathode. This process is known as thermionic emission. The electrons then collide into a target anode, which abruptly slows them down. From this sudden deceleration, energy in the form of x-rays is produced in the form of bremsstrahlung radiation or characteristic radiation. Characteristic radiation, shown in Figure 2.2(a) is when a high-energy electron collides with an inner shell electron, and both are ejected from the tungsten atom, leaving a 'hole' in the inner layer. An outer electron shell fills the vacant core orbital and is associated with a loss of energy emitted as an x-ray photon[6]. Bremsstrahlung radiation, shown in Figure 2.2(b), is the energy lost when an electron passes near the nucleus, it is slowed down, and its path is deflected. Each element has different nuclear binding energies which results in unique characteristic radiations for each material. Both these processes occur simultaneously.

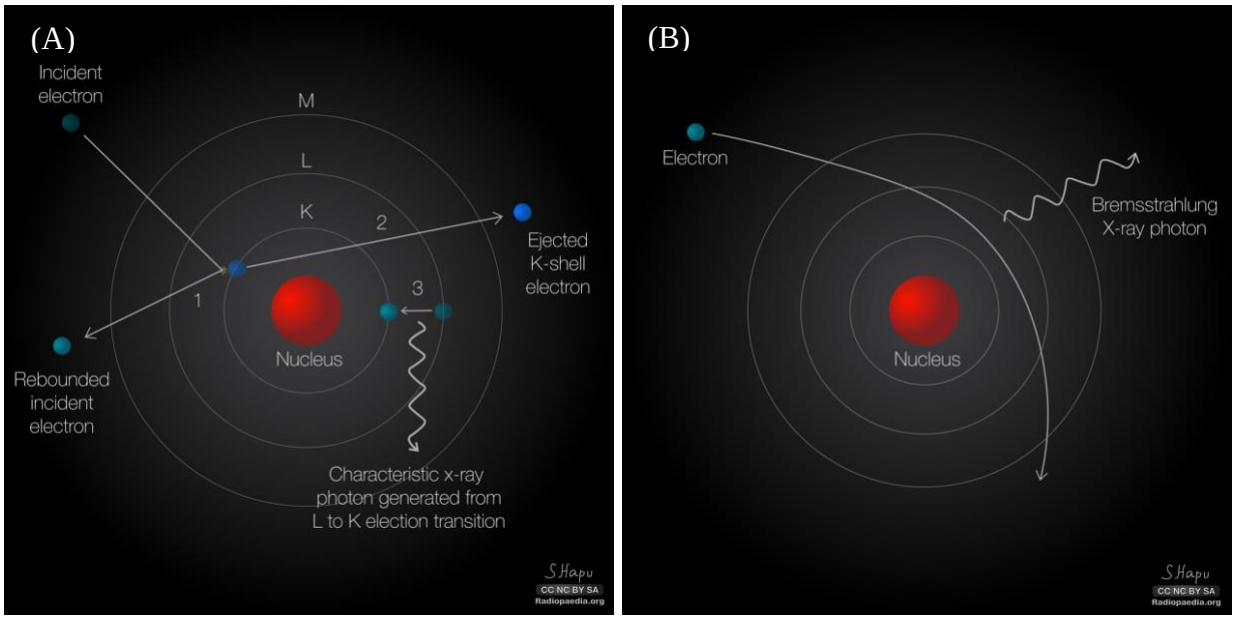

Figure 2.2. (A) The production of characteristic radiation when the high energy incident electron collides with the inner shell electron is shown. This electron as well as the 'ejected' electron are emitted from the atom leaving a 'hole' in the inner layer. One of the electrons in the outer shells can be observed emitting an x-ray photon to drop down to the inner electron shell. Image courtesy of Dr Candace Makeda Moore, Radiopaedia.org. (B) The production of bremsstrahlung radiation[7] is shown when a high energy incident electron passes near the nucleus and releases a photon as it is slowed down and its path is bent. Image courtesy of Dr Konrad Schultz, Radiopaedia.org.

Other applications of x-rays can be appreciated in medicine to view the internal structure of objects such as the human body, in airport security to check for dangerous substances, or in construction to check for damages in building materials.

2.3 Beamline Choice: Synchrotron Radiation vs. Lab x-ray Diffractometer

While gathering all the information described above from an x-ray diffractometer, it is important to highlight why synchrotron radiation was a better choice than a laboratory x-ray diffractometer. The first benefit is that because the velocity of the electrons in synchrotron radiation is very close to the speed of light, the relativistic effect emits radiation in a very narrow angular distribution (i.e., they are condensed into an extremely small angular spread[8]). This offers a significantly better angular resolution of the incident x-rays. Secondly, the x-rays are not produced continuously since the circulating electrons are in bunches separated by 1 ns lasting about 100 ps. The intense x-ray in short pulses allows recording of time-resolved x-ray diffraction patterns. This feature is not amenable with laboratory x-ray diffractometers. Synchrotron radiation also produces a broad end continuous energy spectrum. A single wavelength can be selected with the aid of a monochromator. This highly collimated, intense, and horizontally polarized beam gives superior quality data when compared to a laboratory x-ray diffractometer.

2.3 X-ray Diffraction (XRD) and Bragg's Law

Diffraction is a process by which an incident radiation is scattered elastically (Figure 2.3) as it incidences on a periodic arrays, e.g., crystal lattice or grating. Diffraction only occurs when the path difference travelled by the x-rays is an integer of the wavelength (λ). The diffraction condition is governed by the mathematical quantification of Braggs diffraction law (Equation 2.1) [9].

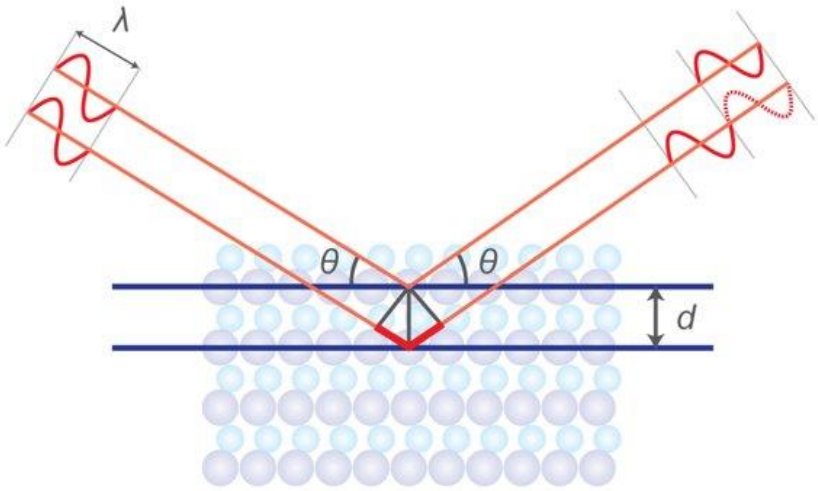

Figure 2.3. Diffraction geometry according to the Bragg's diffraction law[9] is illustrated, where λ represents the incident wavelength, θ represents the incident angle of the energy source and d is the spacing between the crystal layers.

Bragg's Diffraction Law is defined as:

$$n\lambda = 2d\sin\theta \tag{2.1}$$

where:

n = an integer (order of the diffraction)

λ = wavelength of the x-ray

d = spacing of the crystal layers

θ = incident angle

The diffracted waves are subjected to constructive and destructive interference. Constructive interference occurs when the scattered beams emerge 'in-phase' and destructive interference is when the beams emerge 'out-of-phase' at specific angles. The position and intensity of the constructive interference depend on wavelength and the spacing of the atomic plane. The angles at which x-rays are diffracted depend on the distance between the adjacent layers of atoms or ions. Since the wavelengths of x-rays are similar to the distance between atoms in a crystal, x-rays can be used to determine the distance between atoms in a crystal. The study of crystal structures requires electromagnetic radiation with wavelength comparable to the interatomic distances. For example, the typical interplanar spacing between crystals is about 2-3 Å and x-rays have a wavelength of approximately 1 Å.

The crystal essentially acts as a 3D diffraction grating in which the diffraction can be treated as a reflection from multiple equivalent lattice planes (hkl). A perfect crystal produces sharp peaks, an imperfect crystal produces broad peaks, and liquids or gases produce a diffuse, continuous spectrum.

In powder XRD, all possible diffraction directions of the lattice planes are obtained due to the random orientation of the micro-crystalline material[10]. When the angle satisfies the diffraction, a signal is recorded. Each set of planes in a crystal gives rise to a cone of diffraction. Each cone consists of a set of closely spaced dots, representing diffraction from a single crystallite. This cone is known as a Debye cone (Figure 2.4). In a one-dimensional diffraction pattern, the detector scans through an arc that intersects each Debye cone at a single point, giving a discrete diffraction pattern (Figure 2.4).

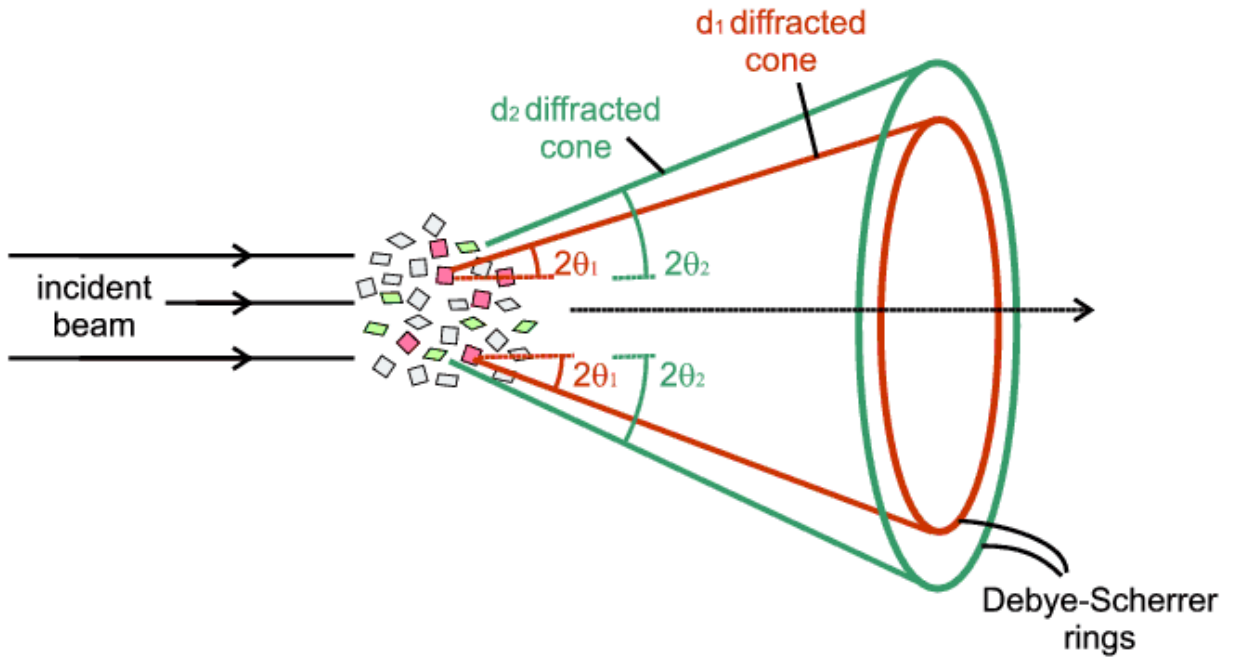

Figure 2.4. A theoretical illustration is shown as to how the Debye cone is formed. The image[11] shows different cones of diffraction depending on the planes of the crystallite. Image shared from Open Access database.

θ is the incident angle defined between the x-ray source and the sample. 2θ is the diffracted angle defined between the incident beam and the detector angle.

A diffraction data pattern is a plot of the intensity of the diffracted x-rays as a function of the scattered angles (2θ). It is important to note here that while θ is the angle between the incident beam and the reflecting plane (i.e., the angle between the reflected beam and the reflecting plane in Figure 2.5), 2θ represents the angle between the transmitted x-rays. A flat photographic plate was used as the detector. Therefore, both reflected and transmitted beam can be observed which means that 2θ is a quantity one can be measured. This is further illustrated in Figure 2.5 below.

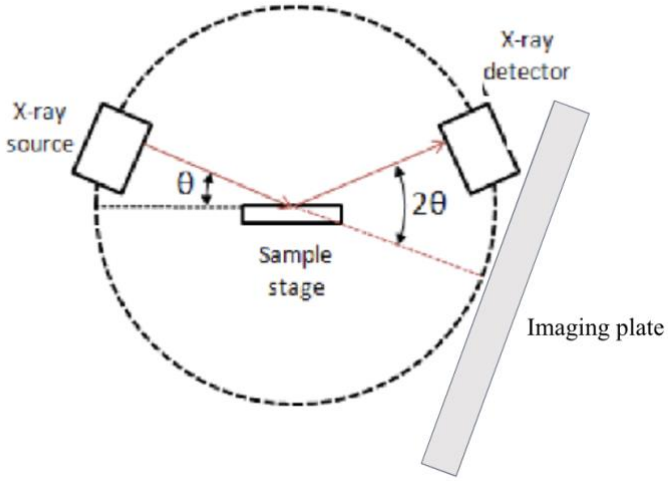

Figure 2.5. Illustration showing[12] the incident beam onto the sample as well as the transmitted beam that is detected by the x-ray detector. The total angle the beam travels is 2θ.

Figure 2.6 below illustrates an experimental diffraction pattern that shows Debye cones recorded on a flat image plate of powder diffraction of CH_4.

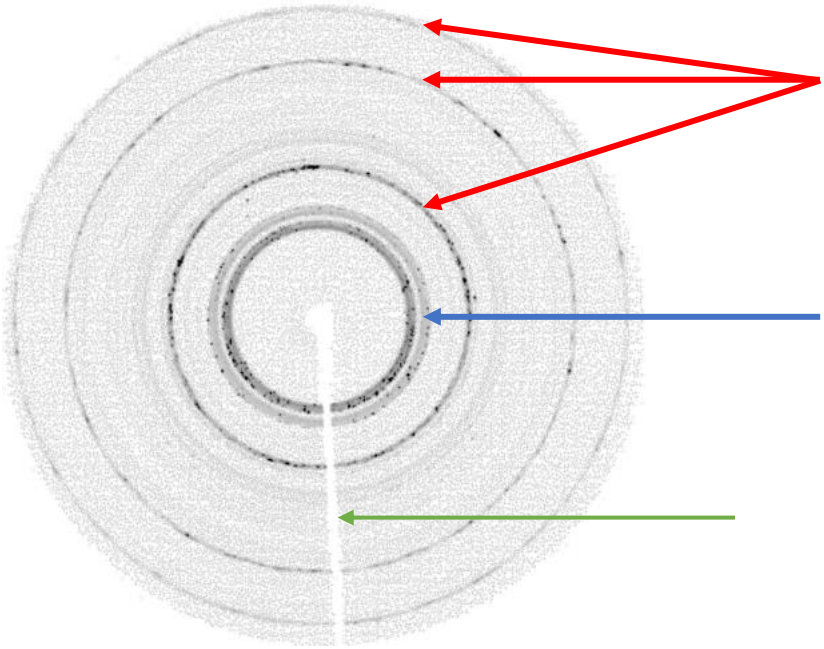

Figure 2.6. An example is shown of a CH_4 diffraction pattern (blue arrows) and the diamond substrate on the diamond (red arrows) imaging plate. It is a practical illustration of the Debye-Sherrer rings. At the center of this figure, there is an outline of the beam stop (green arrow). This ensures that the diffraction pattern is at the correct central position for further data collection.

An example of what the converted 1-D diffraction pattern for diamond recorded at the Brockhouse beamline is shown in Figure 8. This diffraction pattern shows three distinct peaks, at $2\theta = 9.62°$, 15.74°, and 18.48°, which are characteristic of diamond.

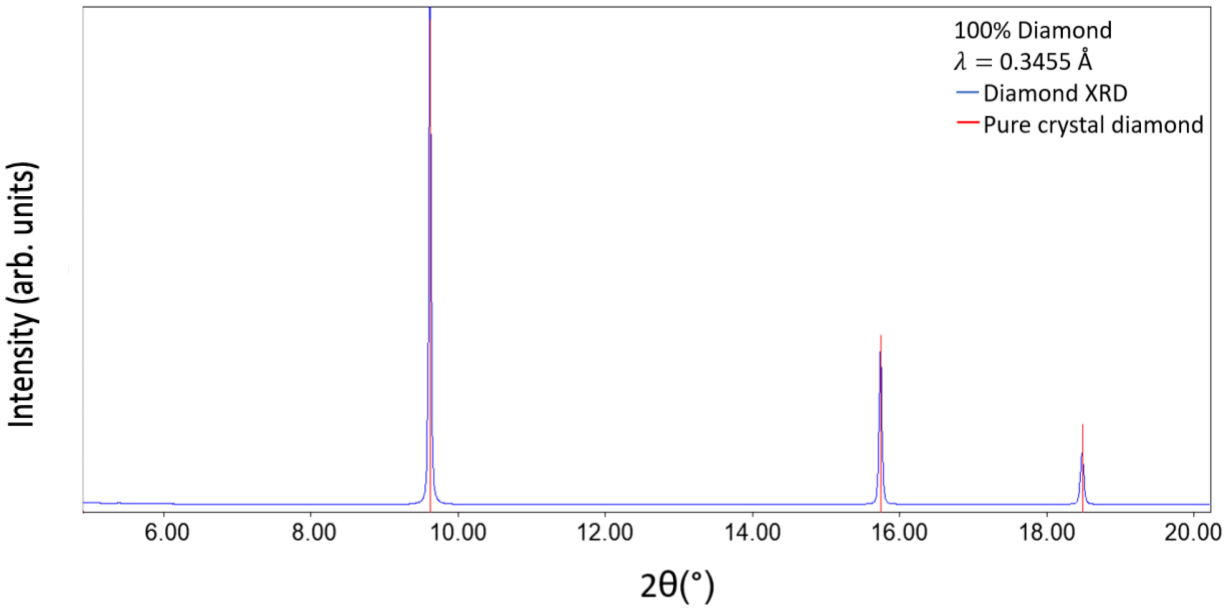

Figure 2.7. Diffraction pattern of 2θ vs intensity is shown for a diamond substrate measured at the Brockhouse beamline. The peaks at 2θ = 9.6°, 15.7°, and 18.5° are the Bragg reflections of diamond.

2.4 Crystal information from XRD

The following information can be derived from the scattering of x-rays by a crystal:

2.4.1 Unit Cell

The primitive unit cell is the smallest unit of volume that allows identical cells to be stacked to fill the geometry space (as described in the previous section, refer to Figure 2.7). The unit cell also ensures that symmetry is maintained in the crystal system. There are 7 main crystal systems that are all based upon the relationship between a, b, c and α, β, γ. The unit cell is the basic repeating unit that defines a crystal. Each primitive cell comprises exactly one motif (or one base, not necessarily one atom). Figure 2.8 summarizes all the possible crystal systems[13].

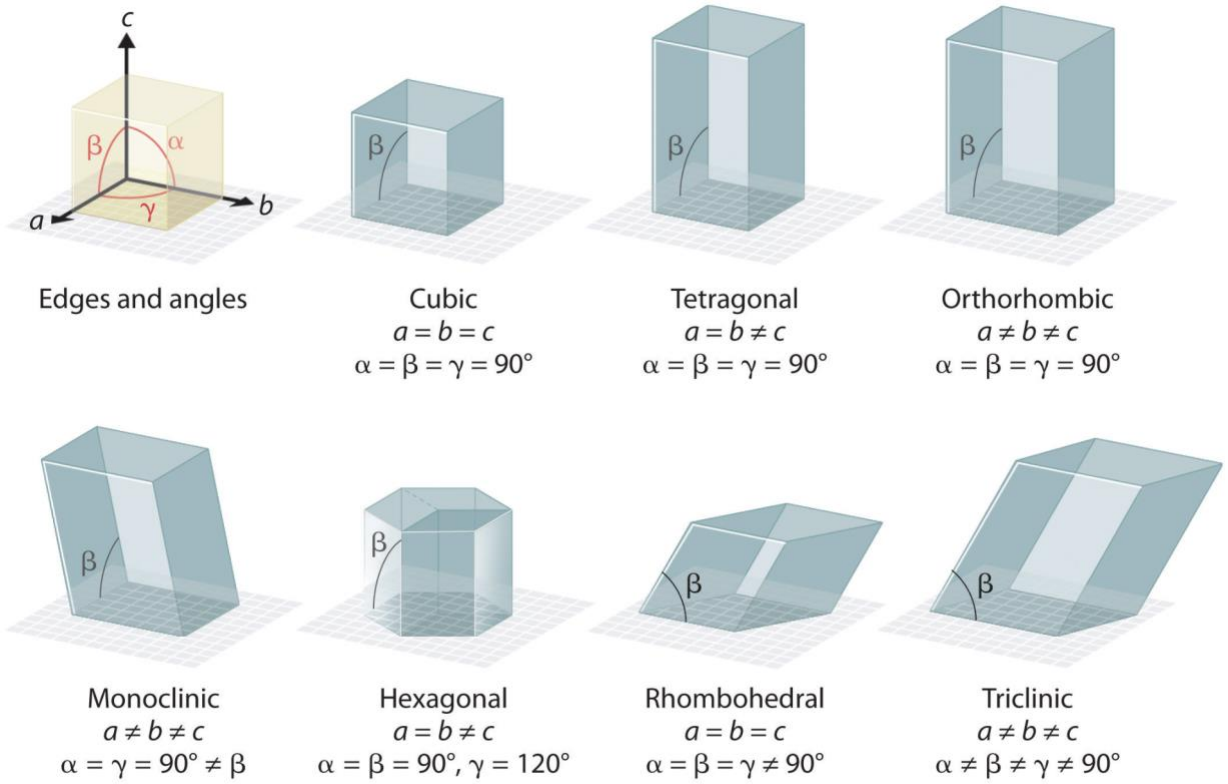

Figure 2.8. A summary of the 7 crystal systems that are based upon the relationship between a, b, c and α, β, γ. Image courtesy of Robert Belford, University of Arkansas under licence CC BY-NC-SA 3.0.

If the symmetry of the lattice points is included, there are 7 more lattices that can be noted – centered lattices. This gives rise to the Bravais lattices. This can be further divided as

- Primitive cell (P) that has no centered point
- Single-sided face-centered C(AB) unit cell that only has a center on 2 of the sides
- Body-centered unit cell (I) in which an additional lattice point is placed exactly in the center of a unit cell.
- Face centered unit cell (F) in which there are additional lattice points at all faces but not inside the unit cell.

An illustration of these Bravais lattices is shown in Figure 2.9[14].

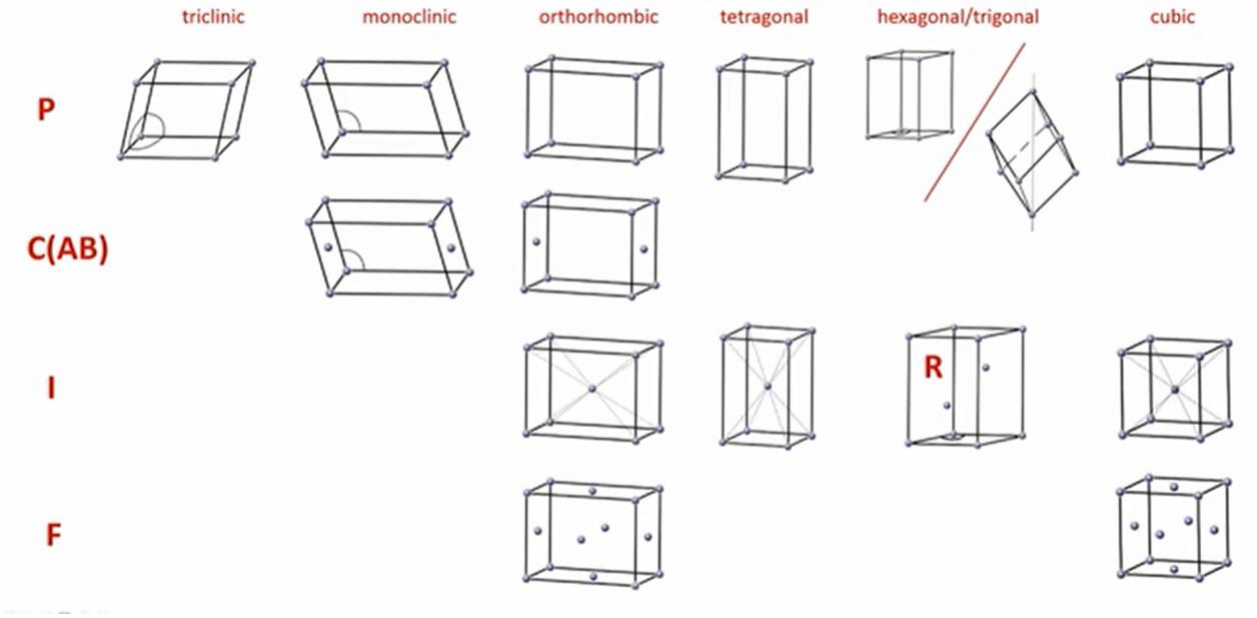

Figure 2.9. Summary of the Bravais lattices and the 7 crystal systems further organized into primitive (P), single-sided face-centered (C(AB)), body-centered (I), and face-centered (F) lattices. Image courtesy of Dr. Frank Hoffmann's course entitled The Fascinations of Crystals and Symmetry, University of Hamburg.

2.4.2 Miller Indices

The Miller indices are a group of three integers (hkl) that serve as a vector representation for the orientation of an atomic plane in a crystal lattice. The lattice planes are defined as the reciprocals of the fractional intercepts that the plane makes with the crystallographic areas. Each set can be found by first determining the intercepts of plane along each crystallographic direction, then taking the reciprocal of the intercepts, and, finally, if there is a fraction result, multiply each by the denominator of the smallest fraction. An example of this has been illustrated in Figure 2.10[15].

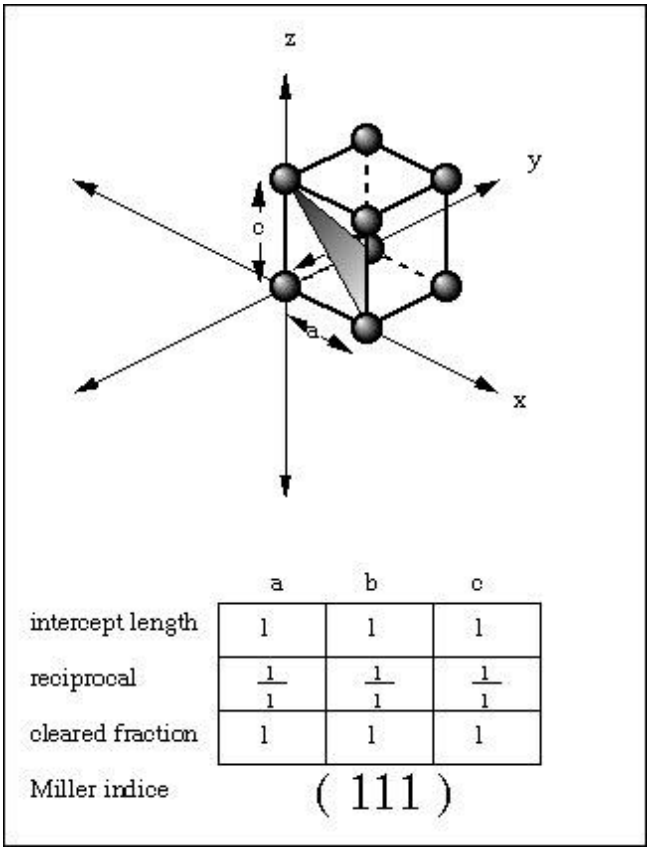

Figure 2.10. A sample calculation of the miller indices from a simple unit cell[18] is illustrated. Image courtesy of Dr. Paul Schroeder. Reprinted with permission.

2.4.3 Structure Factor

From the information of the lattice planes and the atomic positions, the structure factor[16] can be computed. The structure factor (Equation 2.2)[16] describes the amplitude and phase of the diffracted x-ray wave from a crystal that is determined by the crystal planes with Miller indices hkl.

$$\mathbf{F}_{hkl} = F_{hkl} \exp(i\alpha_{hkl}) = \sum_j f_j \exp[2\pi i(hx_j+ky_j+lz_j)] \qquad (2.2)$$

where the sum is over all the atoms in the unit cell

x_j, y_j, z_j = positional coordinates of the jth atom

f_j = scattering factor of the jth atom

α_{hkl} = phase of the diffracted beam.

2.4.4 Intensity of Bragg reflection

The intensity (Equation 2.3) of the diffracted beam is directly proportional to the amplitude of the structure factor.

$$I(q) \propto |F(q)|^2 \tag{2.3}$$

where $q = \frac{4sin\theta}{\lambda}$ is the scattering vector.

The positions and intensities of the diffraction peaks provide information regarding the types and locations of the atoms within a unit cell.

The intensity is dependent on the multiplicity factor, absorption factor, Lorentz factor, polarization factor, temperature factor, structure factor, and background intensity as described by Equation 2.4.

$$I(q) = mALpK|F(q)|^2 + I_b \tag{2.4}$$

where:

m = multiplicity factor

A = absorption factor

L = Lorentz factor

p = polarization factor

K = temperature factor

$F(q)$ = structure factor

I_b = background intensity

2.4.5 Polarization Factor

The polarization factor (p) arises from the fact that an electron does not scatter along its direction of vibration (Figure 2.11 and Equation 2.5 below). In other words, the electrons radiate with an intensity proportional to $\cos^2\alpha$. p is independent of the method used for the data collection[17].

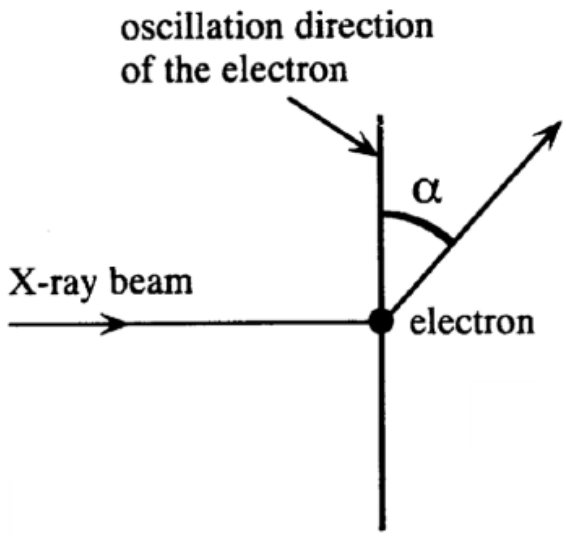

Figure 2.11. Illustration showing scattering from a charged particle by an incident radiation. It shows that when the x-ray beam hits a charged particle such as an electron, the electric field causes this particle to oscillate in the direction of the electric field where α represents the angle at which the incident radiation scatters.

It is defined as:

$$p = \frac{1 + \cos^2 2\alpha}{2} \tag{2.5}$$

2.4.6 Lorentz Factor

The Lorentz factor (L) depends on the precise measurement technique used. It is a correction factor that is applied to each reflection that scales each of the intensities to account for the distortion of the actual intensities. This distortion occurs because the x-ray may not spend the same amount of time on each point on the surface crystal due to its angular velocity. It is defined in Equation 2.6 as:

$$L = \frac{1}{\sin 2\theta} \tag{2.6}$$

This factor applies to diffractometer data obtained by the usual 2θ scans.

2.4.7 Temperature Factor

The temperature factor (Equation 2.7) depends on the amplitude of the atomic vibrations as a function of the temperature, T, and is defined by:

$$K = \exp\left[-B\frac{\sin^2\theta}{\lambda^2}\right] \quad (2.7)$$

Where B is the thermal factor.

2.4.8 Multiplicity and Absorption Factor

The multiplicity factor refers to the fact that there may be a family of hkl planes with different orientations but have the same d and F^2. The absorption factor depends on the angle which modifies the observed intensity. As atoms vibrate about their equilibrium positions in a crystal, the electron density is spread over a larger volume. This means that the atomic scattering factor decreases with $\frac{sin\theta}{\lambda}$ more rapidly at high scattering angles.

2.5 Crystal Structure Parameters

In principle, information on the crystal structure of a crystal can be extracted from the diffraction pattern. However, there are a few important details to highlight:

1. Peak position. The peak positions provide information on the relative orientation of the reflection planes from which lattice parameters such as the shape of the unit cell, space group and, sometimes, the crystal symmetry, can be obtained. The unit cell is the building block of a crystalline solid and its dimensions are related to interatomic distances. The lattice parameters (Figure 2.12) are:
   i. a, b, c = unit cell dimensions along the x, y, z axis respectively
   ii. α, β, γ = angles between b, c (α); a, c (β); a, b (γ)

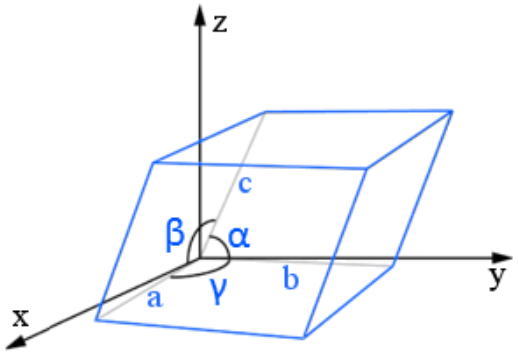

Figure 2.12. Illustration showing the lattice constants (a, b, c) in the x, y, and z direction, respectively, and the angles (α, β, and γ). Image courtesy of Chemicool [18].

2. Peak areas. The peak areas (intensities) of a single phase contain information on the nature of the constituent atom and how the atoms are arranged in the unit cell.
3. Peak widths. The distribution of the peak widths provides two pieces of information:
    i. Full Width Half Maximum (FWHM) is defined as the width of the diffraction peak at a height halfway between the background and the peak minimum. It provides information about the crystallinity of this sample and details about any inhomogeneous composition.
    ii. Integral breadth is the total area under the peak divided by the peak height. This measurement specifically accounts for the tails of the peak as well as the background. It provides information regarding the crystalline size, strain, and disorder
4. Peak shape. The peak shape can give information on the about the crystalline size, strain, and disorder. X-ray diffraction (XRD) is a non-destructive technique that can be used for many applications. These include but are not limited to differentiating between crystalline and amorphous materials, determining the structure of crystalline materials, determining the electron distribution within the atoms and throughout the unit cell, and determining the orientation of single crystals[10].

2.7 Rietveld Refinement

The Rietveld method is a method to determine the crystal structure for powder diffraction patterns. The method starts from a proposed model and adjusts the structural parameters such as the atomic positions to minimize the difference in the calculated and observed structure factors using the least squares method[16]. The strengths of Rietveld analysis are that it uses directly measured intensities and the entire measured diffraction pattern. This is less susceptible to the model and experimental errors. However, the procedure requires high quality diffraction pattern with Bragg peaks measured to high angles. Rietveld programs are also not easy to use, and the refinement often requires some experience.

The software Match! available as a commercial package from Crystal Impact[24], was used to analyze the results from the x-ray diffraction (XRD) measurements. This software can extract peak positions and allows the comparison with a database of known compounds. Unit cell parameters and atomic positions can be obtained from the analysis, and a crystal structure visualization can

be produced using the software Endeavour[19]. The Fullprof Suite[20] embedded within the software provides user-friendly interface to work through systematically. Fullprof has been designed to perform Rietveld analysis on either x-ray powder diffraction data or neutron diffraction[21]. Rietveld analyses were performed on the present data sets to provide information on the lattice parameters (a, b, c), as well as relative composition on the mixture based on the actual calculated intensity of the relevant phases.

2.7.1 Results from a Rietveld Refinement

Rietveld refinement can provide information on:

1. Unit cell dimensions
2. Phase quantities (i.e., how much of each substance is present)
3. Crystalline size and/or shape
4. Atomic coordinates.

The analysis of the diffraction pattern follows the following steps.

The first step of the refinement is to correctly identify the crystal phase, which means that the calculated Bragg reflection peaks must be at the correct measured positions. Then peak width, intensity, and the slightly shifted peak positions can be adjusted. An example of this procedure is illustrated in Figure 2.13. Inspection of the calculated and measured patterns shows that the peaks have been identified in the correct positions but there are some obvious differences.

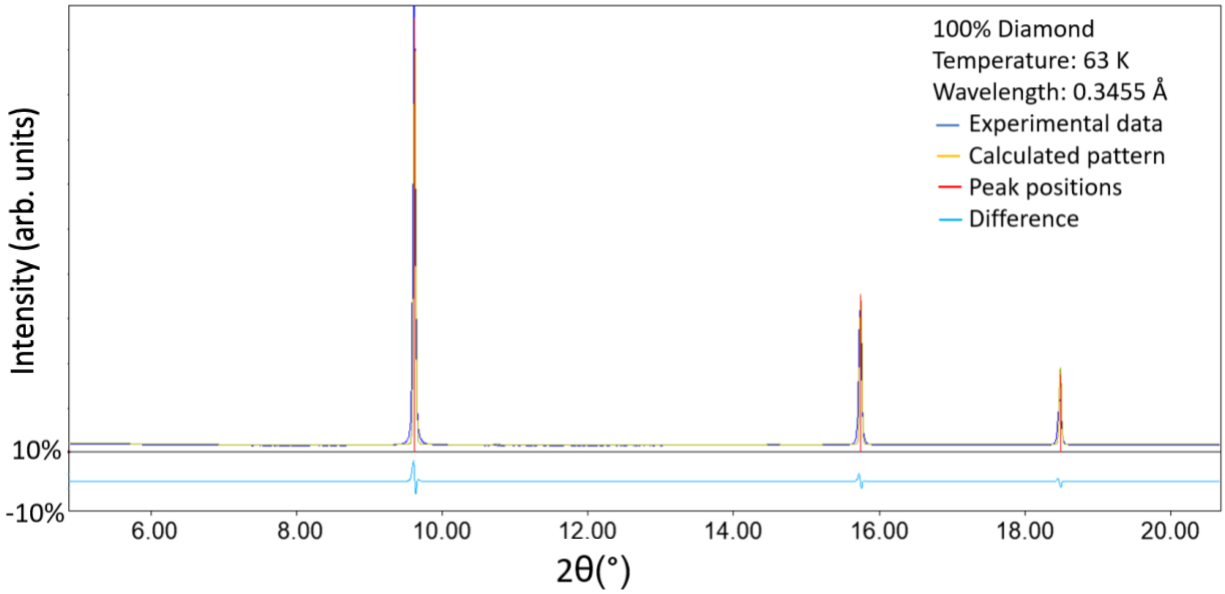

Figure 2.13. Diffraction pattern illustrating how the peak positions are appropriately aligned before further data analysis. The red sticks indicate where the peak positions are in the experimental data for diamond. The Match!

Software then searches its database to find an existing crystal structure to match the experimental diffraction pattern using the peak positions. It then calculates a diffraction pattern and allows the user to compare this with the original experimental pattern. The three peaks identified in this pattern for pure diamond are at 2θ = 9.6°, 15.7°, and 18.5° at the Brockhouse beamline. The light blue difference graph shows what the difference between the experimental and calculated diffraction patterns is. It can be observed that this error is less than 10%.

The next step is to adjust the peak shape. There are two methods of doing this.

1. The most used mathematical function to model the linewidth is the pseudo-Voigt method defined in Equation 2.8. This method was used as the experimental diffraction pattern was neither a pure Lorentzian nor Gaussian. The observed diffraction peals are fitted to this peak shape function.

$$V_p(x) = n * L(x) + (1 - n) * G(x) \tag{2.8}$$

where:

n = between 0 and 1, allowing one to weigh the function more towards pure Lorentzian or pure Gaussian.

$L(x) = \frac{1}{1+\left(\frac{x-x_0}{\omega}\right)^2}$ = Lorentzian curve

$G(x) = \exp\left[-\ln(2) \cdot \left(\frac{x-x_0}{\omega}\right)^2\right]$

x = peak position

x_0 = peak position at maximum

ω = full width at half maximum (FWHM)

The Lorentzian line shape emphasizes the tails of the peak and is somewhat narrower around its maximum as observed in Figure 2.14.

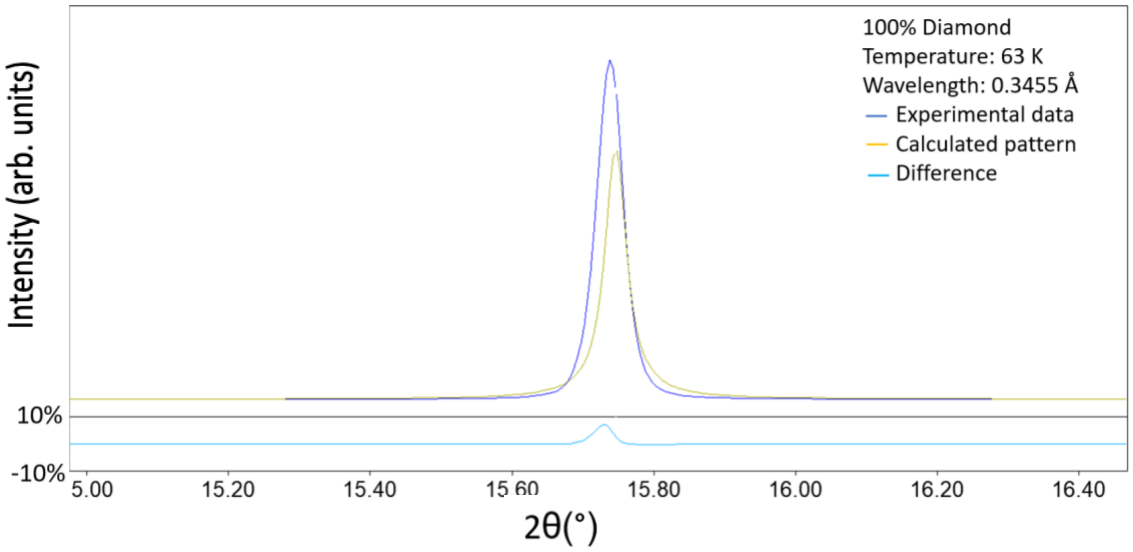

Figure 2.14. Diffraction pattern illustrating a Lorentzian fit for one peak of the experimental diamond diffraction peak at 2θ = 15.7° at the Brockhouse beamline. The calculated pattern shows discrepancy in the intensity when compared to the experimental pattern. However, the tails of the experimental and calculated patterns are in good agreement. The light blue line shows an error of less than 10% between the two diffraction patterns.

The Gaussian method is a typical 'normal' distribution and can be observed in Figure 2.15.

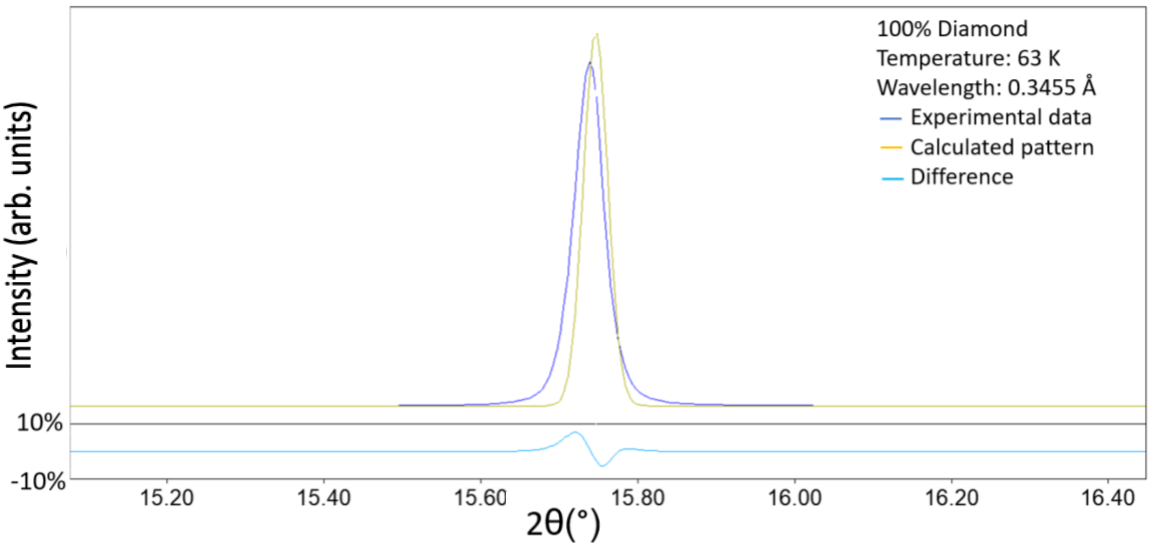

Figure 2.15. Diffraction pattern illustrating a Gaussian fit for one peak of the experimental diamond diffraction peak at 2θ = 15.7° at the Brockhouse beamline. The calculated pattern shows good agreement between the intensity of the experimental and calculated patterns. However, the tails of these patterns are not in good agreement. The light blue line shows an error of less than 10% between the two diffraction patterns.

Both these functions have finite integrals (i.e., the tails or any other component of the functions does not extend out to a significant degree), are limited, and are symmetric about their center points[22].

To take advantage of the properties of the Lorentzian and Gaussian fits, the so-called Pseudo-Voigt function was used. It is a linear combination of the two functions to model the experimental line shape. An example is shown in Figure 2.16, the diffraction profile is now better described. However, there is an apparent discrepancy in the peak position. This is likely due to the lattice parameter and the center (zero shift) of the diffraction pattern that were not adequately refined.

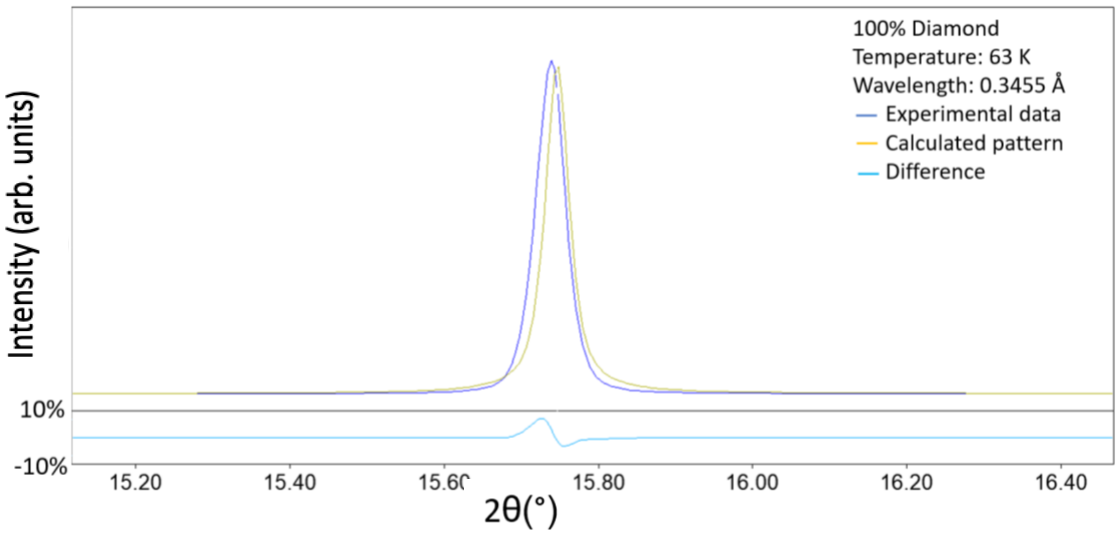

Figure 2.16. Diffraction pattern illustrating the fit with the pseudo-voigt function for one peak of the experimental diamond diffraction peak at 2θ = 15.7° at the Brockhouse beamline. It shows a significantly better fit for the intensity and the tail ends of the peak. The light blue line shows an error of less than 10% between the two diffraction patterns.

Several other mathematical models have their limitations and will not be discussed in detail here as they were not used in the peak shape adjustment but include Gaussian, Lorentzian, and Pearson profile functions.

2. The fundamental parameter approach, which is a profile modeling method, calculates the profile of the peak from the device's configuration. It accounts for the source emission profile (i.e., the wavelength distribution of the x-ray), the individual optical elements in the beam path, and the contributions from the sample.

Finally, these are some of the strategies that can be used for refinement (i.e., matching the calculated with experimental diffraction pattern) on the following parameters:

1. Peak positions
    a. Correction of unit cell dimensions because of sample height displacement or a zero shift.
2. Absolute intensities
    a. Compute the weighing fraction (scaling) for correcting the experimental intensity to the absolute structure factors.
3. Relative intensities
    a. Correct for preferred orientation of the sample which could be affected by the beam, tilt of the experimental system or unevenness in the deposition procedure.
    b. Explore sample texture by correcting for the graininess of the sample
    c. Atomic coordinates
    d. Site occupancies
    e. Thermal displacement parameters
4. Peak widths
    a. Crystallite size
    b. Micro-strain in the crystal structure
    c. To a lesser extent, surface roughness

A detailed example of Rietveld refinement of pure nitrogen can be found in Chapter 5.1.

2.7.2 Convergence on Rietveld Refinement

Weighted Profile R-factor (R_{wp})

R_{wp} is the primary figure of merit to determine the goodness of the fit. The weighted profile R-factor (R_{wp}) is defined as the sum of the square root of the quantity minimized divided by the sum of the weighted intensities to measure convergence as noted in Equation 2.9.

$$R_{wp} = \sqrt{\frac{\sum_i w_i\{y_i(obs) - y_i(calc)\}^2}{\sum_i w_i y_i(obs)^2}} \times 100\% \tag{2.9}$$

where:

$w_i = \frac{1}{\sigma_i^2}$

σ_i^2 = variance of $y_i(obs)$.

While this factor is useful when using Rietveld analysis, different softwares may be programed to sum individual points differently. This could mean that all points are being summed rather than individual points that have an intensity significant enough to measure. This parameter needs to be used cautiously because of the way in which background parameters are refined with Fullprof Suite (i.e., first background parameter refinement and remaining background parameter) affects the $y_i(obs)$ term. A larger $y_i(obs)$ will result in a smaller R_{wp}. So, while the weighted profile R-factor is a useful term, the designers of the Match! software advise against using it has a primary measure of the quality of the match.

Expected R factor (R_{exp})

R_{exp} is essentially the best possible R_{wp}. It is a measure of the data quality as shown in Equation 2.10 below:

$$R_{exp} = \sqrt{\frac{N - P + C}{\sum_i w_i y_i(obs)^2}} \times 100\% \tag{2.10}$$

where:

N = total number of observations

P = number of parameters refined

C = number of constraints used in the refinement

Chi-squared (χ^2)

A chi-squared value (Equation 2.11) can be calculated if the ratio is taken of R_{wp} and R_{exp}.:

$$\chi^2 = \left(\frac{R_{wp}}{R_{exp}}\right)^2 \tag{2.11}$$

If the initial crystal model is poor, χ^2 is large. This value often improves with more refinement cycles. χ^2 should never be < 1 as this means that $\{y_i(obs) - y_i(calc)\}^2$ is less than $y(obs)^2$ which may be a result of an overestimation of standard uncertainties or that too many parameters have

been introduced and the model is adjusting to fit the noise[9]. An ideal χ^2 would be 1 indicating that the R_{wp} exactly matches the R_{exp}.

It is worth noting that the parameters above are statistical values that are affected by data quality, the number of observations (N), and the resolution of the data. Nonetheless, they are useful when used to compare different models for the same set of data. Another benefit of these parameters is that they determine how well the match is being refined. If there is an increase in any of the factors above (R_{wp}, R_{exp}, χ^2) while the experimental pattern is compared to the reference pattern, it would indicate that there is an error in the refinement process. For example, a refined R_{wp} (ideally less than 5) and a high χ^2 indicates to the user that their refinement is likely good but that there may be systematic errors such as the shape profile of the refined pattern. A combination of a low χ^2 and R_{wp} is more reassuring that a good fit has been found.

CHAPTER 3: INSTRUMENTATION

The following chapter will discuss the instrumentation used for the experimental set up at the HXMA and Brockhouse beamlines at the CLS.

3.1 Monochromators

The purpose of using synchrotron radiation is to select a specific wavelength to probe the sample. The following formula can be used to convert energy and wavelength.

$$\mathrm{E\ (eV)} = \frac{1240\ \mathrm{eV \cdot nm}}{\lambda\ \mathrm{(nm)}} \tag{3.1}$$

To extract the precise radiation of a particular wavelength or energy, a monochromator is needed to monochromatize the broadband wavelength into a single energy.

The principle of this is to use the method of diffraction, as discussed previously. In addition to having the correct wavelength, the resolution must also be considered. Synchrotron radiation has the advantage of very intense wavelength and a broad distribution of wavelengths. If the spread of wavelength is not precise, the resolution will not be ideal either - i.e., the image will be blurred. A basic set up of monochromators is to focus radiation onto a crystal with a selected diffraction plane to select the appropriate wavelength for the experiment.

3.1.1 HXMA Beamline

The HXMA (Hard X-ray Micro-Analysis) beam at the Canadian Light Source that has a radiation with range of 5-40 keV, suitable for crystal structure analysis.

The HXMA beamline employs a double crystal monochromator. In the design of this system, the first crystal acts to monochromatize the synchrotron radiation (this is done using the energy spectrum as a function of incident angle[23]). The second crystal adjusts the beam height and the direction. At the HXMA beamline, an x-ray with E = 24.5 keV was used. The photon flux of the HXMA[24] beamline is around 10^{12} photon/m^2/s at 12 keV. At 24 keV, the photon flux is 5 x 10^{12} photon/m^2/s.

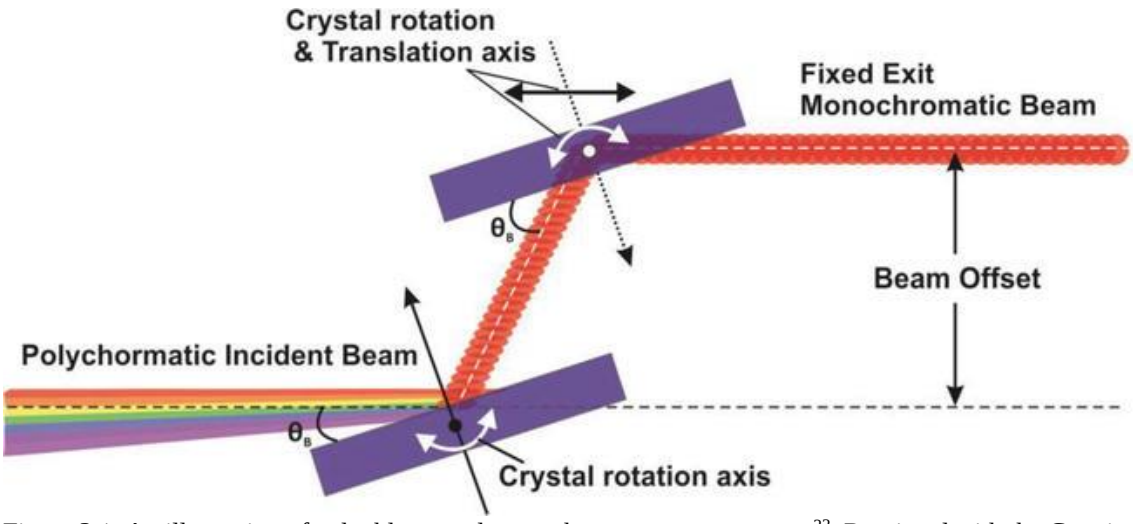

Figure 3.1. An illustration of a double crystal monochromator system set up[23]. Reprinted with the Creative Commons Attribution License (http://creativecommons.org/licenses/ by/3.0).

3.1.2 Brockhouse Beamline

The Brockhouse High Energy Wiggler Beamline beam at the Canadian Light Source can provide photon in the energy range between 20-94 keV. It makes use of a bent Laue Bragg crystal monochromator. This device uses a Si crystal that is cylindrically bent so that a vertical tangent to the center point of a spherical concave grating has a diameter equal to the radius of the curvature of the bent crystal. The benefit of having a single bent Laue Bragg crystal monochromator is that it allows the user to have an increase of magnitude of flux (compared to the double crystal monochromator). This crystal system is also able to reduce the resolution broadening by focusing the beam in one direction (i.e., the resolution gets better). At the Brockhouse beamline, x-ray with E = 35 keV was used.

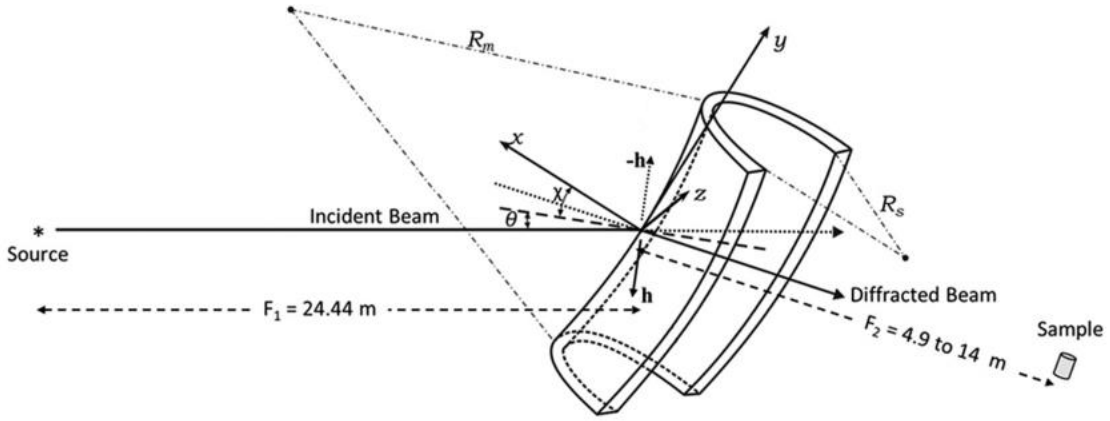

Figure 3.2. A schematic view[25] of bent Laue Bragg crystal system where θ (°) is Bragg angle and h is diffracting Bragg plane.

Resolution at the Brockhouse beamline is 2.5×10^{-4} at 12.9 keV to 4.5×10^{-4} at 22.5 keV with a maximum photon flux of 1×10^{12} to 5×10^{12} ph/s.

In the ensuing discussion, the diffraction patterns of co-deposition of methane and nitrogen measured at the two beamlines will be presented.

3.3 Vapour Deposition System

X-ray diffraction was performed using a partially polarized x-ray with a wavelength of 0.5092 Å at the HXMA (high energy x-ray for materials analysis) beamline and a wavelength of 0.3455 Å at the Brockhouse beamline of the Canadian Light Source. The diffraction pattern was recorded

with a CCD detector with time resolution of less than 1 second. The system was calibrated for distance and detector orientation using the x-ray diffraction pattern of the thin diamond plate attached to the cold finger of a cryostat on to which the sample was deposited. Prior to any set of gas deposition, the system was purged with vacuum. It is important to note here that this experiment was operated in a high vacuum while thin films were deposited so that the gas could be easily pumped out. Previous studies, mentioned in the Introduction, were performed under equilibrium conditions on bulk samples.

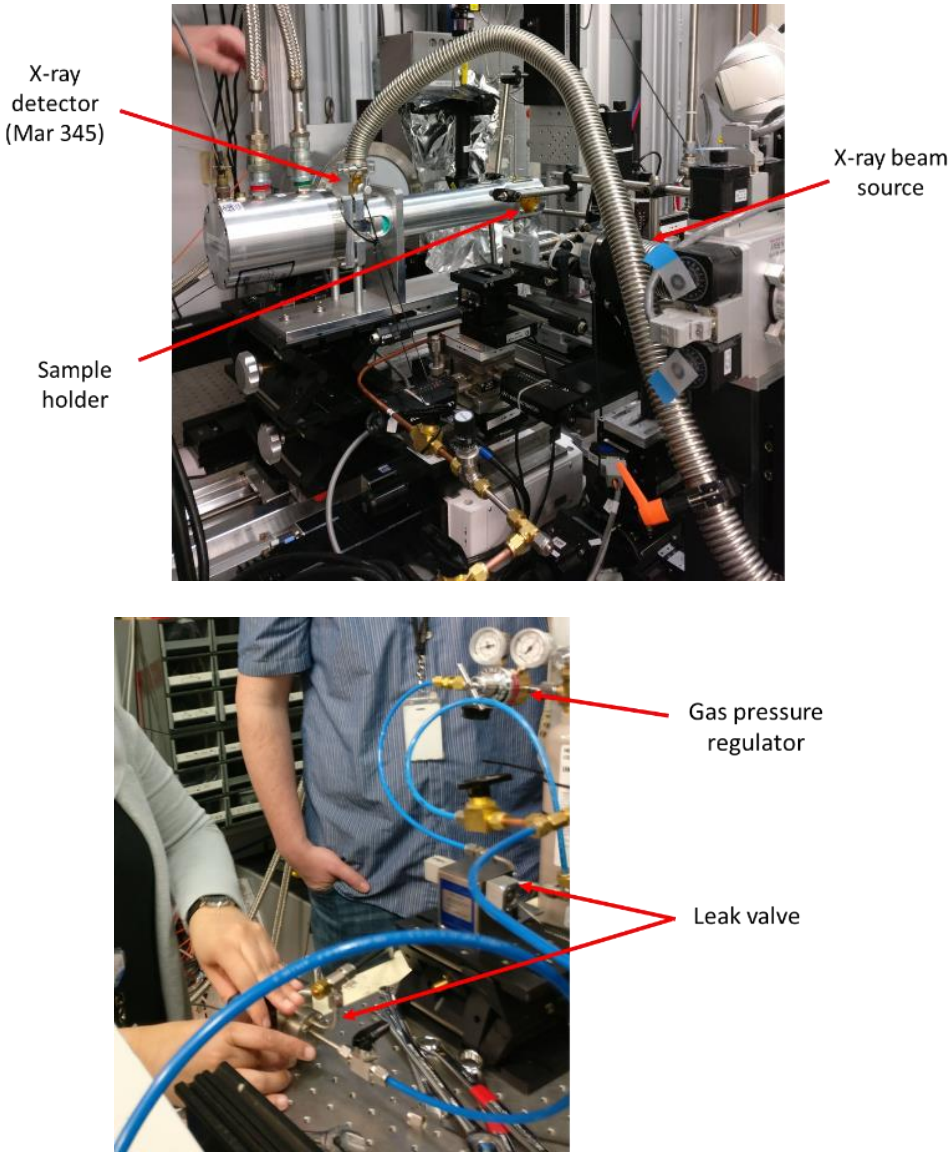

Figure 3.3. The experimental set up on the HXMA beamline is shown. The red arrows indicate the manual leak valve used at this beamline. The gas pressure regulator was used to control the gas pressure as it was leaked into the deposition system.

For each set of measurements, the system was evacuated to 10^{-7} – 10^{-8} torr and cooled down to 10K. Then the gas or gas mixtures were deposited for 20-30 minutes to produce a thin film on the diamond plate. Due to the heat of adsorption, the dose rate is controlled such that the temperature of the deposition is maintained at ±2K. The diffraction pattern was then recorded using a CCD (charged coupled device) x-ray detector. The sample was then slowly warmed up with diffraction patterns obtained at every increment of temperature change. It was warmed up to the melting temperature of the sample with the lowest melting point. Note that the thermodynamic melting point for nitrogen is 63.15 K and is 91.15 K for methane.

The purpose of the experiment was to co-deposit CH_4 and N_2 on a cold substrate and measure their diffraction patterns. The deposition was performed at high vacuum. A manual leak valve was used at the HXMA beamline and a programmed leak valve at the Brockhouse beam line to adjust the relative concentration of the gases.

3.4 Leak Valves

3.4.1 Manual Leak Valve

Commercially available 99% pure methane (CH_4) gas and nitrogen (N_2) gas were mixed at different concentrations and deposited onto a thin diamond film (70 µm) attached to the cold end of the DISPLEX in a specially designed system at cryogenic temperatures. This system was originally developed and tested by Tse et al. on a variety of applications. At the HXMA beamline, the relative concentration of the two gases was adjusted manually using a mechanical leak value for each gas (203 Variable Leak Valve). Table 3.1 shows the concentrations that were used during the first set of data acquisition:

Table 3.1. This table shows the concentrations for N_2 and CH_4 used in the experiment at the HXMA beamline with manually controlled valves.

Experiment	N_2 (%)	CH_4 (%)
1	100	0
2	75	25
3	43	57
4	20	80
5	0	100

There were some concerns about human error when manually adjusting these leak valves. The system was first tested by trial and error with a sample set and then fine-tuned to collect the bulk of the data.

Table 3.2 shows the dial settings for leak valve (shown in Figure 3.4) values for the mixing of the two gases at different concentrations. The settings are determined by the molecular weights and the diffusion rate of the respective gases from Graham's law of diffusion shown in Equation 3.2. The manual also gives instructions[31] that "Twenty-seven turns of the driver handle, or 270 counter numbers above the sealed position reference number, changes the leak from full closed mass spectrometer leak tight to full open.". A closed leak valve will have a reading of 0010.

$$\frac{r_1}{r_2} = \sqrt{\frac{M_2}{M_1}} \tag{3.2}$$

where:

r_1 = rate of diffusion for gas 1

r_2 = rate of diffusion for gas 2

M_1 = molar mass of gas 1

M_2 = molar mass of gas 2

Table 3. 2. The leak valve setting for the preparation of CH4-N2 gas mixtures at the HXMA beamline.

Experiment	N_2 (turns)	CH_4 (turns)
100% N_2	1720	-
75% N_2 and 25% CH_4	1720	570
43% N_2 and 57% CH_4	1300	1300
20% N_2 and 80% CH_4	535	2850
100 % CH_4	-	1300

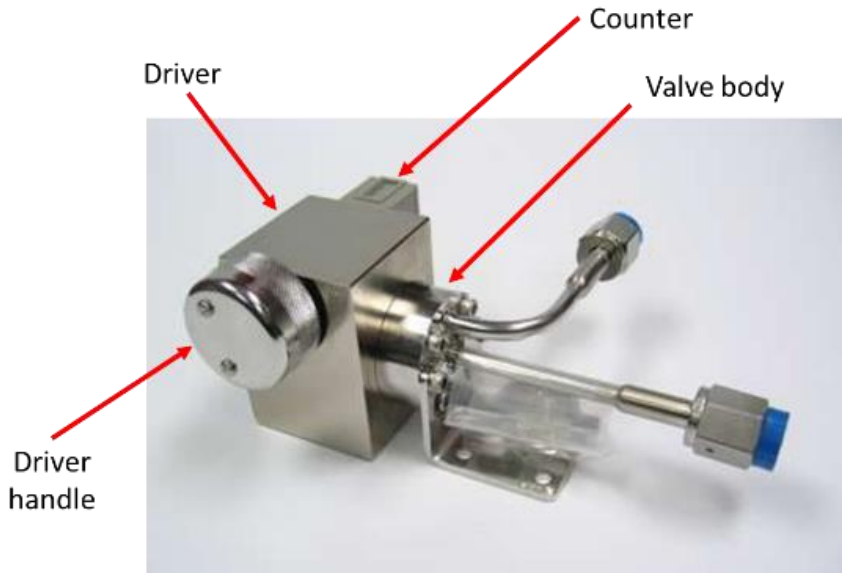

Figure 3.4. This is the manual leak valve[26] used in the setup at the HXMA beamline. The counter is used to control the leakage conductance giving better control over how much gas is leaked into the DISPLEX.

3.4.2 Programmed Leak Valve

The data collected at Brockhouse beamline used the programmable Bronkhurst mass flow control valves (Series F-200CV; Figure 3.5). They were calibrated specifically for N_2 and CH_4. The valve was controlled by a computer software through RS-232 connections. The RS-232 connection was used for communication and the EZ-Flow software for control. This allowed setting a set point to control the flow of gases and monitor the flow rates[27]. Use of a computer-controlled valve allowed more fine control over the rates with feedback from the valve.

Figure 3.5. This is the computer-controlled valve[28] used on the Brockhouse beamline for gas deposition.

3.5 Diffraction Patterns from Dioptas

The raw diffraction data (diffraction images) were converted into one-dimensional 2θ vs intensity files using the Dioptas software[29]. This software is designed to handle batch processing of data collected from a synchrotron. Using Dioptas, the data was calibrated with Diamond. As the distance of the sample to the detector cannot be measured with Å resolution[30], the diamond diffraction pattern was used for calibration. Diamond is known to have low x-ray absorption and a low-thermal expansion, making it ideal to use for this low temperature experiment.

Dioptas was also used to correct for the tilt (~1.3 degrees) of the image plate with respect to the incident x-ray using diamond as a reference. It takes the raw spectrum and allows calibration of the images via batch processing.

3.5.1 Raw Diamond Diffraction Pattern

A raw diffraction pattern of diamond generated by the Dioptas software is shown below:

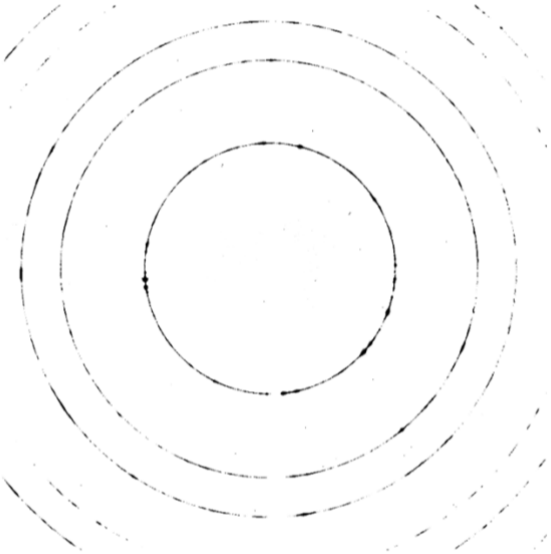

Figure 3.6. Raw diffraction pattern of diamond on the Brockhouse beamline at 60 K.

The diamond peaks are then identified:

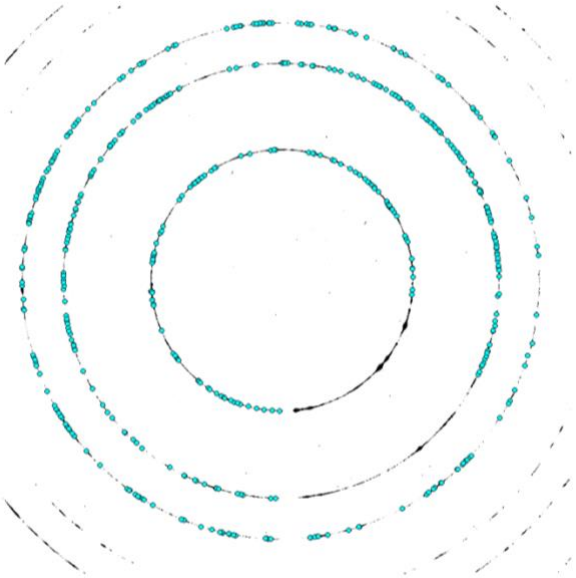

Figure 3.7. Diamond peaks identified on raw the diamond pattern on the Brockhouse beamline at 60 K.

Then, the 1-D flattened image (pancake plot) is examined to assess how good the data calibration was.

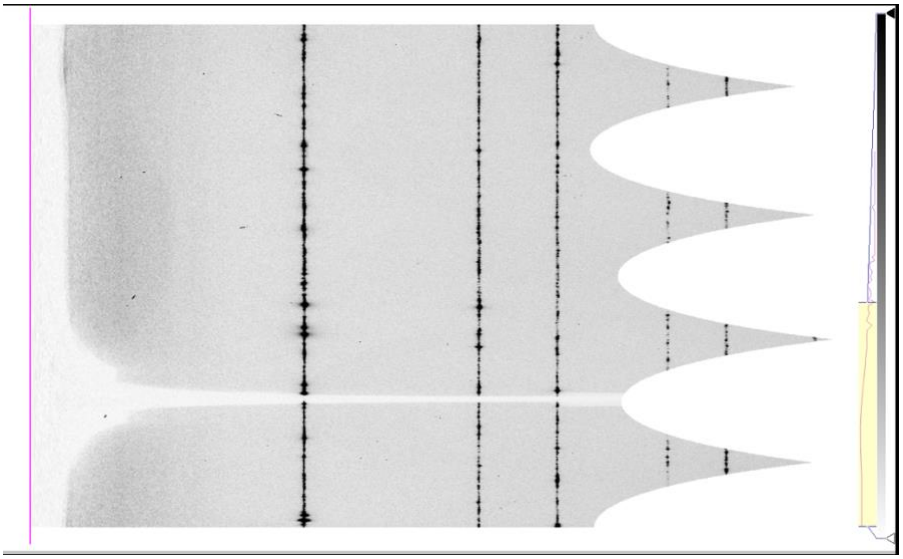

Figure 3.8. A pancake plot of the raw pattern for diamond on the Brockhouse beamline at 60 K.

The vertical lines correspond to a good calibration. This essentially serves as a check point to ensure that the calibration of the raw pattern was done appropriately[29]. Wavy lines could mean that the geometry of the diffraction may be potentially incorrect. An example of this is illustrated in Figure 3.9.

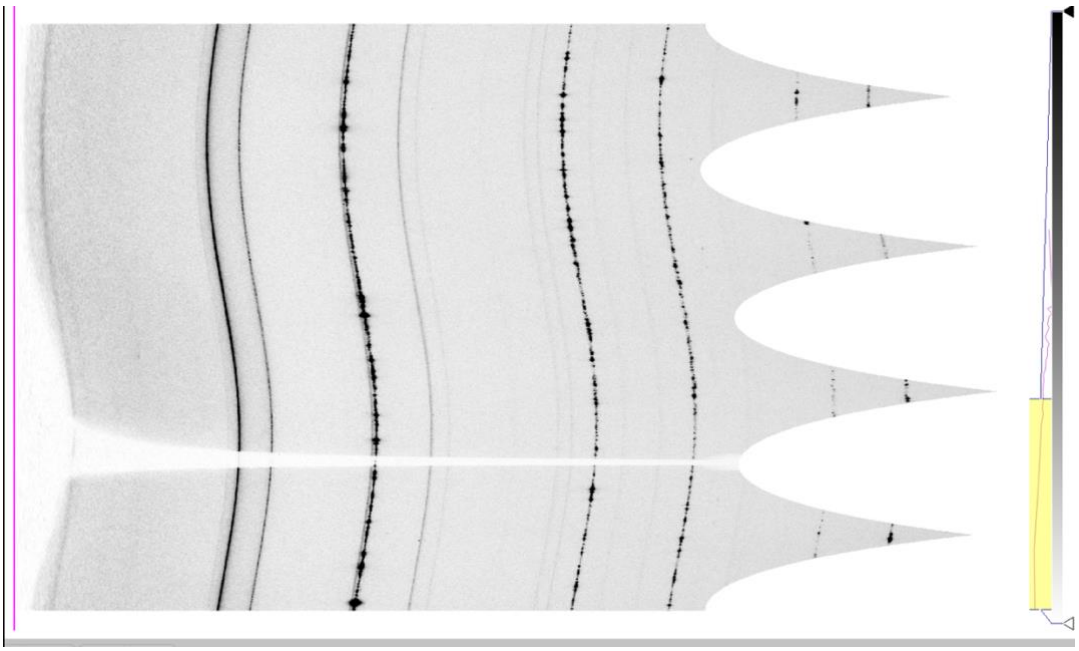

Figure 3.9. An example of poor calibration of the diamond diffraction pattern on the Brockhouse beamline at 60 K.

This is a result of poor selection of the calibrant peak. The wavy cake pattern indicates that the calibration was not performed properly. An incorrect wavelength or incorrect calibration file can also result in similar errors. This must be rectified before batch processing the rest of the data in order to avoid systemic errors in data analysis, and more specifically during the Rietveld refinement.

Files that did not have good diffraction patterns were identified here (due to loss of beamline, unexpected closure of the shutter, or poor pattern due to micromovements) and removed from further data analysis.

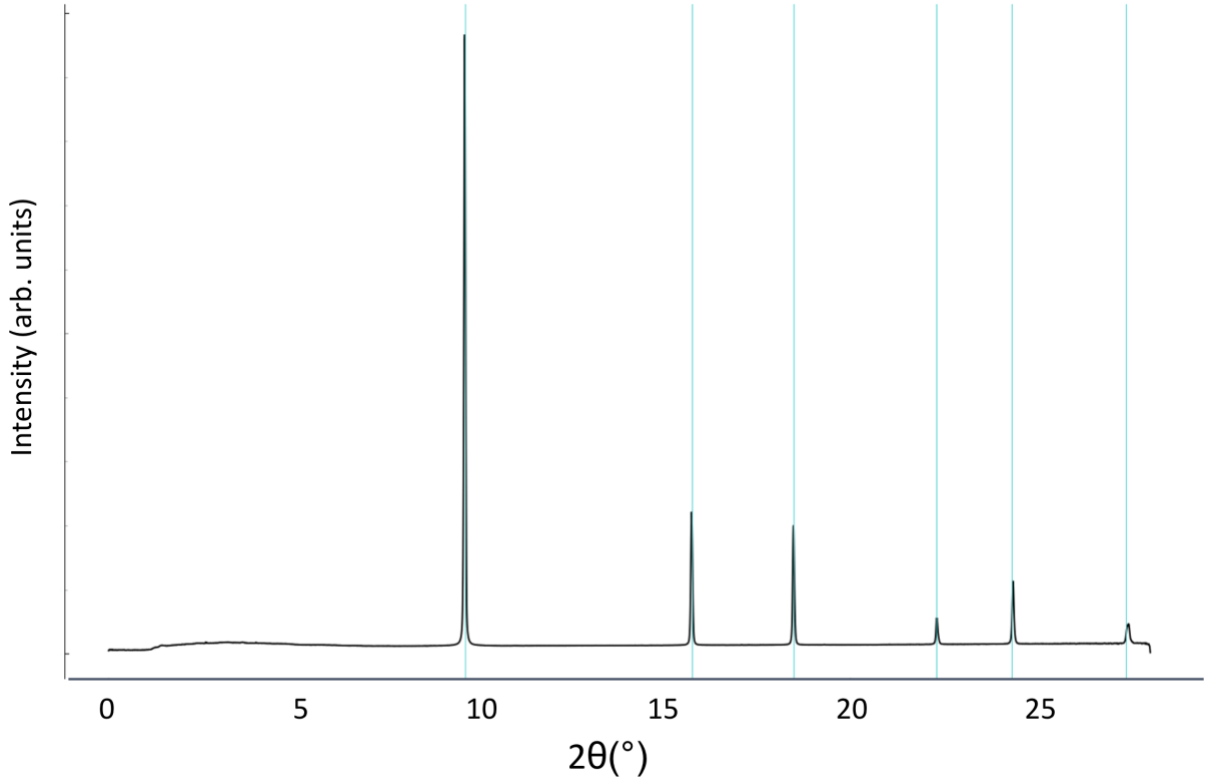

Figure 3.10. A diffraction pattern of the raw diamond data in Figure 3.6 at 60 K. The blue lines represent the diffraction peaks of diamond.

Figure 3.10 shows the diffraction pattern of the diamond substrate of the deposition system (see Figure 3.6). Usually, diffraction features below $2\theta < 5°$ and higher than $2\theta > 20°$ are discarded. The low angle cut-off is to reduce the contribution of the direct beam. The cut-off at the higher angle is to exclude incomplete diffraction rings due to the rectangular imaging plate.

For example, the diamond peaks that are identified from this calibration are at 2θ (°) = 9.61°, 15.29°, 18.47°. These peaks will be used in the Rietveld refinement to identify the correct peak positions of N_2 and CH_4.

3.5.2 Raw Nitrogen Diffraction Pattern

To illustrate the difference between the reference diamond peaks observed in Figure 3.6, Figure 3.11 below shows a 100% Nitrogen diffraction pattern and the corresponding pancake plot in Figure 3.12.

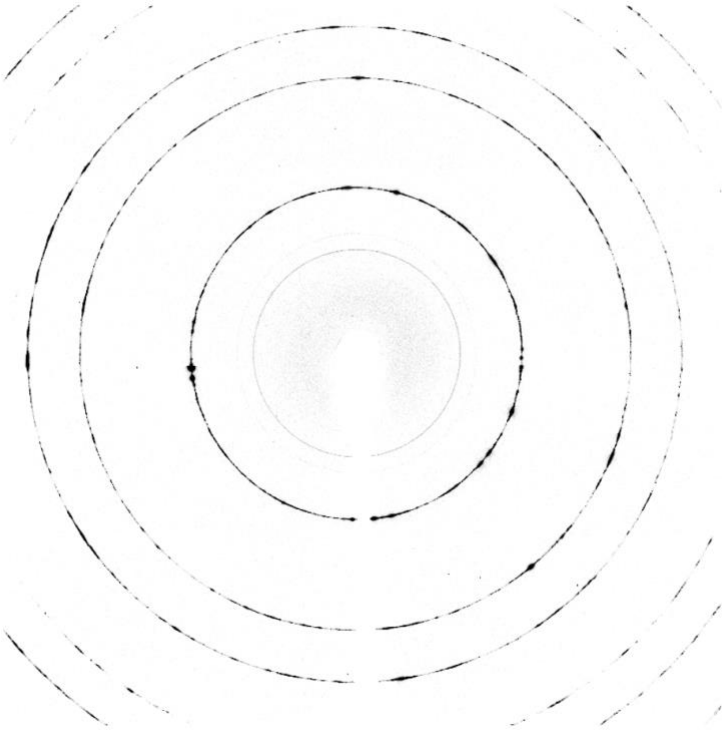

Figure 3.11. A raw diffraction pattern of pure nitrogen measured at the Brockhouse beamline at 15 K.

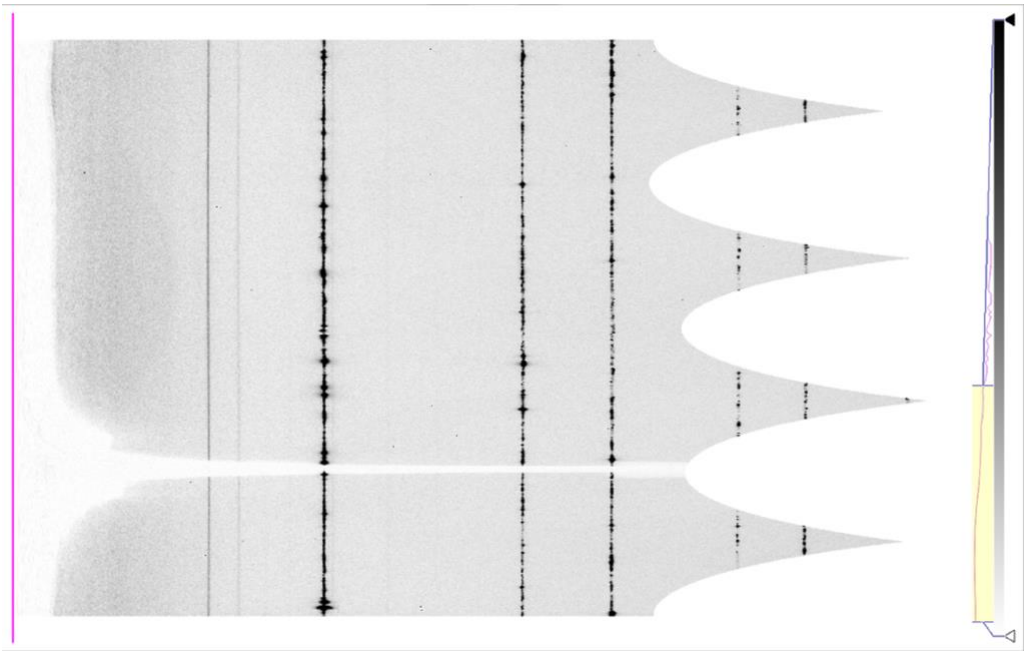

Figure 3.12. A pancake plot of the raw pattern for pure nitrogen measured at Brockhouse beamline at 15 K.

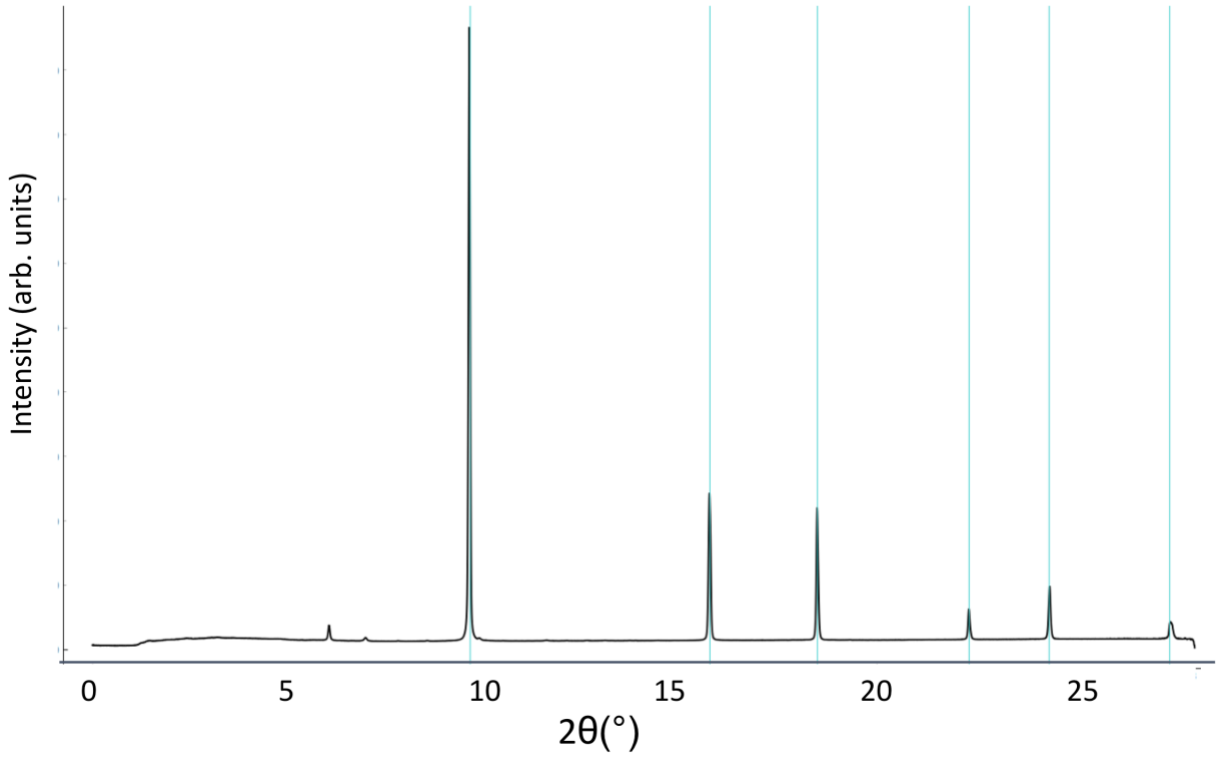

Figure 3.13. A diffraction pattern of the pure nitrogen measured at the Brockhouse beamline at 15 K. The blue lines represent the diffraction peaks of diamond.

Figure 3.13 shows that the calibrated lines are vertical and parallel to each other. This means that there is a good calibration for this set of data. The red lines in the Figure 3.13 correspond to the diamond calibration peaks (2θ (°) = 9.61°, 15.29°, 18.47°). From this diffraction pattern, two distinct N_2 peaks at 2θ (°) = 6.03°, 6.97° can be identified. It is important to highlight here that the diamond peaks are much stronger in intensity compared to the N_2 peaks. The strongest N_2 peak at 2θ = 6.03° has an absolute intensity of ~ 100 arbitrary units compared to the strongest diamond peak at 2θ = 9.61°, which has an absolute intensity of ~ 1900 arbitrary units. This means that the N_2 diffraction pattern has only a relative intensity of approximately 5% of the diamond pattern. In addition to this, there are several other weaker N_2 peaks observed at ~ 7.8°, 8.2°, 9.7°, 11.1°, and 11.6°, 12.2°, 12.8°, 13.9°. A closer view of this can be observed in Figure 3.14.

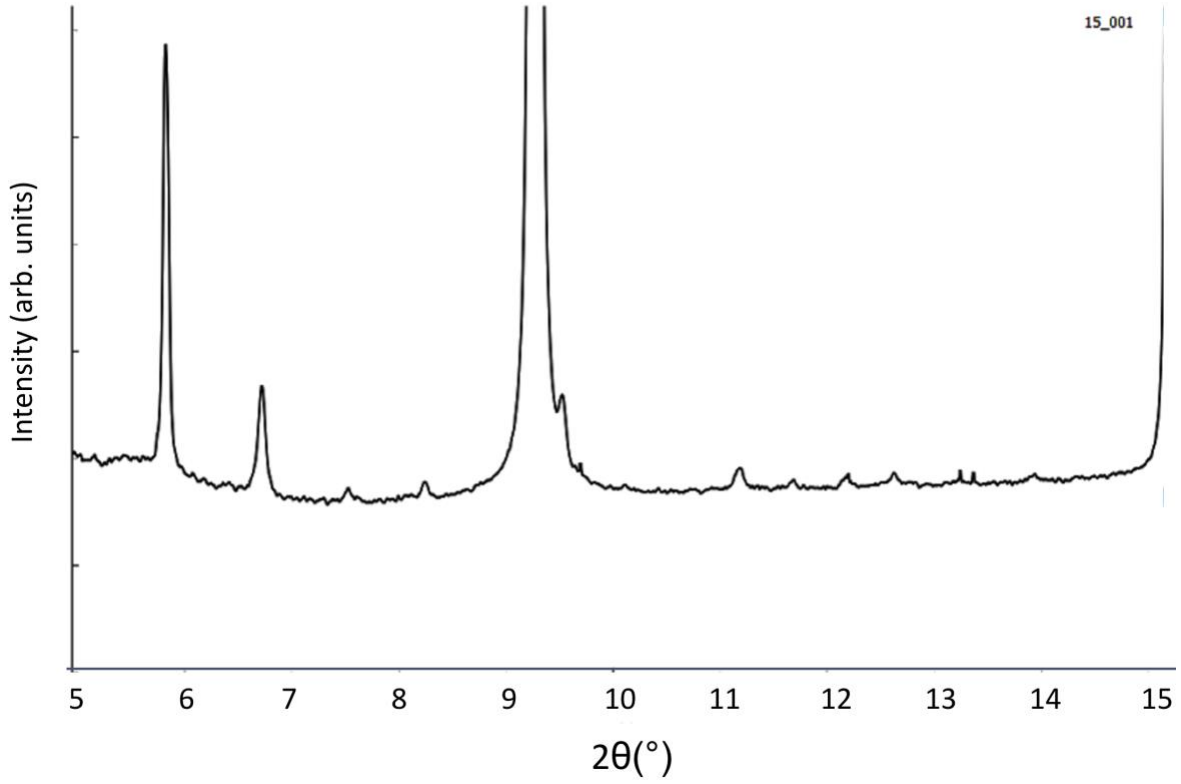

Figure 3.14. Diffraction pattern of the pure N_2 measured at the Brockhouse beamline limited to between 5° and 15° where the peaks at 9.6° and 15.3° represents diamond and all other peaks represent N_2.

3.5.3 Raw Methane Diffraction Pattern

The figure below shows a 100% Methane diffraction pattern and the corresponding pancake plot:

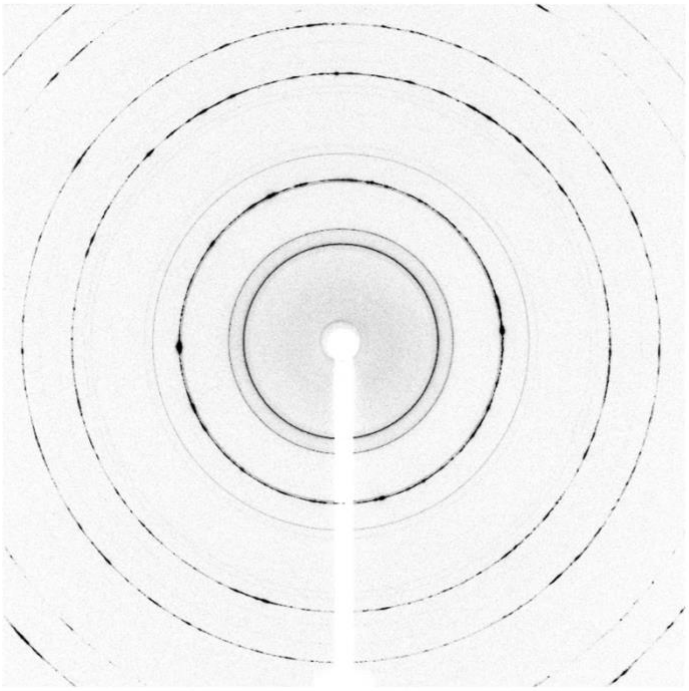

Figure 3.15. Raw diffraction pattern of pure methane measured at the Brockhouse beamline at 13 K.

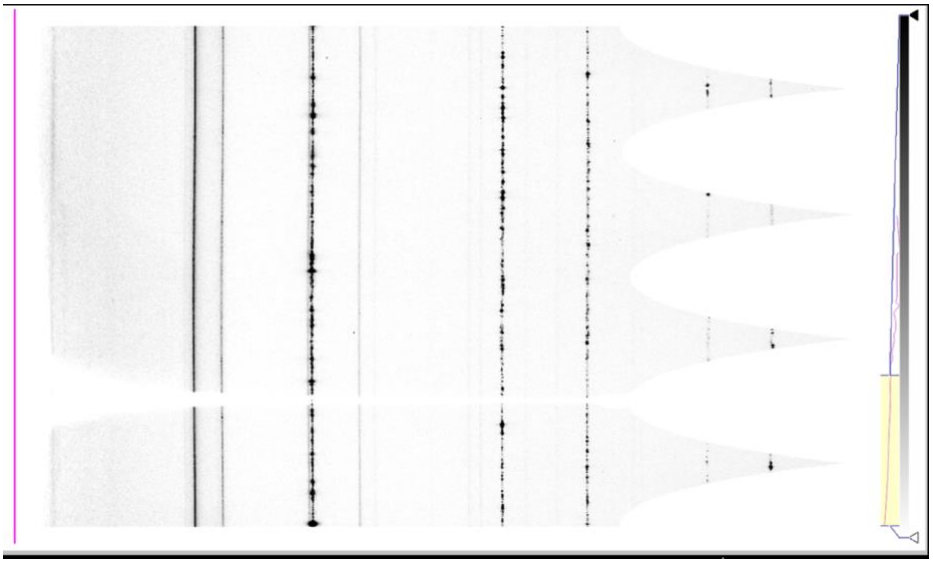

Figure 3.16. Pancake plot of the raw pattern of pure methane measured at Brockhouse beamline at 13 K.

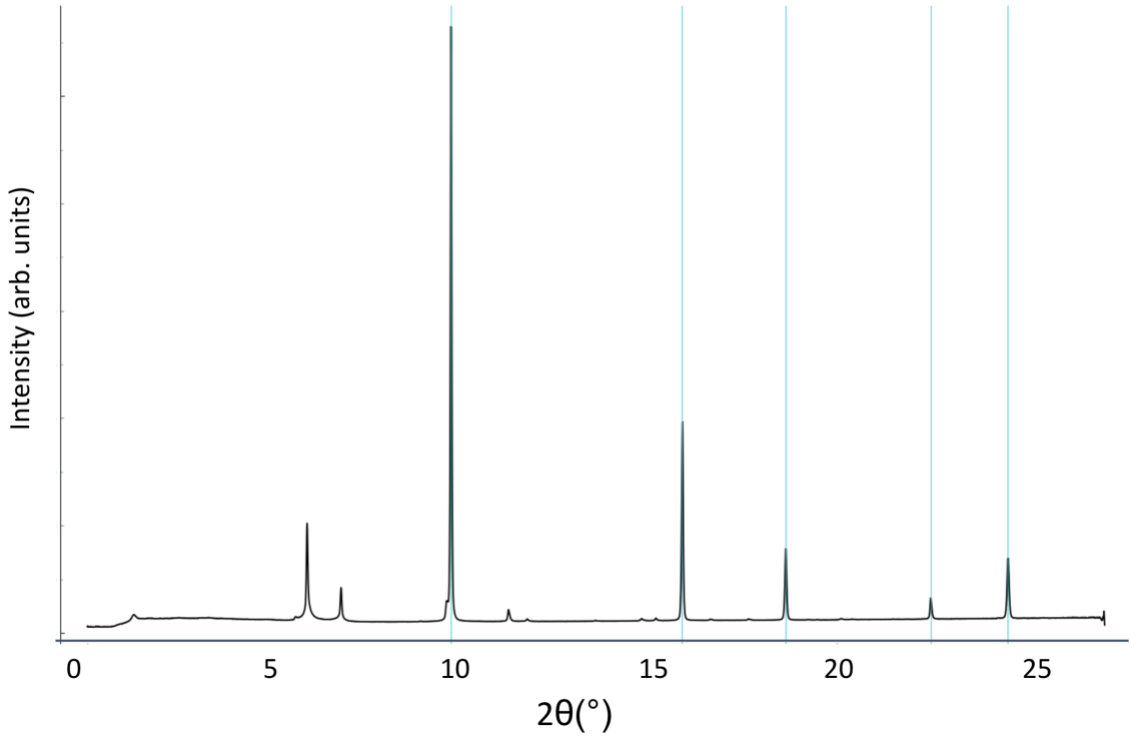

Figure 3.17. A diffraction pattern of the pure methane measured at the Brockhouse beamline at 13 K. The blue lines represent the diffraction peaks of diamond.

Figure 3.16 shows that the calibrated pattern is parallel to each other, which is reassuring that it is a good correction. Once again, the blue lines in the Figure 3.17 correspond to the diamond calibration peaks at 2θ (°) = 9.6°, 15.3°, 18.5°. Several distinct methane peaks at 2θ (°) = 5.8°, 6.7°, 9.6°, 11.2° can be identified. The diamond peaks are much stronger in intensity compared to the CH_4 peaks. The strongest methane peak at 2θ = 5.8° has an absolute intensity of ~ 200 arbitrary units compared to the strongest diamond peak at 2θ = 9.6°, which has an absolute intensity of ~ 1100 arbitrary units. This means that the methane diffraction pattern has a relative intensity of approximately 18% of the diamond pattern. There are several other weaker methane peaks observed at ~ 11.6°, 13.1°, 14.2°, 14.9°, 15.8°, 17.1° and 19.1° as observed in Figure 3.18.

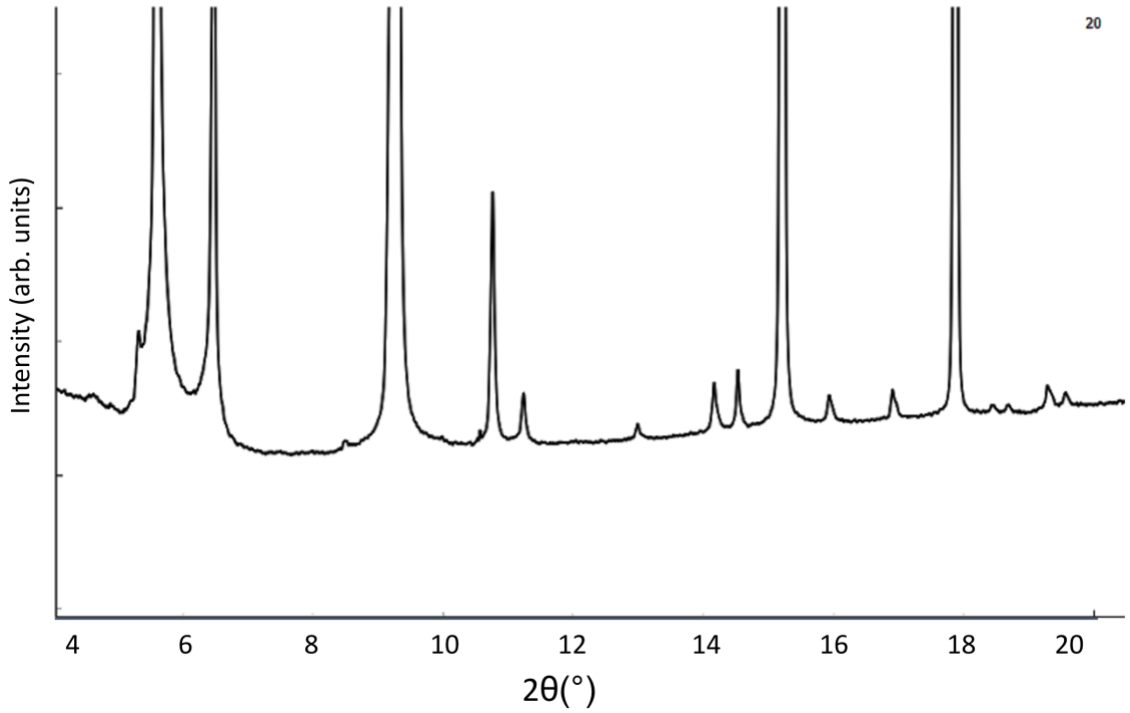

Figure 3.18. This enlarged diffraction pattern of the pure CH_4 on the Brockhouse beamline limited to between 5° and 20° where the peaks at 9.6°, 15.3°, and 18.5° represent diamond and all other peaks represent CH_4.

The diffraction due to the sample is less than 10% of the total scattering.

CHAPTER 4: COMPARING X-RAY DIFFRACTION AT HXMA AND BROCKHOUSE

4.1 Data Processing

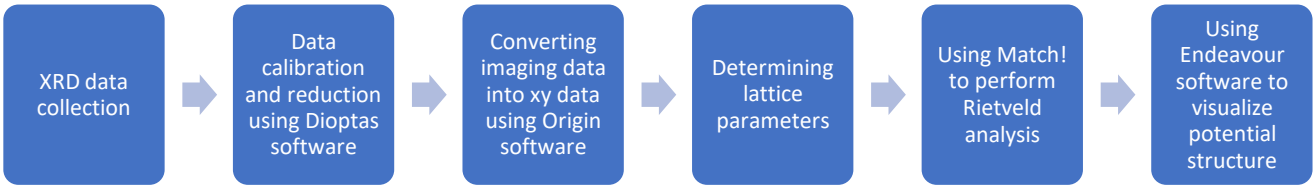

Figure 4.1. A flowchart summarizing the analysis of the x-ray diffraction data.

A flowchart for the analysis of the diffraction results is presented in Figure 4.1. The 2D diffraction recorded on an imaging plate is first corrected for the orientation and then data is extracted to have a 1D diffraction pattern, using the Dioptas software. The raw diffraction is converted to a simple (x,y) file using the Origin software. The diffraction pattern is indexed and analyzed using Rietveld analysis. The Endeavour software is then used for visualization.

In a typical experiment, the measured x-ray diffraction (XRD) data was compared to reference patterns of the pure sample in the Match! Software database to determine what phases were present in the sample. Sharp peaks represented the reference pattern. The goal of this study was to match the reference patterns and experimental patterns as closely as possible while acknowledging that there will be a marginal mismatch of the position and intensity of the data and the reference pattern. The reason for this error is due to the temperature and pressure at which the reference patterns were measured. A literature search on the cif (crystallographic information files) files for N_2 revealed many patterns from which the ones suited to the experimental condition were selected and then used for the Rietveld analysis. A similar literature search for CH_4 was performed but, unfortunately, no cif files were available at low temperatures. Neumann et al.'s paper[31] listed the individual parameters from which a crystallographic information file (cif) was created using the

VESTA software[32]. A cif file contains information about atom type properties, data to describe the structural refinement parameters, as well as cell parameters for a particular material. This was then imported into the data analysis software (Match!)[20].

4.1.1 HXMA Co-deposition

The following section discusses the vapor co-deposition of methane and nitrogen experiments at the HXMA beamline where a total of five sets of deposition were done. After setting up the equipment, the gases were leaked into the vapor deposition system using the manual valve where it was assumed that the gases are depositing on the diamond substrate. Diffraction patterns were collected after each deposition and this data was then calibrated. After processing each data set in Dioptas, the software converts the diffraction patterns into x-y data format files. These files were then imported into Origin to create waterfall plots to visualize pattern changes with increasing temperature. Figures 4.4, 4.11, 4.19, 4.22, and 4.26 below show the raw diffraction pattern for each concentration of N_2 and CH_4 as a function of temperature on the HXMA beamline (energy of 24.5 keV and wavelength of 0.5092 Å). The plots illustrate the progression of the diffraction peaks with increasing temperature, which reflects changes in crystalline structure for each sample. Table 4.3 below will summarize the samples and peak locations at the HXMA beamline.

4.1.2 Brockhouse Co-deposition

A similar approach to data collection as described above was used for the data collected on the Brockhouse beamline. An energy of 35 keV and wavelength (λ) of 0.3455 Å was used. The following section will also discuss the results of the vapor co-deposition of methane and nitrogen at the Brockhouse beamlines where five sets of deposition were done. After setting up the equipment, once again, the gases were leaked into the vapor deposition system using the programmed valve where it was assumed that the gases are depositing on the diamond substrate.

Figures 4.7, 4.14, 4.20, 4.24, and 4.29 below show the raw diffraction pattern for each concentration of N_2 and CH_4 as a function of temperature on the Brockhouse beamline. The plots illustrate the progression of the diffraction peaks with increasing temperature, which reflects changes in crystalline structure for each sample. Table 4.4 will summarize the samples and peak locations at the Brockhouse beamline.

4.2 Diamond

The following section presents the result for pure diamond on the HXMA and Brockhouse beamlines. This will allow for a discussion about the properties of each beamline using a diamond that has been well studied and has strong diffraction peaks. The quality of the data will be compared.

4.2.1 Diamond HXMA

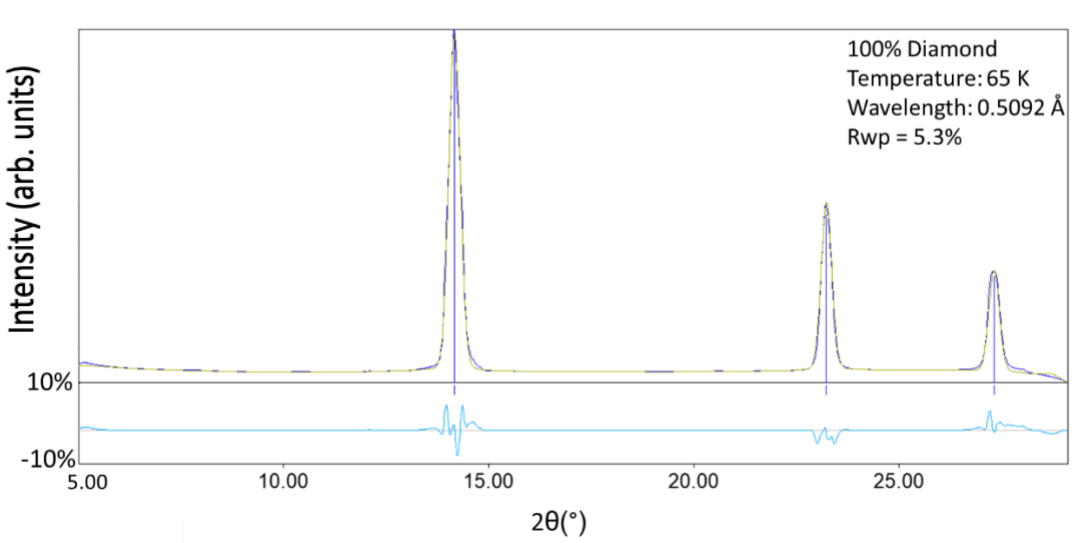

Figure 4.2. A diamond diffraction pattern measured at the HXMA beamline at 65 K. The blue sticks indicate the peak positions for diamond at 2θ = 14.1°, 23.3°, and 27.4°. The blue diffraction pattern represents the experimental data, and the yellow diffraction pattern represents the calculated pattern. The light blue line signifies that the difference between the calculated and the experimental pattern is less than 10%. R_{wp} is the weighted Bragg – R factor that is used to assess the merit of the calculated pattern.

Figure 4.2 shows the diamond diffraction pattern measured at the HXMA beamline with an energy of 24.5 keV (wavelength (λ) of 0.5092 Å). Diffraction peaks at 2θ = 14.1°, 23.3°, and 27.4° were

observed. There is good agreement between the observed diffraction pattern (blue) and the calculated diffraction pattern with Rietveld refinement (yellow) as indicated by the low weighted Bragg-R factor. Figure 4.2 also shows the difference plot between the observed and calculated diffraction pattern, illustrated as a light blue line. The maximum difference in the intensity is in the first peak. Hence, the maximum difference between the measured and calculated intensity is about 6%. The features observed in the intensity difference plot can be attributed to the pseudo-voigt function as the line shape is not a perfect representation. After the Rietveld refinement process, a weighted Bragg-R factor of 5.3% calculated indicating that there was good agreement between the experimental and calculated patterns.

4.2.2 Diamond at Brockhouse

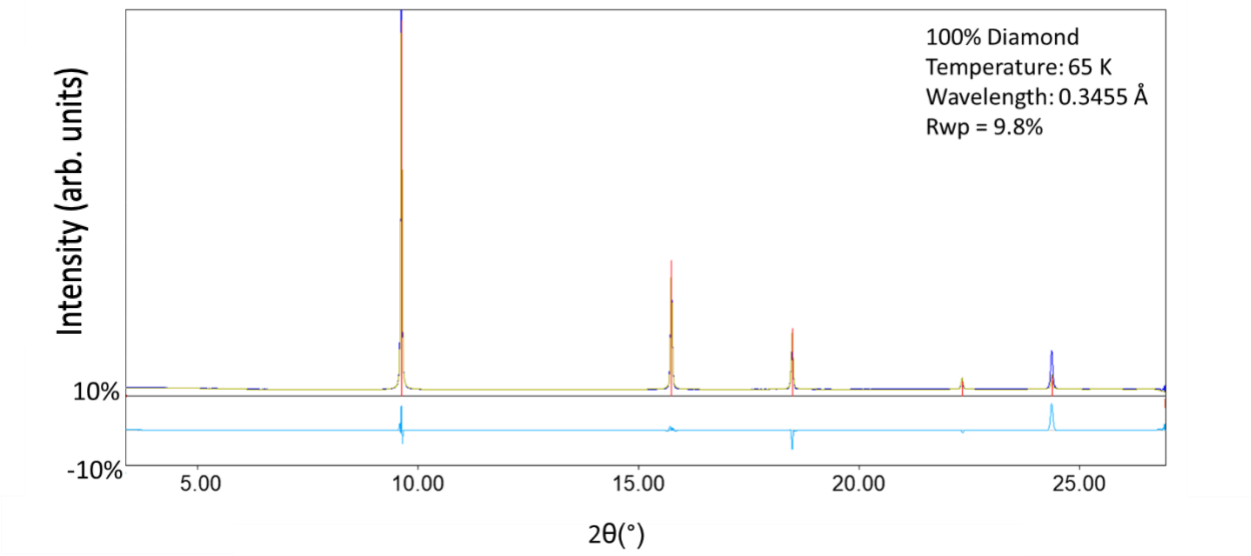

Figure 4.3. A diamond diffraction pattern measured at the Brockhouse beamline at 65 K. The blue sticks indicate the peak positions for diamond at 2θ = 9.6°, 15.7°, 18.5°, 22.3°, and 24.4° The blue diffraction pattern represents the experimental data, and the yellow diffraction pattern represents the calculated pattern. The light blue line signifies the difference between the calculated and the experimental pattern is less than 10%. R_{wp} = 9.8%, which is an acceptable value.

Figure 4.3 shows the diffraction pattern for 100% diamond measured at the Brockhouse beamline. The energy used at this beamline was 35 keV (and a wavelength (λ) of 0.3455 Å). The diamond diffraction peaks at 2θ = 9.6°, 15.7°, 18.5°, 22.3°, and 24.4° were observed. More peaks were observed at this beamline as the incident x-ray has a shorter wavelength. Once again, there is acceptable agreement between the experimental diffraction pattern (blue) and the fitted diffraction

pattern (yellow). The overall weighted Bragg-R factor is 9.8%, which means that there is acceptable error between the calculated and the experimental diffraction patterns on the Brockhouse beamline. The features observed for the first diffraction peak is typical of a slight difference in the FWHM. The reason for a large, weighted Bragg R-factor for the data measured at Brockhouse is mainly due to the difference between the measured and calculated intensities of the third and fifth diffraction peaks, as observed in Figure 4.3. The difference may be attributed to a small crystallinity of the diamond substrate. However, the pseudo-voigt function gave a better description of the line profile on HXMA. Additionally, since only three peaks were measured at HXMA, this resulted in a fortuitous Bragg R-factor.

Overall, at the Brockhouse beamline, more diffraction peaks were observed with a less scattering and a higher energy (35 keV). On the HXMA beamline, there were less diffraction peaks but had a much lower Bragg R-factor, indicating better quality data.

4.3 Data sets for Pure Nitrogen

4.3.1 HXMA

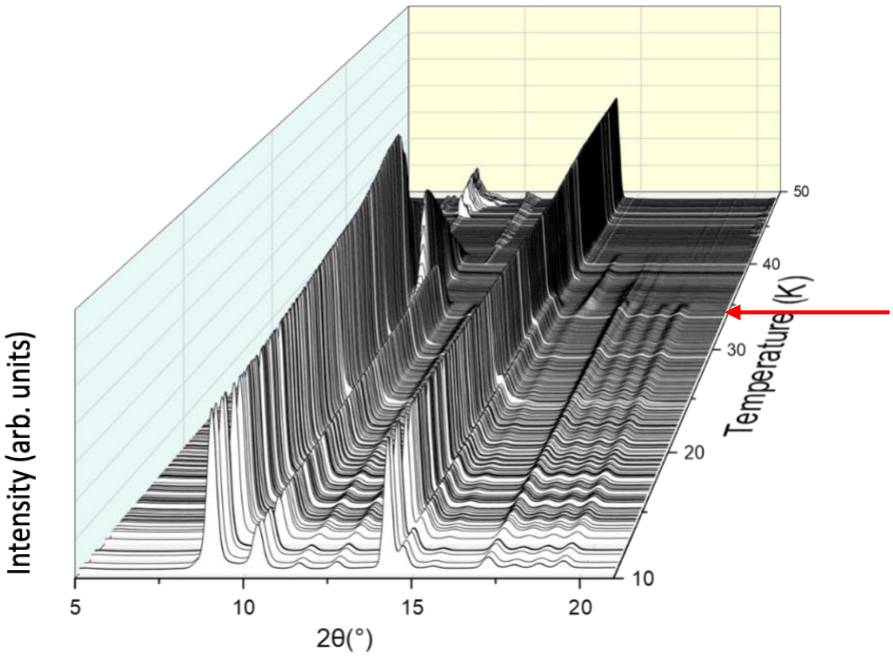

Figure 4.4. The diffraction patterns examine the phase changes of pure N_2 and diamond as it is warmed from 10K to 50K. The red arrow indicates a change in diffraction pattern for the N_2 crystal structure at 34 K. The diamond peak is observed at $2\theta = 14.1°$.

Figure 4.4 contains N_2 and diamond diffraction peaks. This sample is warmed from 10 K to 50 K. The diamond peak is observed at $2\theta = 14.1°$ and it remains almost constant throughout the warmup process. There appears to be changes in the diffraction pattern features after 34 K as indicated by the red arrow. After approximately 40 K, crystalline N_2 is no longer present. The peaks for diamond and nitrogen have been summarized in Table 4.1 below.

Table 4.1. Summary of diamond and nitrogen peaks for the HXMA beamline.

Diamond Peaks	Nitrogen (N_2) Peaks Melting point: 63.15 K
14.1°	8.9°
23.3°	10.2°
27.4°	11.3°
	12.6°
	14.6°
	17.4°
	18.2°
	18.8°
	19.5°
	21.8°

Figure 4.5 below examines more closely at the changes in the diffraction pattern at 34 K. There is a clear decrease in the intensity of the peaks as well as the appearance of new peaks at 9.7°, 12.0°, and 15.8°.

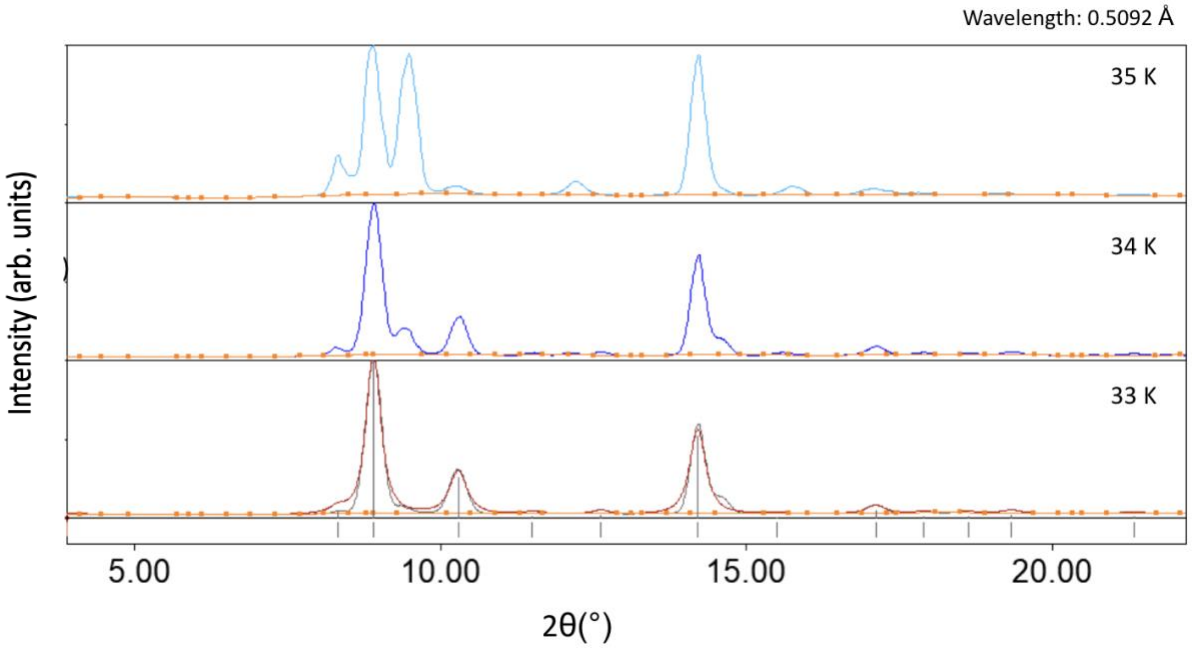

Figure 4.5. Diffraction patterns shown at the phase changes of pure N_2 as below, at, and above 34 K at the HXMA beamline. The diamond peak remains constant 14.1°. As temperature increases, the N_2 peaks previously observed at 8.9°, 10.2°, 11.3°, 12.6°, 14. 6°, 17.4°, 18.2°, 18.8°, and 19. 5° are not appreciated at 34.5 K. Instead, new peaks at 9.7°, 12.0°, and 15.8° are observed. The grey sticks along the x-axis represent the experimental peaks identified by the Match! Software.

The second point to highlight is the relative intensities between the strongest diamond and nitrogen peaks. In Figure 4.6 below, the relative intensities of the nitrogen peak at 8.9° and diamond peak at 14.1° are 1000 arb. units and 800 arb. units respectively. This means that the nitrogen diffraction pattern has a relative intensity of approximately 125% to the diamond pattern. Knowing what the relative intensities of each of the compounds in the sample will be important for interpreting the results of the Rietveld refinement later.

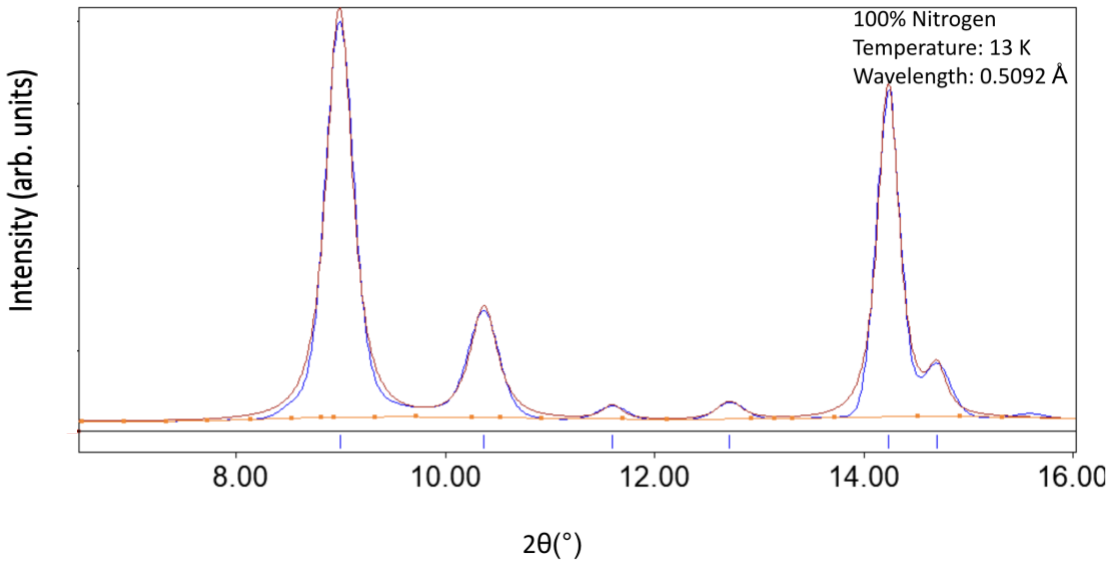

Figure 4.6. This diffraction pattern illustrates the relative intensity between the strongest diamond (14.1°) and nitrogen (8.9°) peaks on the HXMA beamline. It highlights that the strongest N_2 peak has a greater relative intensity than the diamond peak ~ 125%.

4.3.2 Brockhouse

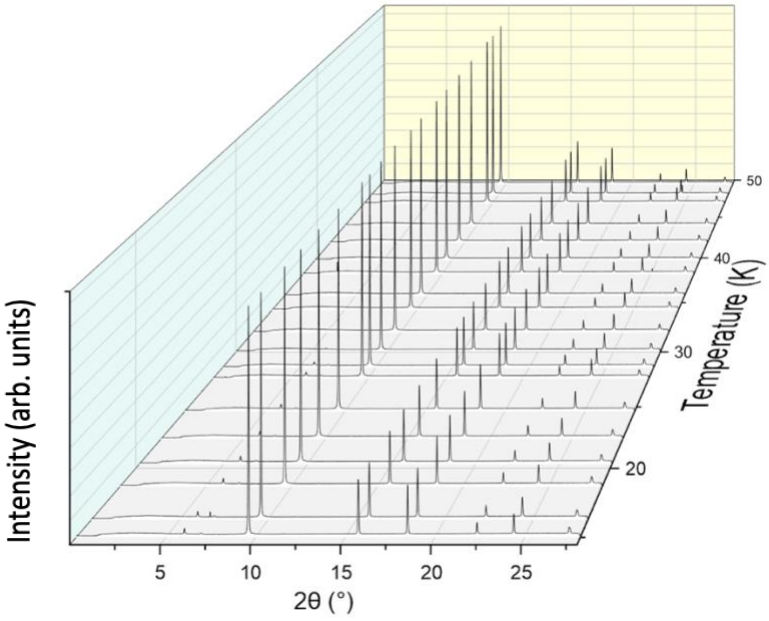

Figure 4.7. The diffraction patterns illustrate the phase changes of pure N_2 as it is warmed from 10K to 50K on the Brockhouse beamline.

Figure 4.7 shows a waterfall plot of the diffraction patterns of pure nitrogen on the Brockhouse beamline relative to temperature. At this beamline, it is obvious that the diamond peaks have a

much stronger intensity than the nitrogen peaks. In Figure 4.8 below, the relative intensities of the nitrogen peak at 6.0° and diamond peak at 9.6° are 40 arb. units and 1000 arb. units respectively. This means that the nitrogen diffraction pattern has a relative intensity of approximately 4% to the diamond pattern. This is significantly lower than how much nitrogen was deposited in the system at HXMA. It will have implications in which phase changes are observed, how quickly the sample is pumped out of the system, and how good the Rietveld refinement results are.

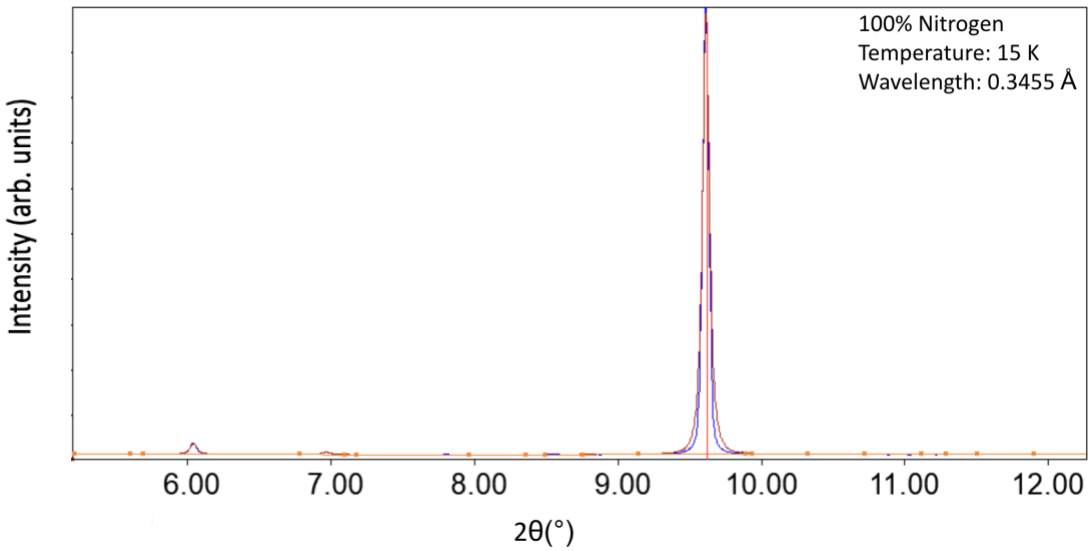

Figure 4.8. This diffraction pattern illustrates the relative intensity between the strongest diamond (9.6°) and nitrogen (6.0°) peaks on the Brockhouse beamline ~ 4%.

In Figure 4.8, the diamond peaks can be observed at $2\theta = 9.6°$, 15.7°, 18.5°, 22.5° and 24.8°. These 5 peaks remain almost constant throughout the warmup procedure due to the low thermal expansivity of diamond. To better visualize the low intensity N_2 peaks, we limit the diffraction pattern between 5° and 15° to eliminate the high amount of scatter at lower angles and to focus in the N_2 peaks as observed in Figure 4.9.

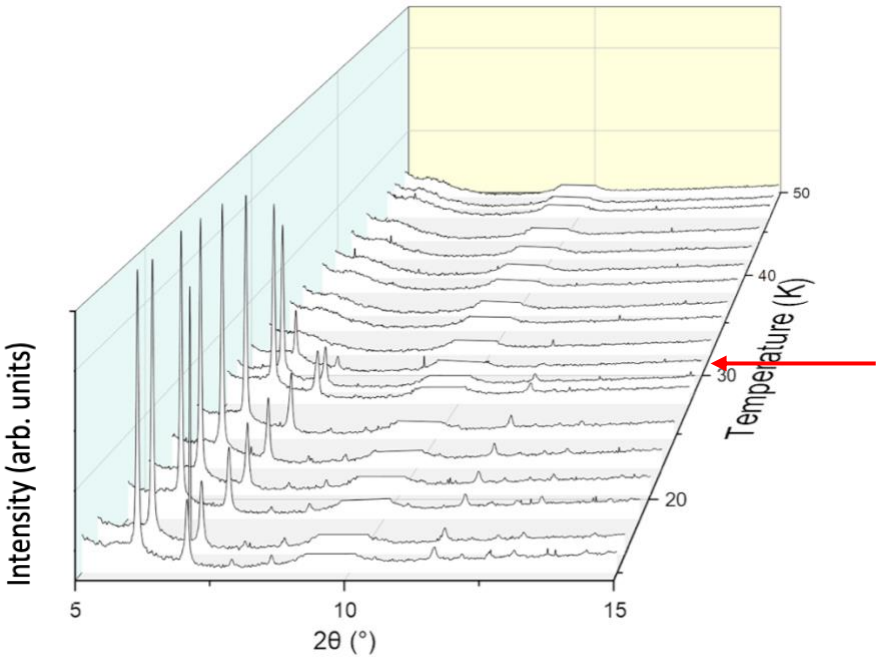

Figure 4.9. Waterfall plot of diffraction patterns illustrates the phase changes of pure N_2 as it is warmed from 10K to 50K at a limited angular range with the diamond peaks removed at 9.6° to reveal the weaker peaks at the Brockhouse beamline. The red arrow indicates the temperature at which the peaks disappear suggesting the N_2 gas is no longer crystalline.

No changes in diffraction pattern are observed here as it appears that the sample was pumped out of the vacuum system by 32 K. Figure 4.9 shows the same diffraction pattern as Figure 4.7 with the diamond peaks removed from the pattern. This allows a better visualization of the N_2 peaks. Figure 4.10 illustrates when nitrogen evaporates from the system at 32 K.

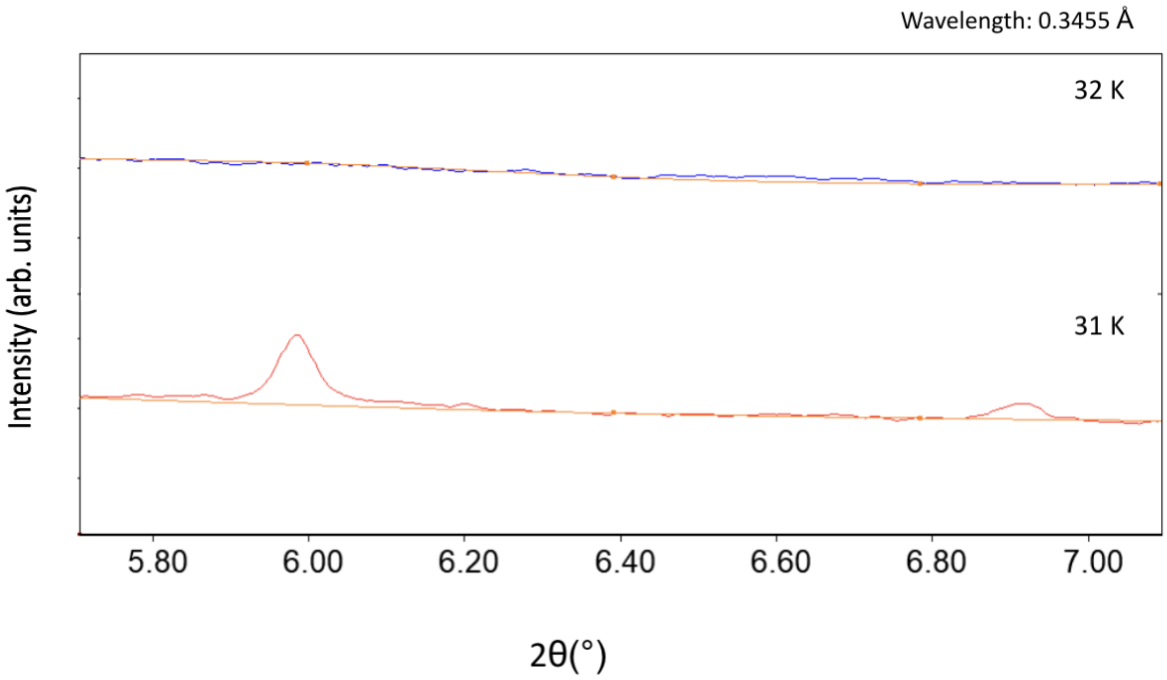

Figure 4.10. Diffraction patterns show that there are no phase changes of pure N_2 apparent at 31 K and 32 K at the Brockhouse beamline.

These results are contrary to what was observed on the HXMA beamline. On HXMA, a change in diffraction pattern was observed at 34K. Unfortunately, at Brockhouse, the sample had been pumped out entirely from the system at 32 K, which may suggest that a very small amount of N_2 was deposited via the computer-controlled valve. As a result of this, it was only able to form a thin layer on the diamond substrate. Summary of the nitrogen and diamond peaks is provided in Table 4.2.

Table 4.2. Summary of diffraction peaks for the Brockhouse beamline for diamond and nitrogen

Diamond Peaks	Nitrogen (N_2) Peaks Melting point: 63.15 K
9.6°	6.0°
15.7°	6.9°
18.5°	7.9°
22.5°	8.4°
24.8°	11.3°

4.4 Data sets for Pure Methane

4.4.1 HXMA

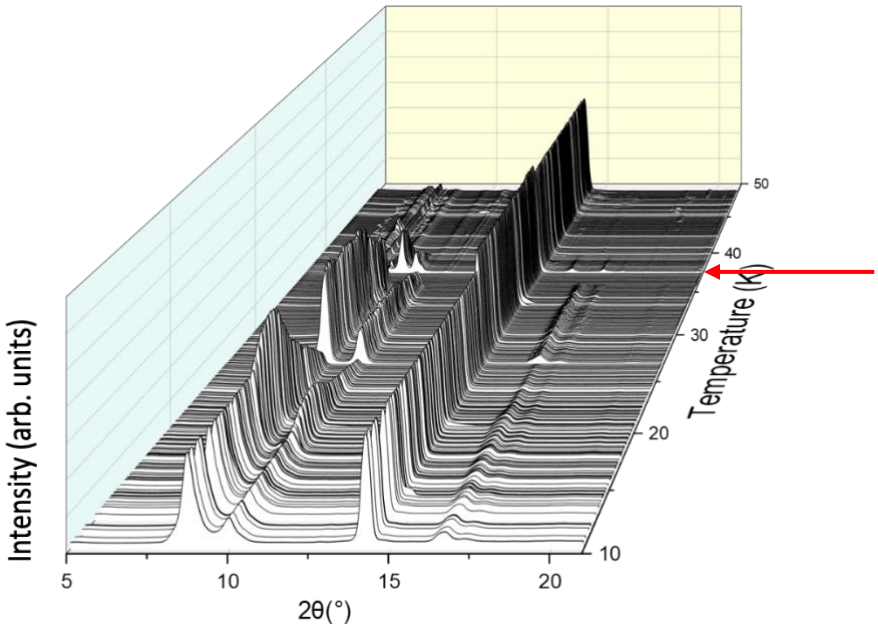

Figure 4.11. Waterfall plot of diffraction patterns illustrates at the phase changes of pure CH_4 as it is warmed from 10K to 65K at the HXMA beamline. The red arrow at 37 K shows a change in diffraction pattern.

Figure 4.11 shows the diffraction pattern of methane and diamond diffraction peaks. A summary of the peaks in these diffraction patterns is presented in Table 4.3. This sample is warmed from 10 K to 50 K. The diamond peak is observed at $2\theta = 14.1°$ and it remains constant throughout the warmup process. The relative intensities were computed first to compare the relative intensities of the strongest methane and diamond peaks.

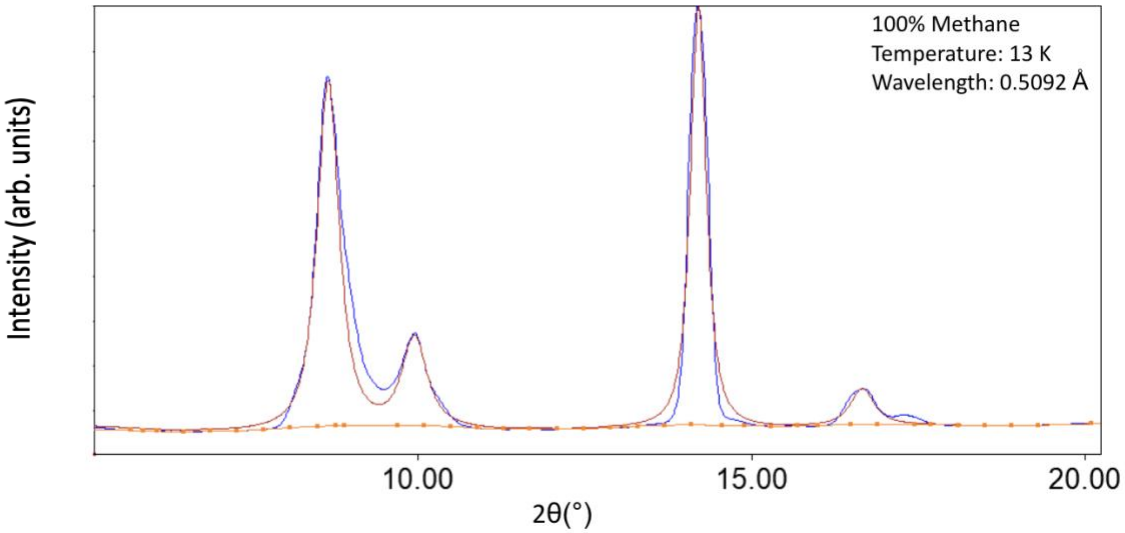

Figure 4.12. The diffraction pattern illustrates the relative intensity between the strongest diamond and methane peaks on the HXMA beamline ~ 85%.

The relative intensities of the methane peak at 8.6° and diamond peak at 14.1° are 850 arb. units and 1000 arb. units respectively, shown in Figure 4.12. This means that the methane diffraction pattern has a relative intensity of approximately 85% to the diamond pattern. Furthermore, it appears that there is some variation in the intensity of the methane peaks at 27 K but there are no changes in peak position that would otherwise suggest a possible phase change. However, there does appear to be a change in diffraction pattern at 37 K. The cause of this variation is not known but some aspect of it may be attributed to beam instability, although it is highly unusual. This is explored further in Figure 4.13 below.

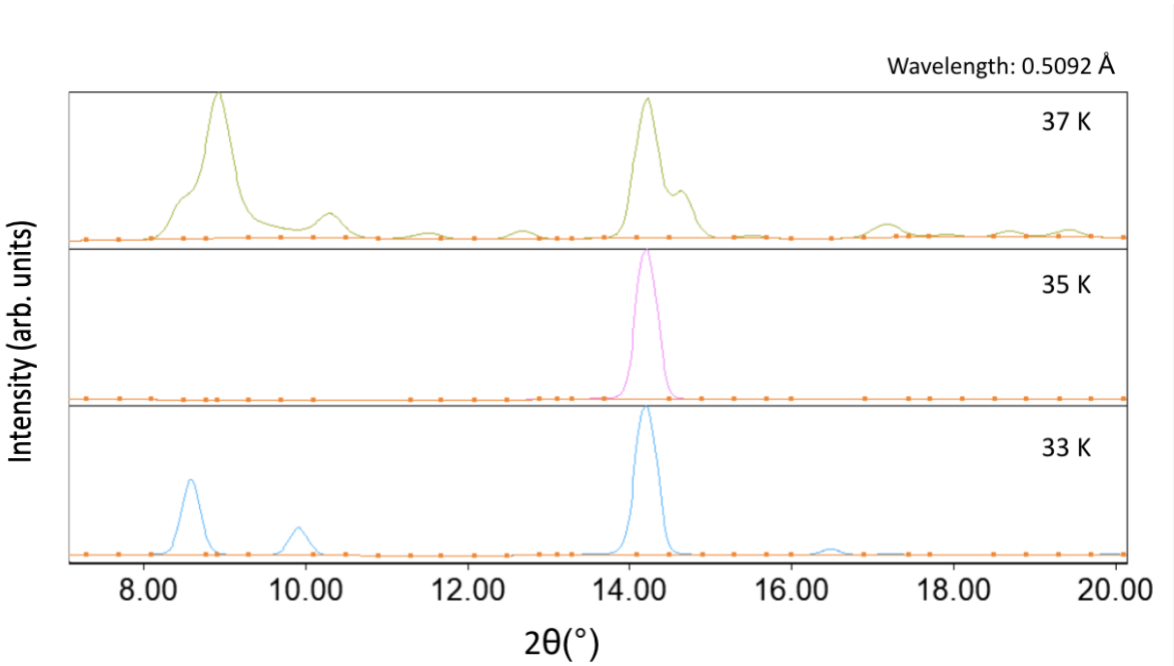

Figure 4.13. The diffraction patterns examine the phase changes of pure CH_4 from 33 K to 37 K at the HXMA beamline to study the change in diffraction pattern at 37 K.

In Figure 4.13, the diffraction pattern seems to disappear at 35 K and reappear at 37 K. It is assumed that this is a result of a crystal-to-crystal phase transition via an amorphous state. It is possible that the peaks broadened at 35 K and blended into the background at this temperature. At a temperature of greater than 37 K, there appears to be a new crystal structure of methane peaks at $2\theta = 8.9°$, 10.3°, 11.5°, 12.7°, 14.6°, 17.1°, 18.7°, and 19.2°.

Once again, the diamond peaks are almost constant throughout the warmup procedure due to the very low coefficient of thermal expansion of diamond.

The CH_4 peaks as well as the previous diamond and nitrogen peaks for the HXMA beam line outlined in Table 4.1 are summarized in Table 4.3.

Table 4. 3. Summary of diffraction peaks for the HXMA beamline.

Diamond Peaks	Methane (CH_4) Peaks Melting point: 91.15 K	Nitrogen (N_2) Peaks Melting point: 63.15 K
14.1°	8.6°	8.9°
23.3°	9.9°	10.2°
27.4°	14.1°	11.3°
	16.7°	12.6°
		14.6°
		17.4°
		18.2°
		18.8°
		19.5°
		21.8°

4.4.2. Brockhouse

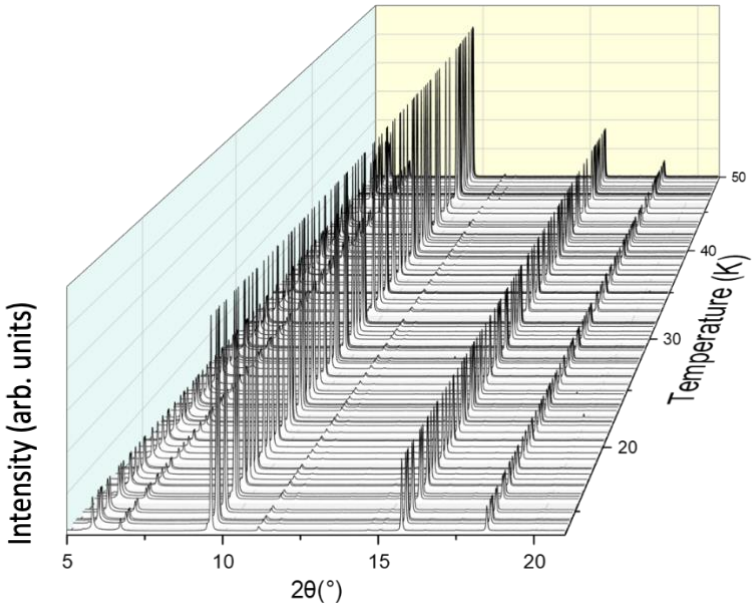

Figure 4.14. The diffraction patterns examine the phase changes of pure CH_4 as it is warmed from 10K to 50K on the Brockhouse beamline.

The trend of CH_4 diffractions as the sample is warmed from 10 K to 50 K at the Brockhouse beamline is illustrated in Figure 4.14. The diamond peaks can be observed at $2\theta = 9.6°$, 15.7°, and 18.5°. It is evident that the diamond peaks have a strong intensity and, as a result, almost drown out the CH_4 peaks with lower intensity shown in Figure 4.15 below. This is similar to what was observed at the Brockhouse beamline with N_2 where the relative intensity of nitrogen to diamond was 4%. Nevertheless, the resolution of the detector reveals useable diffraction patterns of CH_4. For Figure 4.14, the relative intensities of the methane peak at 5.8° and diamond peak at 9.6° are

200 arb. units and 1000 arb. units respectively, shown in Figure 4.15 below. This means that the methane diffraction pattern has a relative intensity of approximately 20% to the diamond pattern.

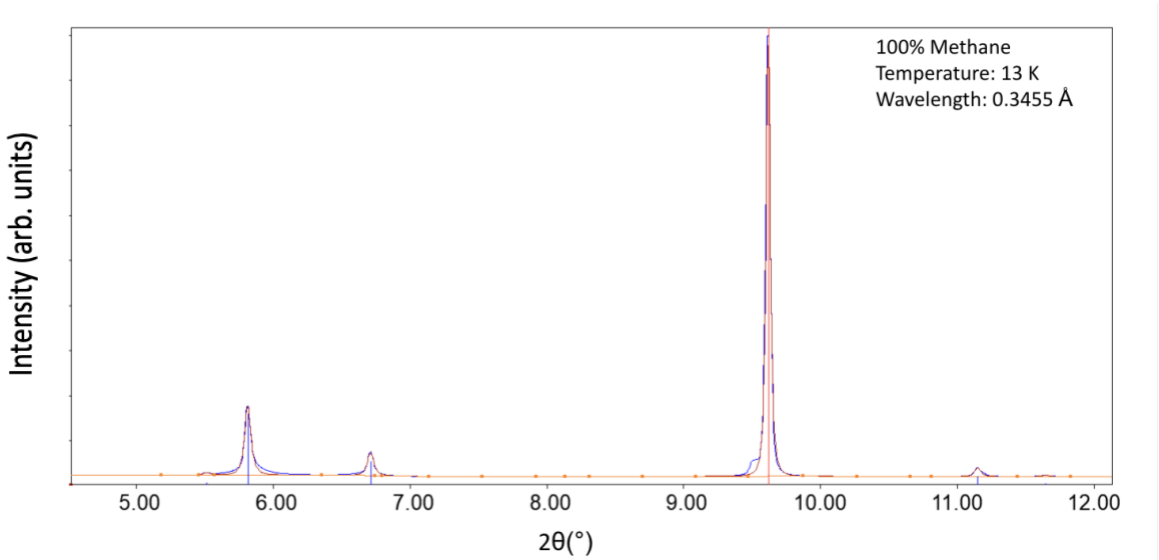

Figure 4.15. This diffraction pattern illustrates the relative intensity between the strongest diamond (9.6°) and methane (5.8°) peaks on the Brockhouse beamline ~ 20%. The blue sticks represent the methane in the pattern and the red stick represents diamond.

To better evaluate the trend of diffraction pattern over temperature, the 2θ angle was limited to between 5° and 15° to assess the trend of CH_4, as illustrated in Figure 4.16.

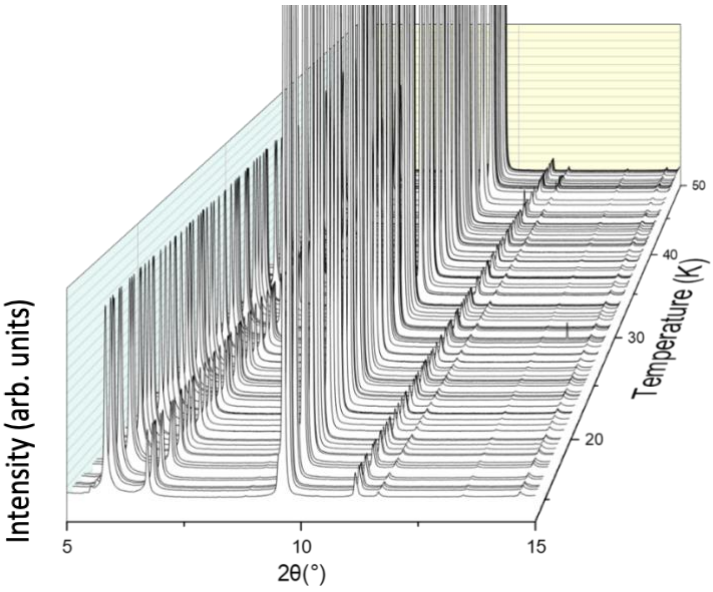

Figure 4.16. The diffraction patterns examine the phase changes of pure CH_4 as it is warmed from 10K to 50K on the Brockhouse beamline with the 2θ limited to 5° and 15°.

The diamond peak at 9.6 ° was removed from this data set as it was difficult to assess if there were changes in the diffraction patterns at the lower angles due to this strong peak as shown in Figure 4.17.

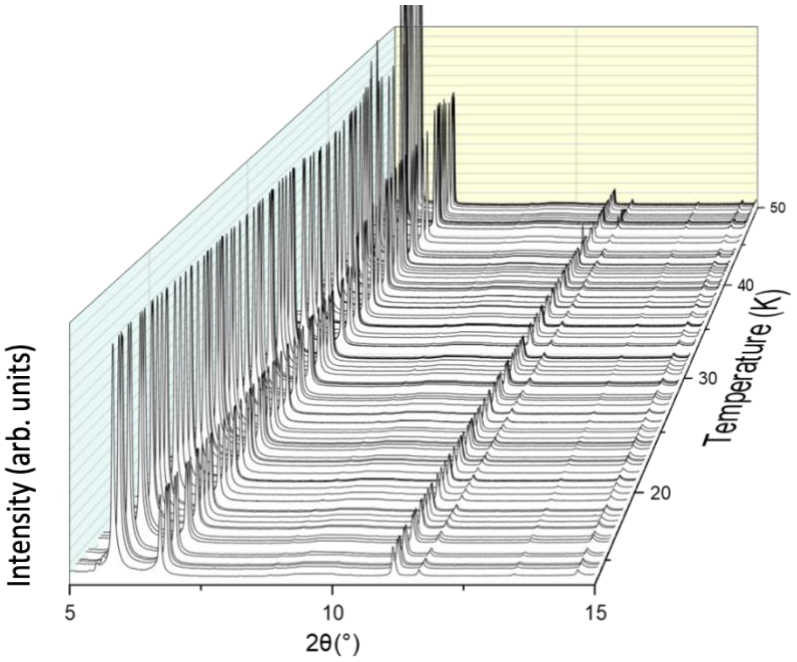

Figure 4.17. Waterfall plot of diffraction patterns illustrates the phase changes of pure CH_4 as it is warmed from 10K to 50K at a limited angular range with the diamond peaks removed at 9.6° to reveal the weaker peaks at the Brockhouse beamline.

There appears to be no phase change in the CH_4 crystal structure as there are no changes in the position of the diffraction peaks shown in Figure 4.17. To ensure a change in diffraction pattern was not hidden in the waterfall, a closer study was performed, shown in Figure 4.18.

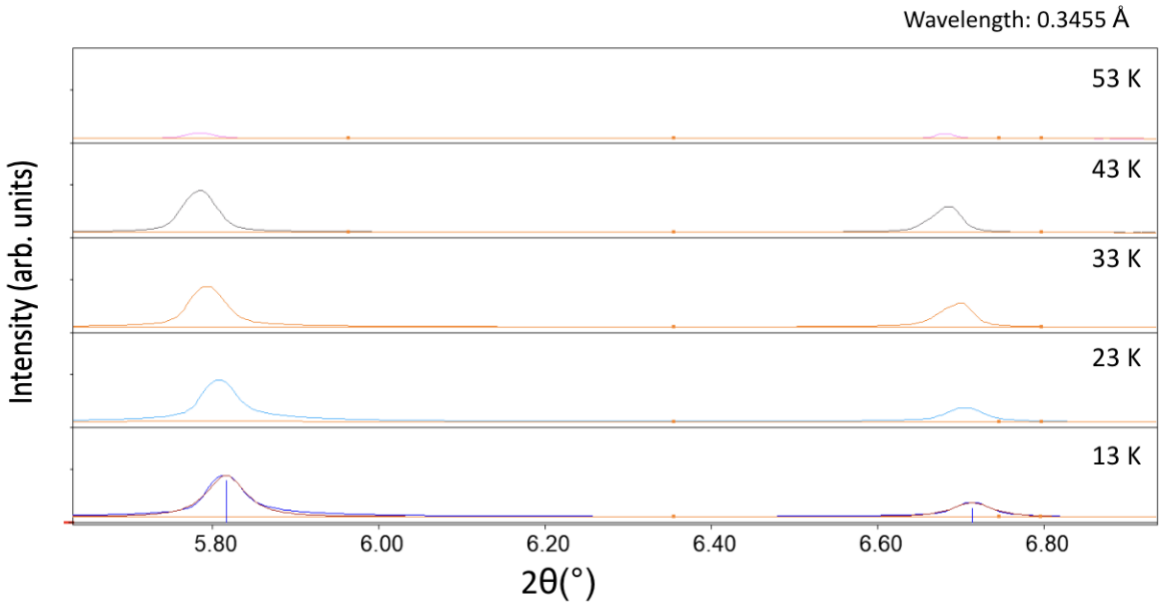

Figure 4.18. The diffraction patterns examines if there is a phase change of pure CH_4 from 13 K to 53 K at the Brockhouse beamline. There is a leftward shift in the peak positions with an increase in temperature which can be attributed to the gases transitioning to an amorphous state before they are no longer seen in the system.

Previous diffraction studies of 100% CH_4 show either no changes[33] in crystal methane structure below 90 K or that there is a transformation point[34] at 20.4 K. The results from Brockhouse reflect previous studies that there are no changes in diffraction pattern analysis at low temperatures. However, the HXMA beamline shows some interesting features of a phase change at 37 K (Figure 4.13) that has not previously been noted in literature. Summary of all the peaks at the Brockhouse beamline have been summarized in Table 4.4 below.

Table 4.4. Summary of diffraction peaks for the Brockhouse beamline

Diamond Peaks	Methane (CH_4) Peaks Melting point: 91.15 K	Nitrogen (N_2) Peaks Melting point: 63.15 K
9.6°	5.8°	6.0°
15.7°	6.8°	6.9°
18.5°	11.2°	7.9°
22.5°	11.8°	8.4°
24.8°	13.1°	11.3°
	14.8°	

4.5 25% Methane and 75% Nitrogen Mixtures

4.5.1 HXMA: 25% Methane and 75% Nitrogen

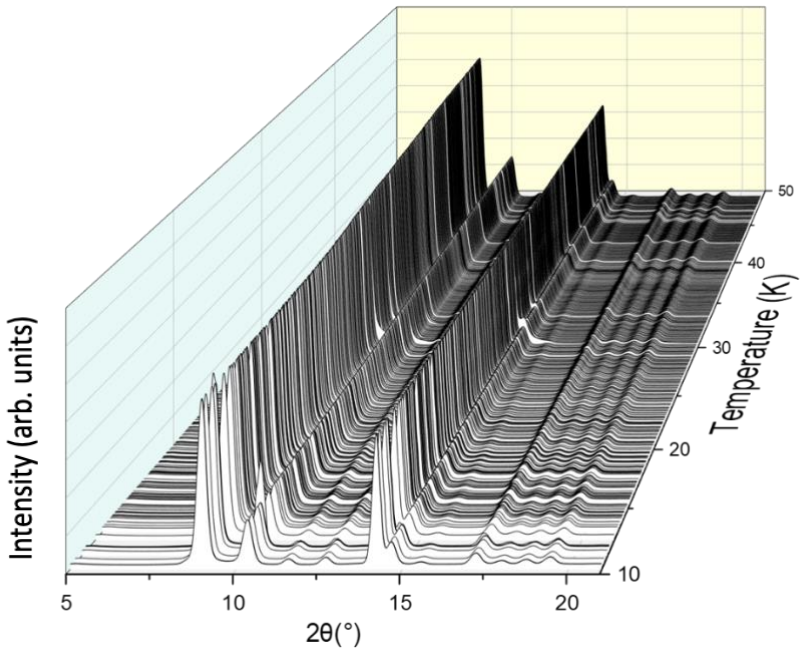

Figure 4.19. Waterfall plot of diffraction patterns illustrates the phase changes of 25% CH_4 and 75% N_2 as it is warmed from 10 K to 52 K at the HXMA beamline.

At the HXMA beamline, the manual leak valves for N_2 and CH_4 were adjusted according to the settings in Table 3.2. The gases were leaked into the system simultaneously. The assumption was made that the gases were diffusing at comparable rates and that they were homogenously deposited on the diamond substrate. Figure 4.19 shows the diffraction patterns of a nominal 75% N_2 and 25% CH_4 mixture at the HXMA beamline as the system was warmed from 10 K to 52 K. Peaks that were previously observed and summarized in Table 4.3 for N_2 and CH_4 can be appreciated in these diffraction patterns. The results show no changes in the diffraction pattern as temperature increased. The integrity of the two components is maintained indicating that there is no significant interaction between N_2 and CH_4. This set of data also does not appear to be affected by the increase in temperature, meaning that there are no obvious crystal phase changes observed in the diffraction pattern. This apparently surprising finding can be explained by the fact that the pressure in the CH_4 cylinder was found to be very low after the completion of the deposition. The very low pressure may indicate that the amount of CH_4 was not as much as anticipated.

Quantification of how much methane and nitrogen was deposited would have been helpful for data analysis. It was known that the manual valves were set to deposit 25% methane and 75% nitrogen. However, when analyzing the data to get accurate values, the nitrogen peaks were significantly more predominant than methane which prevented the Match! software from identifying any methane peaks in the diffraction pattern. It essentially showed that each diffraction pattern in Figure 4.19 reflected 100% nitrogen at all temperatures.

4.5.2 Brockhouse: 25% Methane and 75% Nitrogen

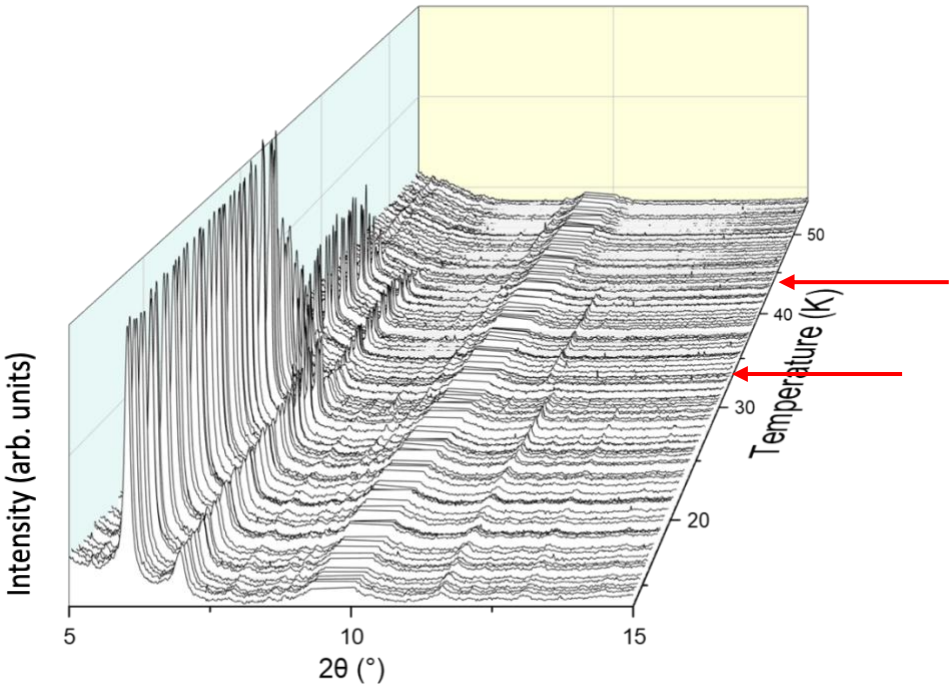

Figure 4.20. The diffraction patterns examine the phase changes of 25% CH_4 and 75% N_2 as it is warmed from 10K to 52 K with the diamond peaks removed at 9.6° to reveal the weaker peaks at the Brockhouse beamline. The red arrows indicate phase changes at 33 K and shows that the gasses have been pumped off at 44 K.

The results of co-deposition of 25% CH_4 and 75% N_2 are illustrated in Figure 4.20. At 33 K, there are changes in the diffraction pattern that a crystal structure change for N_2. The study by Connelly et al.[2] documented a phase change of N_2 at 36 K. The previous section (4.2.2) showed that the nitrogen sample at the Brockhouse beamline had been pumped off at 32 K. As a result of this, no phase changes for CH_4 were observed. There were also no changes observed for pure methane on the same beamline. As discussed previously, literature that discusses pure CH_4 shows either no changes[43] in crystal methane structure below 90 K. After 44 K, it appears as if both gases have likely been pumped out of the system as the intensities abruptly disappear.

Figure 4.21 examines this phase change more closely.

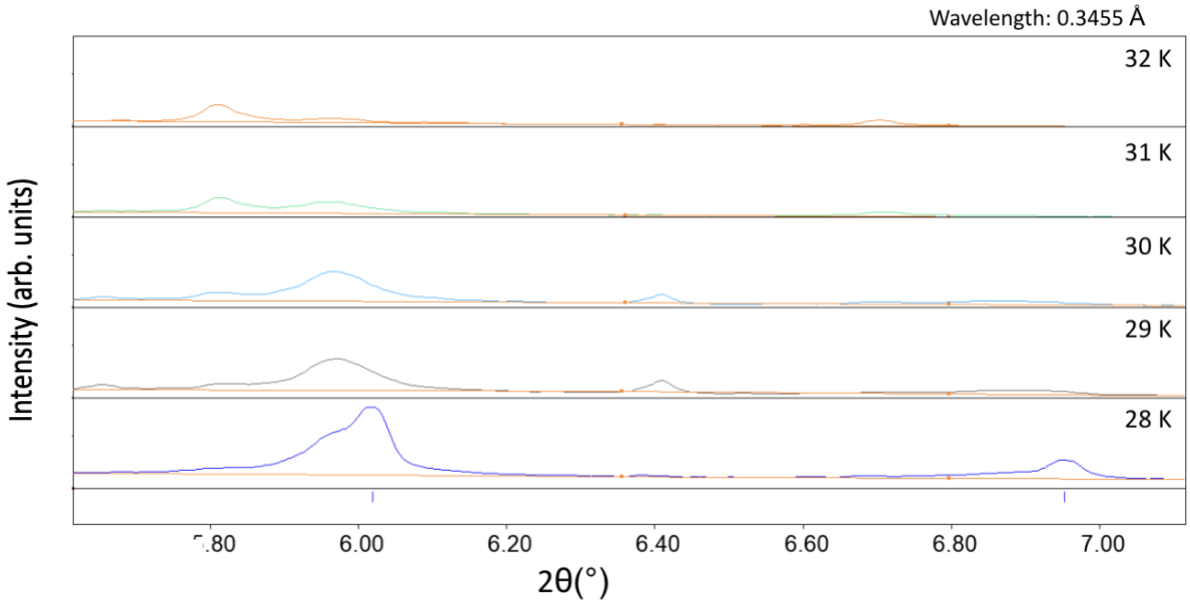

Figure 4.21. The diffraction patterns illustrate the phase changes of 25% CH_4 and 75% N_2 from 28 K to 32 K at the Brockhouse beamline.

In Figure 4.21, there are two distinct N_2 peaks at 6.0° and 6.9° at 28 K that have been previously observed (Figure 4.9) and summarized in Table 4.3. It is known that CH_4 has peaks at 5.8° and 6.8° but they are not immediately obvious in Figure 4.21. The results for 100% N_2 on the Brockhouse beamline (Figure 4.9) showed that the sample was entirely pumped out at 32 K, so no changes in diffraction pattern after that temperature were observed. As mentioned previously, it is likely that a very thin layer of CH_4 was deposited on the diamond substrate using the computer-controlled leak valves. The results for 100% CH_4 at the Brockhouse beamline (Figure 4.17) did not show any phase changes either. In this mixture, however, there are changes in the diffraction pattern at 32 K. The peak at 6.0° decreases in intensity and shifts towards lower angles as temperature increases. The peak at 6.9° essentially disappears at 30 K. At 29 K, there is the appearance of a new peak at 6.4°. At 32 K, there are three distinct peaks observed at 5.8° and 5.9°. It is possible that the 5.8° peak is due to the 25% methane in the system, however, it is strange that it is not observed at lower temperatures. This could be due to the stronger intensity of the N_2 peaks that may have masked the methane and as temperature increased, the N_2 was pumped out of the system to reveal the lower intensity methane peaks. Regardless, the peaks at 5.9° and 6.4° were not noted in previous literature results.

The differences observed in the 25% CH_4 and 75% N_2 sample at the HXMA and Brockhouse beamline could have several reasons. Firstly, since the HXMA gas deposition was controlled by a manual valve, it is possible that the gas was not controlled consistently meaning that one gas could have preferentially deposited faster than the other. Secondly, it was more difficult to identify the CH_4 peaks on the HXMA beamline either due to difference in molecular density or slower rate of diffusion. Finally, while gas deposition was better controlled at the Brockhouse beamline using computerized mass flow meter, the rate of deposition was much slower and resulted in significantly smaller peak intensities compared to diamond. This would have interfered with how many of the peaks were realistically identified for each gas.

Furthermore, while an attempt was made to deposit 25% methane and 75% nitrogen, the Match! software allowed quantification how much of each gas was present at 15 K at the Brockhouse beamline. A ratio of 1:3 of CH_4: N_2 was expected but found that it was 10:1. This could be due to preferential deposition of methane, absorption properties of the gasses, or the rate of deposition. If the nitrogen concentration deposited is significantly lower, it stands to reason that as temperature increases, the gas will be pumped out of the system. This could be why methane peaks are observed on the diffraction patterns after 32 K.

4.6 50% Methane 50% Nitrogen Mixtures

4.6.1 HXMA: 50% Methane 50% Nitrogen

An initial attempt was made to deposit a 50% methane and 50% nitrogen mixture, however due to the limitations of the manual valve, it was estimated that the mixture had a composition of 47% N_2 and 53% CH_4 which was as close to the desired gas percentages as possible (Table 4.1).

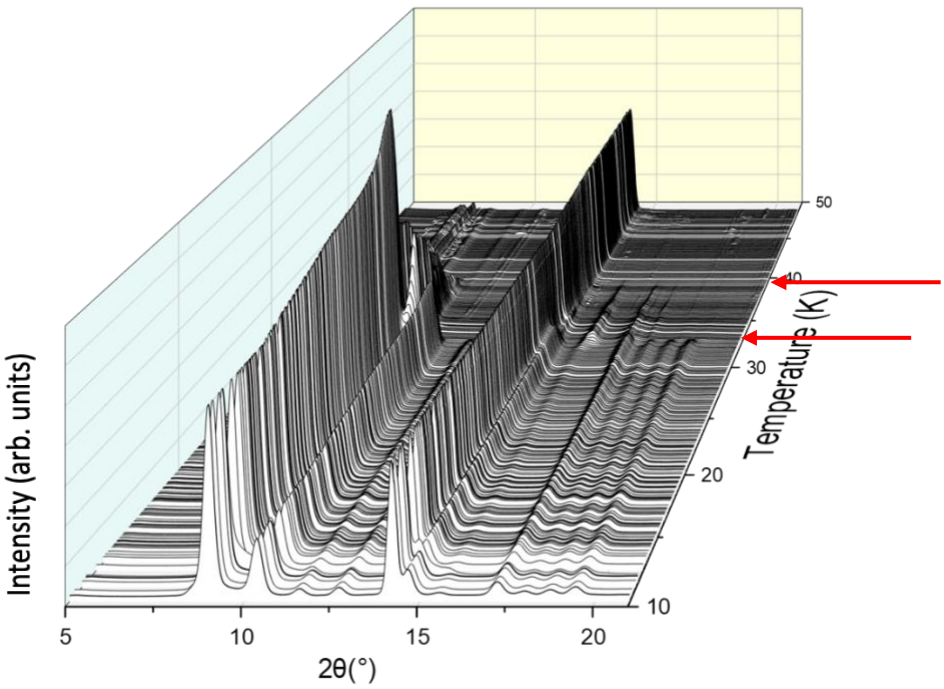

Figure 4.22. Waterfall plot of diffraction patterns illustrates the phase changes of 57% CH_4 and 43% N_2 as it is warmed from 10K to 60K on the HXMA beamline. The red arrow indicates the change in diffraction pattern at 34 K and that the gases have been pumped off at 38 K.

The results of co-deposition of 57% CH_4 and 43% N_2 are illustrated in Figure 4.22. The waterfall plots show the diffraction patterns as the sample is warmed from 10 K to 60 K. It also shows a change in diffraction pattern at approximately 34 K. Figure 4.23 will examine this phase change more closely.

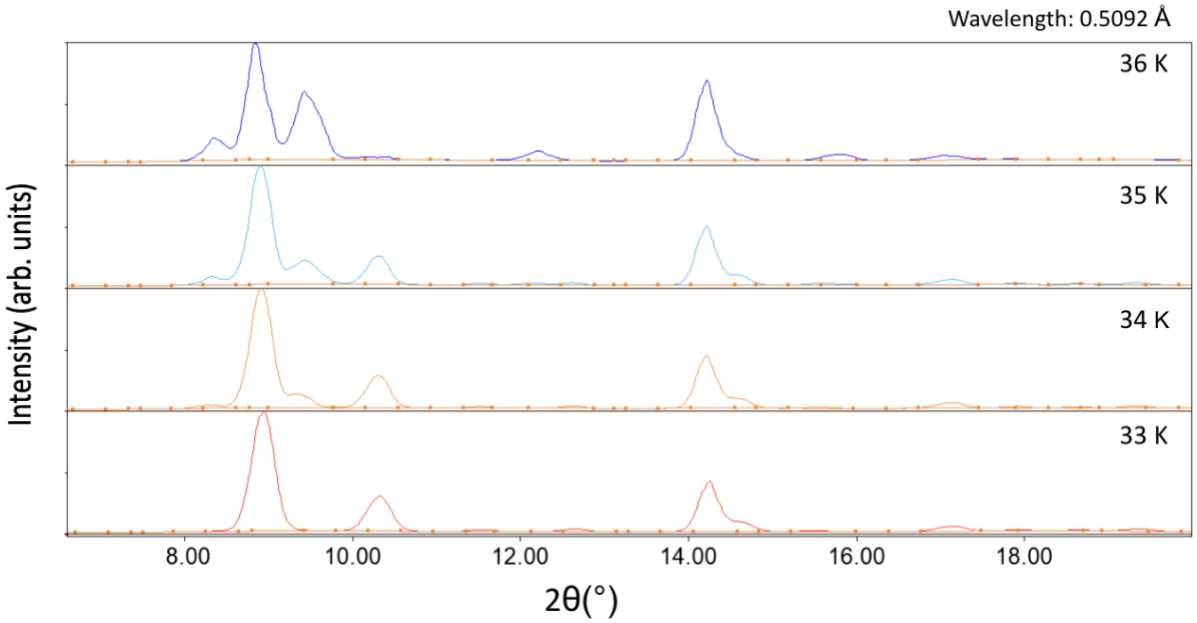

Figure 4.23. The diffraction patterns illustrate the changes in patterns of 57% CH_4 and 43% N_2 from 33 K to 36 K at the HXMA beamline. 58.

The first step to study the change in diffraction pattern is to identify which peaks are present in the system. In Figure 4.23, peaks at 8.8°, 10.2°, 11.4°, 12.5°, 14.1°, and 17.1° are identified at 33 K. There are also peaks with weaker intensities identified at 17.9°, 18.7°, and 19.4°. The peak at 14.1° corresponds to diamond. From the identified peaks, we know that diamond peaks remain fairly constant throughout the warming procedure which is an indication of the very small thermal expansion. From previous results, it is known (from Table 4.3) that methane has a diffraction peak at 8.6° and nitrogen has a diffraction peak at 8.9°. It is possible that the peak observed at 8.8° contains components of nitrogen and methane. The peaks at 10.2°, 11.4°, and 12.6° correlate with previously observed diffraction peaks of nitrogen. As the system warms up to > 34 K, the peaks at 8.8°, 10.2° and 11.4° decrease in intensity and the emergence of new peaks at 8.4°, 8.9°, 9.5°, 12.2°, and 15.8° is observed. The newer peaks do not correlate to either methane or nitrogen independently, so likely represent a new structure due to the mixture of the two gases.

The Match! software allowed quantification of how much of each gas was present. At 15 K, the expected ratio was 1:1 of CH_4: N_2 but found that it was 1:147. However, at 35 K, the ratio of CH_4:N_2 was 1:4. This could be a result of preferential deposition of the gases, the differences in the diffusion rates, or how quickly the gases were pumped out of the system.

4.6.2 Brockhouse

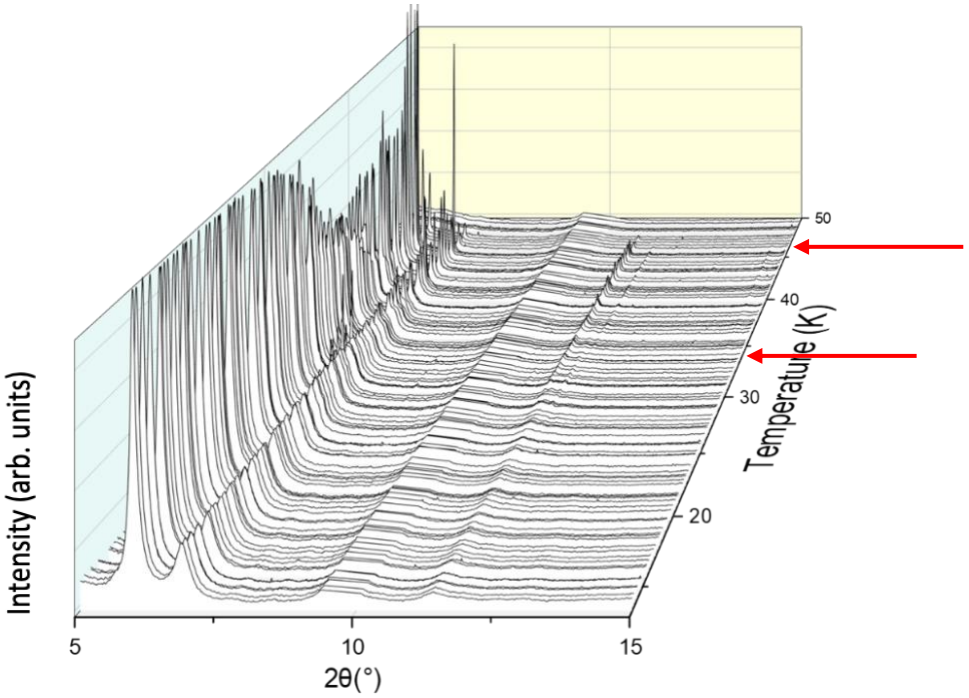

Figure 4.24. The diffraction patterns illustrate the phase change of 50% CH_4 and 50% N_2 as the system is warmed from 10K to 50 K with the diamond peaks removed at 9.6° to reveal the weaker peaks at the Brockhouse beamline. The red arrow indicates the change in N_2 structure at 34 K and shows that the gas is pumped off at 46 K.

Figure 4.24 shows a waterfall graph of 50% methane and 50% nitrogen diffraction patterns. As with previous data on Brockhouse, the diamond peaks have been truncated from the diffraction patterns to better study the lower intensity methane and nitrogen peaks. A change in the diffraction pattern is noted at 34 K (indicated by the red arrow on the figure). Figure 4.25 explores this change further.

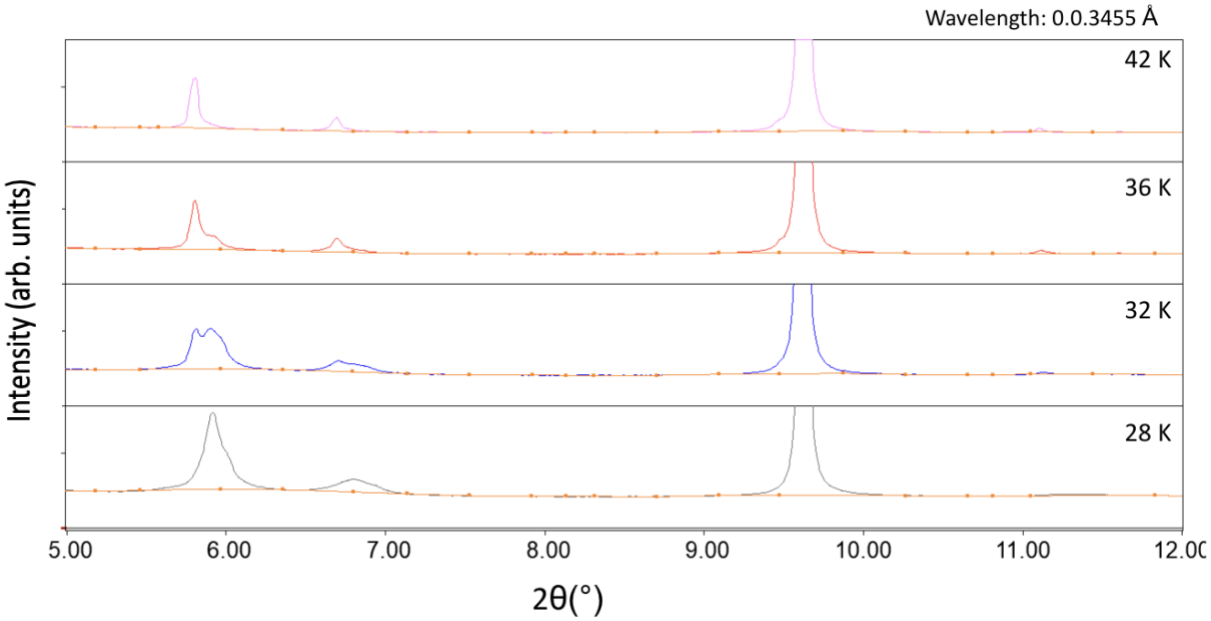

Figure 4.25. The diffraction patterns illustrate the changes in diffraction pattern of 50% CH_4 and 50% N_2 from 28 K to 42 K on the Brockhouse beamline.

In Figure 4.25, peaks at 5.9°, 6.8°, and 9.6° are observed at 28 K. There is also a peak at 11.2° but the intensity of this peak is extremely weak but discernable from the background. Again, the peak at 9.6° corresponds to diamond remains and it fairly constant throughout the warm out procedure. From previous results (Table 4.4), it is known that methane has a diffraction peak at 5.8° and nitrogen has a diffraction peak at 6.0°. It is likely that the peak observed at 5.9° contains both components. It is also known that methane has a diffraction peak at 6.8° and nitrogen has a diffraction peak at 6.9°. The peak observed at 6.8° likely has contribution from both gases. Finally, the peak at 11.2° (if distinctly identified) would correspond to a known methane peak at 11.2° but may have contribution from the nitrogen peak at 11.3°. However, as the system is warmed to > 34 K, peak positions change. Peaks are now observed at 5.8°, 6.8°, and 11.1°. It is difficult to determine whether these peaks are purely from methane or nitrogen as the positions for both these compounds at lower angles are similar. For nitrogen specifically, the expected peaks 7.9° or 8.4° are not observed.

Additionally, an attempt was made to deposit 50% methane and 50% nitrogen, the Match! software allows quantification how much of each gas was present. At 15 K, from Equation 3.23, a ratio of 1:1 of CH_4:N_2 was expected and found to be 4:3.

4.7 75% Methane and 25% Nitrogen Mixtures

4.7.1 HXMA: 75% Methane and 25% Nitrogen

As with the previous HXMA data set, an initial attempt was made to create a 75% methane and 25% nitrogen mixture, however due to the limitations of the manual valve that was used, a composition of 80% nitrogen and 20% methane was more achievable.

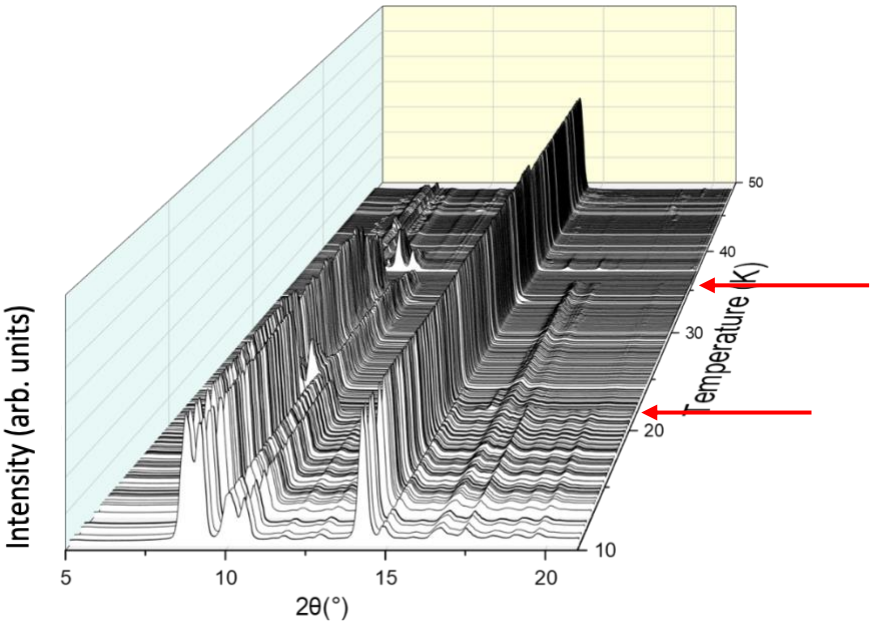

Figure 4.26. The diffraction patterns illustrate the phase changes of 80% CH_4 and 20% N_2 as it is warmed from 10K to 70K on the HXMA beamline The two red arrows highlight changes in the crystal structure at 22 K and 36 K. 61

Figure 4.26 shows the waterfall diffraction patterns for 80% methane and 20% nitrogen as it is warmed from 10 K to 70 K. There are a few interesting features in this pattern. Firstly, at approximately 22 K, there are obvious diffraction pattern changes (indicated by the red arrow on the figure). Figure 4.27 below will explore this in more detail.

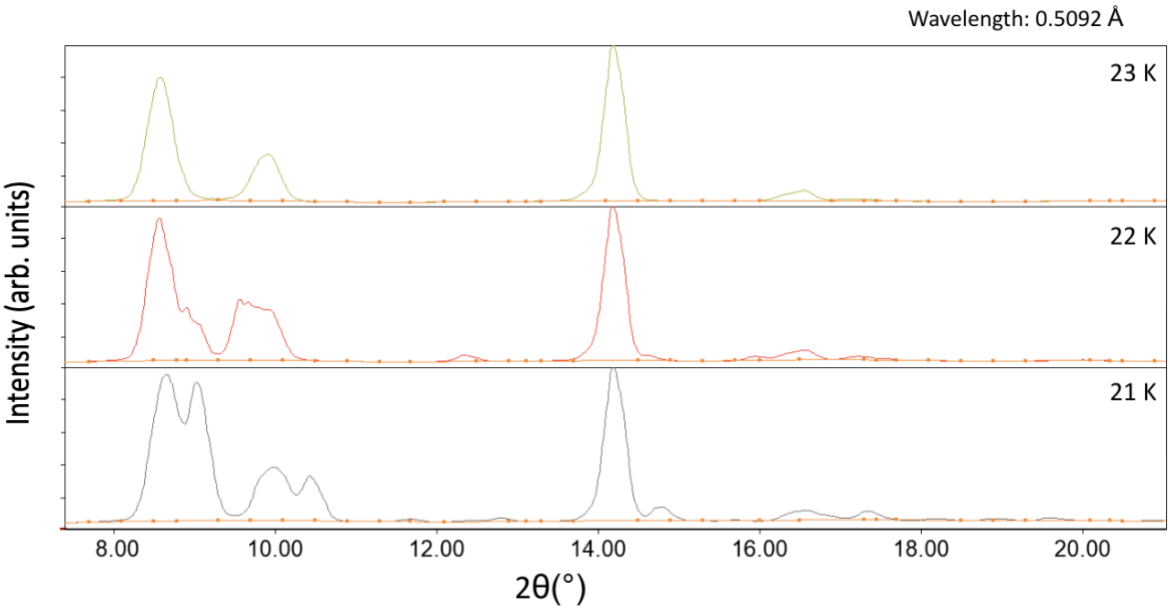

Figure 4.27. The diffraction patterns illustrate the changes in diffraction pattern of 80% CH_4 and 20% N_2 from 21 K to 23 K at the HXMA beamline.

Figure 4.27 shows diffraction peaks at 8.6°, 9.0°, 9.9°, 10.4°, 14.1°, 14.7°, 16.6°, and 17.4° at 21 K. Once again, it is known that diamond has a diffraction peak at 14.1° which remains fairly constant throughout the warm out procedure. It is also known (from Table 4.3) that methane has diffraction peaks at 8.6°, 9.9°, and 16.7°. All three of these peaks are observed in the diffraction pattern in Figure 4.27. Nitrogen diffraction peaks at observed at 8.9°, 10.2°, and 17.4°. However, at > 22 K, it appears as the nitrogen is pumped out of the system as the diffraction pattern is only left with the diffraction peaks that correspond to methane.

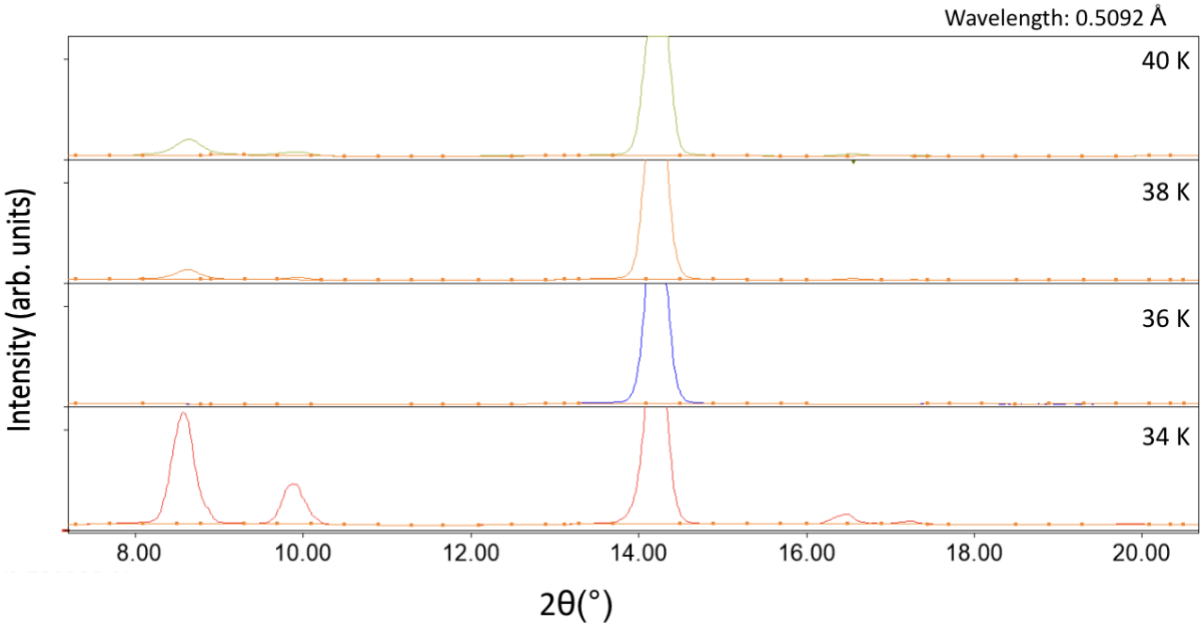

Figure 4.28. The diffraction patterns illustrate the changes in diffraction pattern of 80% CH_4 and 20% N_2 from 34 K to 40 K at the HXMA beamline.

Secondly, there are further changes in the diffraction pattern at 36 K. It appears as if all the gases are pumped out of the system beyond 35 K as the diffraction pattern only shows the diamond peaks. However, at temperature greater than 36 K in Figure 4.28, the methane peaks reappeared. This was observed previously on the HXMA beamline (Figure 4.13) at 36 K for pure methane. At temperatures of greater than 37 K, there were new methane peaks observed. This could indicate a crystal-to-crystal structure change via an amorphous state at 35-36 K.

Figure 4.28 illustrate the previously observed methane peaks at 8.6°, 9.9°, and 16.5° as well as the known diamond peak at 14.1°. As temperature increases, the intensity of the methane peaks decreases. However, at 37 K, these peaks reappear with lower intensity but all at the same positions.

Finally, the Match! software allowed one to quantify how much of each gas was present in the deposition. At 15 K, a ratio of 4:1 of CH_4: N_2 was expected but found that it was 5:2.

4.7.2 Brockhouse: 75% Methane and 25% Nitrogen

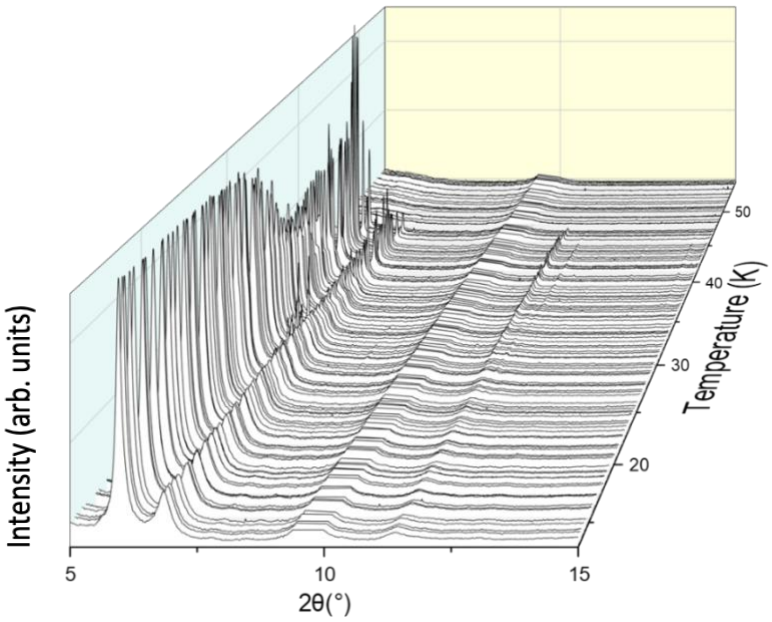

Figure 4.29. The diffraction patterns illustrate no phase changes for 75% CH_4 and 25% N_2 as the sample is warmed from 10K to 52 K with the diamond peaks removed at 9.6° to reveal the weaker peaks at the Brockhouse beamline.

Figure 4.29 shows the waterfall diffraction pattern for 75% methane and 25% nitrogen. As with previous diffraction patterns measured at Brockhouse, the diamond peaks have been subtracted from the patterns to reveal the peaks with lower intensities. There are changes in the diffraction pattern observed. While there are obvious changes in the intensity of the peaks after 36 K, there are no changes in the peak positions. The two primary peaks observed in this pattern are at 5.8° and 6.8°. Both can be assigned to the methane that has been previously identified at the Brockhouse beamline (Table 4.4). As noted previously, the intensities on the Brockhouse beamline for nitrogen and methane were quite low (4% and 20% respectively) relative to diamond. There may be some nitrogen contribution to the peaks. Due to the low intensity, it is difficult to confidently verify this. As expected with methane, there are no phase changes observed. This agrees with what has been noted in literature.

Lastly, the Match! software allowed one to quantify how much of each gas was present. At 15 K, a ratio of 3:1 of CH_4: N_2 was expected but found that it was 141:1.

CHAPTER 5: DATA ANALYSIS

5.1 Rietveld Analysis of Pure Nitrogen

5.1.1 Detailed Representative Rietveld Analysis for Pure Nitrogen Measured at HXMA

This section reports Rietveld refinement on a pure nitrogen sample obtained at the HXMA beamline with λ = 0.5092 Å (E = 24.5 keV) at 11 K. A series of plots shown below is to demonstrate a systematic improvement of results upon the refinement of the parameters described above.

Firstly, an unsupervised refinement in Figure 4.8 with the default settings of the Match! Software will be demonstrated. The automatic refinement runs the refinement process in 10 cycles[26] with standard pre-defined variables that are varied in each refinement cycle. In the first cycle, the software adjusts the scale factors and the shift on the 2θ axis. In the second cycle, it refines these scale factors and the specimen displacement (i.e., the positions of the CH_4 and N_2 peaks). In the third cycle, it refines the scale factors, specimen displacement, unit cell parameters, profile shape parameters and the background coefficient. In the fourth cycle, it refines the scale factors, unit cell parameters, background coefficient and the Caglioti half-width parameters. The Caglioti half-width parameters refines the peak shape by adjusting the FWHM. In the fifth cycle, the software refines the scale factors, unit cell parameters, background coefficient, overall isotropic displacement parameters and the Caglioti half-width parameters. This cycle then repeats five times to minimize the weighted Bragg R-factor and the final reduced chi-squared value.

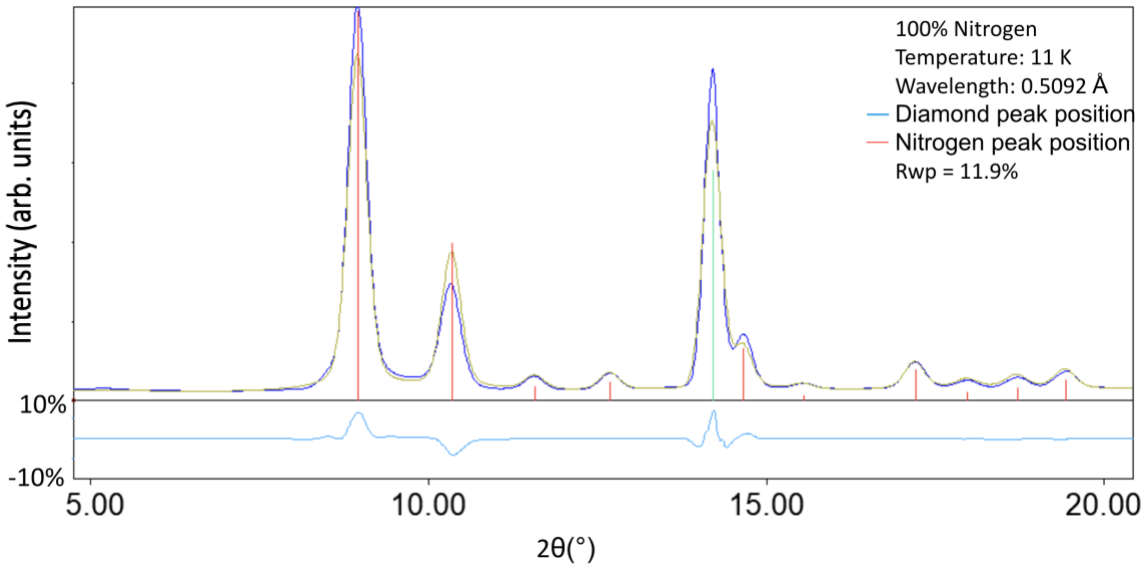

Figure 5.1. Example of automatic refinement of pure nitrogen on HXMA beamline. The red sticks represent the peak positions for nitrogen and the green stick represents the peak position of diamond. The dark blue pattern signifies the calculated diffraction pattern and the yellow signifies the experimental diffraction pattern. The light blue difference plot shows the difference of less than 10% between the calculated and the experimental patterns. The R_{wp} is the weighted Bragg R-factor which is a measurement of quality of the Rietveld refinement. In this case, it is 11.9% which is acceptable but not ideal.

The automatic Rietveld refinement is useful in cases where the peaks are easily identified and can be automatically indexed by the program. However, in much of this experiments' data analysis, manual refinement was necessary to ensure the best reduced weighted Bragg R-factor value as well as a visualization of the difference between the experimental and calculated profiles.

In Figure 5.1, while the difference between the experimental and calculated peaks is less than 10%, there are some discrepancies between the two. Firstly, the nitrogen peak positions are at slightly higher diffraction angle from the experimental peak. Secondly, there are obvious differences in the intensities of the calculated and experimental peaks. And finally, the Rwp (weighted Bragg-R factor) is higher than 10% (which is not ideal).

To reduce the weighted Bragg R factor and to improve the shape of the calculated profiles, the next parameter refined was the profile shape parameters, illustrated in Figure 5.2.

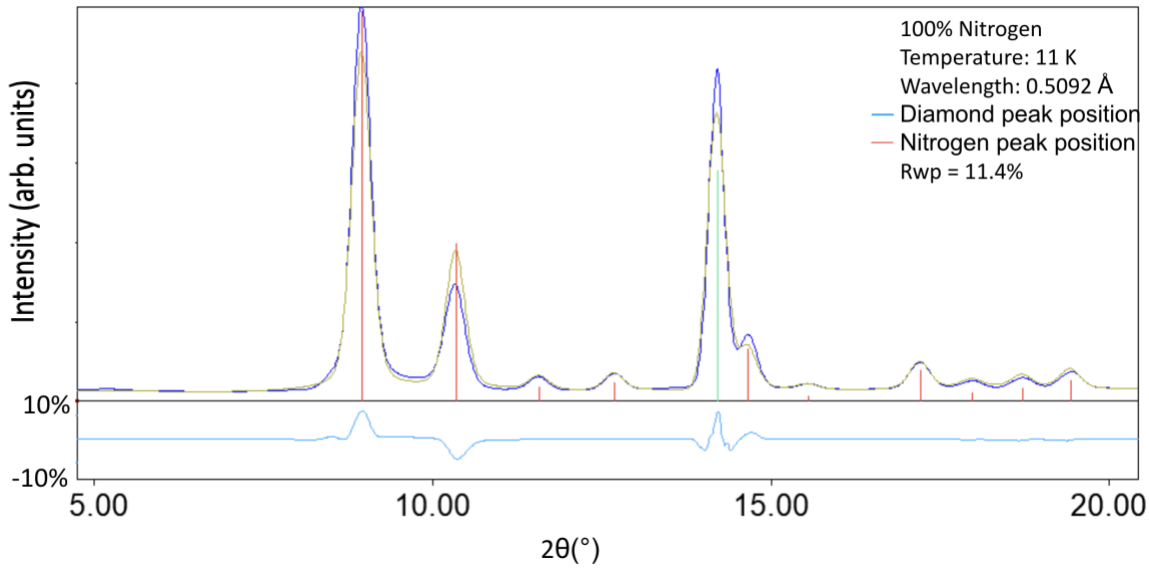

Figure 5.2. An example of profile shape adjustment for pure nitrogen on the HXMA beamline. The pseudo-Voight line shape model was implemented for this diffraction pattern. The R_{wp} (weighted Bragg R-factor) is 11.4%, which is a slight improvement from the previous figure but not ideal. The difference between the calculated and experimental patterns is less than 10%.

As shown, in Figure 5.2, the line width parameter did not make any significant improvement. There are still significant discrepancies between the intensities of the Bragg peaks. The next step is to refine the intensity of all the phases. The result is illustrated in Figure 5.3.

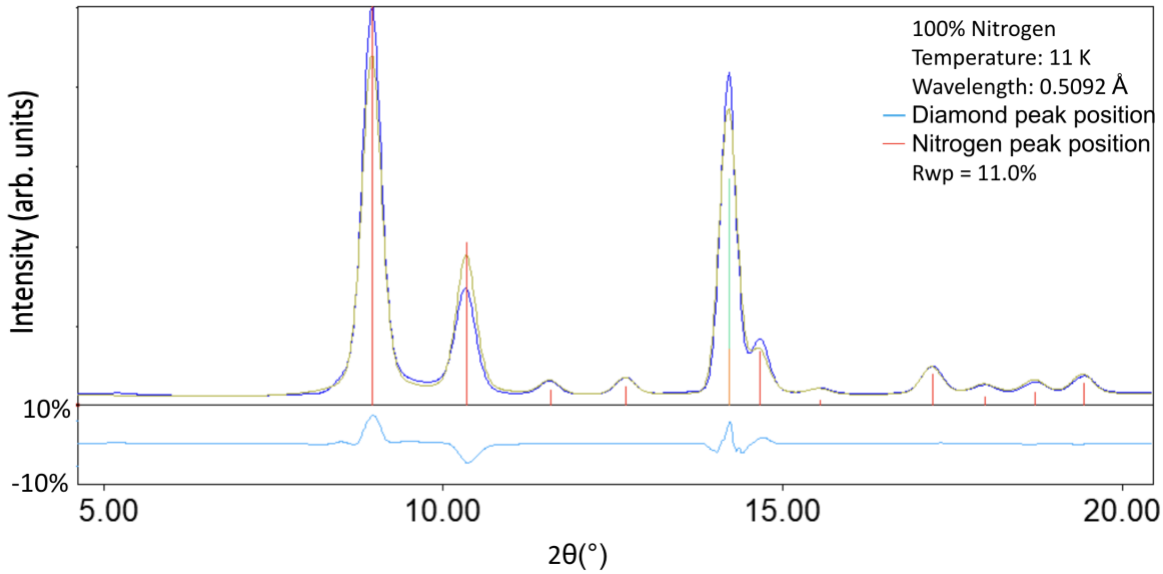

Figure 5.3. An example of intensity adjustment for pure nitrogen at the HXMA beamline. The intensity of the calculated pattern was scaled to approximate the experimental pattern better. The R_{wp} (weighted Bragg R-factor) is 11.0%. The difference between the calculated and experimental patterns is still less than 10%.

From Figure 5.3, the calculated peak intensities still do not match the experimental. In a final trial, the orientation parameter is refined. This assumes that the deposited N_2 crystallites do not have a homogeneous orientation.

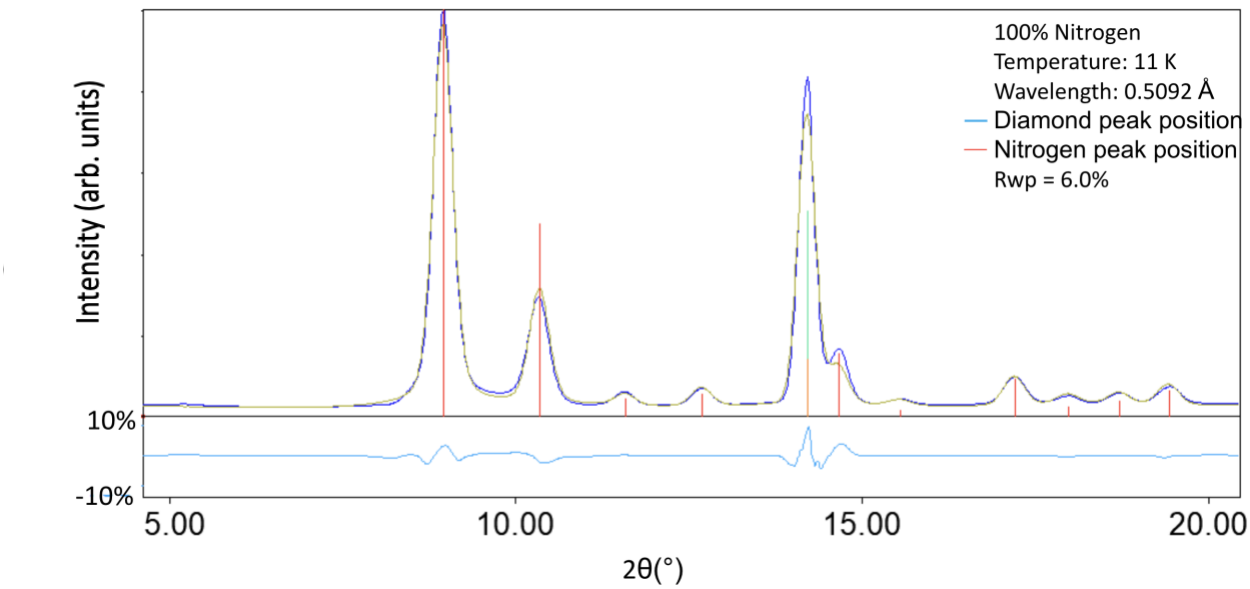

Figure 5.4. An example of phase orientation adjustment for pure nitrogen on the HXMA beamline. The R_{wp} (weighted Bragg R-factor) is 6.0%, which is a significant improvement from the previous figure. The difference between the calculated and experimental patterns is still less than 10% but there is visibly much better agreement between the two patterns.

With this phase orientation adjustment, the peak intensities of both calculated and experimental diffraction patterns are now in better agreement. The weighted Bragg R factor is lower at 6.0% and the maximum error in profile difference is less than 10% mainly due to the diamond diffraction at 14.1°. Finally, the background for the sample was refined, Figure 5.4.

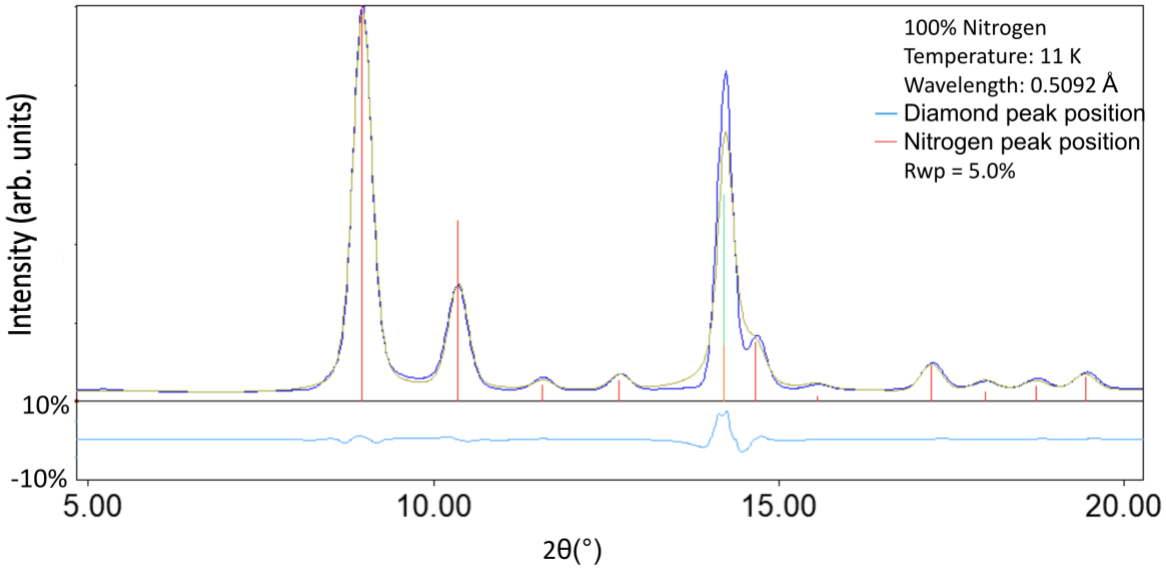

Figure 5.5. Refined example of pure nitrogen on the HXMA beamline. The R_{wp} (weighted Bragg R-factor) is 5.0% indicating that there is good agreement between the calculated and the experimental patterns. The biggest discrepancy is between the intensity of the diamond peak at 14.1°.

This final diffraction pattern reduces the discrepancy of the first peak and only slightly improves the overall agreement with a final weighted Bragg-R factor of 5%, an acceptable value.

5.1.2 Rietveld Refinement of Pure Nitrogen at Measured HXMA

A similar analysis was performed for several diffraction patterns for 100% nitrogen measured at the HXMA beamline. This exercise served two purposes. Firstly, to better understand how to use the match! software and understand the implications of increasing temperature on changes in crystal structure. Secondly, to practice the various adjustment parameters that are available in the Fullprof software.

Table 5.1. Summary of the results of Rietveld refinement for pure N2 with increasing temperature at the HXMA beamline.

Temperature (K)	a = b (Å)	c (Å)	x = y	z	α =β (°)	γ (°)	Volume (Å^3)	Crystal structure	Space Group
11.6	5.643(28)	5.644(44)	0.0522	0.0536	90	90	179.76	Cubic	P 2 3 (195)
13.2	5.649(78)	5.649(78)	0.0522	0.0523	90	90	180.34	Cubic	P 2 3 (195)
13.2	5.638(12)	5.639(12)	0.0523	0.0520	90	90	179.26	Cubic	P 2 3 (195)

13.9	5.651(18)	5.6512(18)	0.0540	0.0540	90	90	180.47	Cubic	P 2 3 (195)
13.9	5.641(17)	5.641(17)	0.0529	0.0529	90	90	179.50	Cubic	P 2 3 (195)
14.1	5.654(29)	5.654(29)	0.0524	0.0535	90	90	180.72	Cubic	P 2 3 (195)
15.8	5.652(21)	5.652(21)	0.0521	0.0520	90	90	180.58	Cubic	P 2 3 (195)
17.6	5.654(19)	5.654(19)	0.0523	0.0523	90	90	180.71	Cubic	P 2 3 (195)
18.9	5.655(18)	5.655(18)	0.0540	0.0540	90	90	180.85	Cubic	P 2 3 (195)
20.6	5.654(71)	5.653(71)	0.0540	0.0540	90	90	181.20	Cubic	P 2 3 (195)
23.1	5.664(20)	5.662(20)	0.0519	0.0521	90	90	181.51	Cubic	P 2 3 (195)
25.9	5.654(88)	5.654(88)	0.0518	0.0518	90	90	180.72	Cubic	P 2 3 (195)
27.6	5.671(17)	5.671(17)	0.0540	0.0540	90	90	182.35	Cubic	P 2 3 (195)
32.2	6.391(58)	11.464(22)	0.0494	0.0494	90	90	468.22	Tetragonal	P 4 (75)
33.5	10.012(22)	3.479(22)	0.0483	0.0484	90	90	348.68	Tetragonal	P 4 (75)
34.9	6.855(42)	14.067(11)	0.3333	0.2911	90	90	661.01	Tetragonal	P 4 (75)
35.9	7.627(18)	7.935(23)	0.3333	0.2716	90	90	461.63	Tetragonal	P 4 (75)
36.8	9.258(13)	6.650(23)	0.3333	0.2976	90	90	569.97	Tetragonal	P 4 (75)
37.9	5.217(23)	11.976(61)	0.3333	0.3380	90	90	325.90	Tetragonal	P 4 (75)
38.8	9.282(60)	6.669(748)	0.3333	0.3380	90	90	574.60	Tetragonal	P 4 (75)
39.9	11.747(51)	11.119(1256)	0.3333	0.3380	90	90	1534.2	Tetragonal	P 4 (75)
40.9	4.7334(71)	16.596(125)	0.5519	0.5519	90	90	371.83	Tetragonal	P 4 (75)

Table 5.1 summarizes that the results (with Rietveld refinement). The table shows that there is a phase change at 32 K.

Inspection of individual diffraction pattern show there are shifts in the positions of the Bragg peaks indicating that there are structural transformations of the N_2 crystal upon heating. The crystal starts with a cubic P23 structure which transforms to a tetragonal P4 system after 28 K. The observed transformation sequence differs from that reported in the literature. It was reported by Connolley et. al.[2] that pure N_2 has an fcc structure up until 36 K after which it has an HCP (hexagonal closed packed) structure. This discrepancy can be attributed to the experimental conditions. In this

experiment, the crystal is under high vacuum and on a diamond substrate compared to the previous work under atmospheric pressure. It is important to note here that there are weak interatomic forces (van der Waal's) that may favor one type of closed packed system over another (fcc vs hcp). Analysis of the N_2 and CH_4 mixtures will gives further insight into this. This will be explored in the following section.

Figures 5.6 to 5.10 show the results from the Rietveld analysis as the pure N_2 system was warmed. As mentioned previously, to use the Match! Software, an existing N_2 cif file is used to identify the diffraction peaks, then the experimental pattern is refined. As temperature increases, the N_2 peaks in the sample change due to phase changes. To ensure this was accounted for, different N_2 reference patterns were used for temperatures greater than 30 K.

Rietveld analysis at 13 K

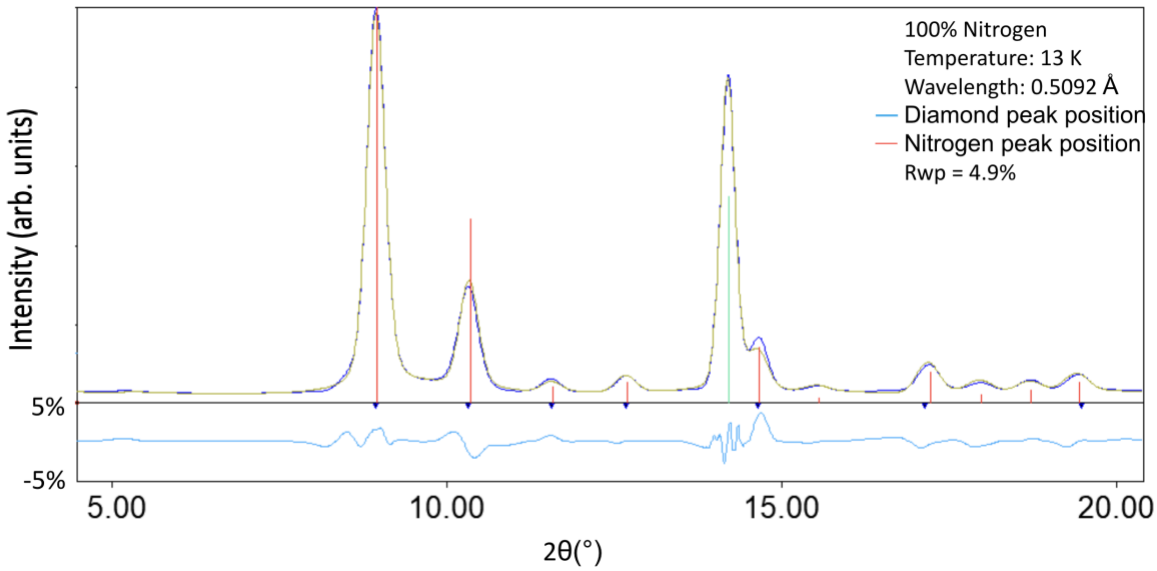

Figure 5.6. Rietveld analysis of pure N_2 at HXMA beamline at 13 K. The red sticks represent nitrogen peak positions, and the green stick represents diamond peak positions. The dark blue diffraction pattern corresponds to the experimental diffraction pattern and the yellow diffraction pattern corresponds to the one calculated by the Match! Software. The light blue graph represents the difference between the calculated and experimental diffraction patterns. The difference between the two patterns for pure N_2 at 13 K is less than 5%. The R_{wp}, which represents the weighted Bragg R-factor, is 4.9%.

Figure 5.6 shows the diamond peak at 2θ (°) = 14.1°. This peak will remain constant throughout the warmup of pure nitrogen (Figures 5.6-5.12). The N_2 peaks can be observed at 2θ (°) = 8.9°, 10.2°, 11.3°, 12.6°, 14.6°, 17.4°, 18.2°, 18.8°, and 19.5° as previously shown in Table 4.3. The Rietveld analysis for this diffraction pattern has a weighted Bragg R-factor of less than 5%, which

is satisfactory. Visual comparison shows that there is good agreement between the calculated and the experimental profiles (calculated is the blue, experimental is yellow).

Rietveld analysis at 20 K

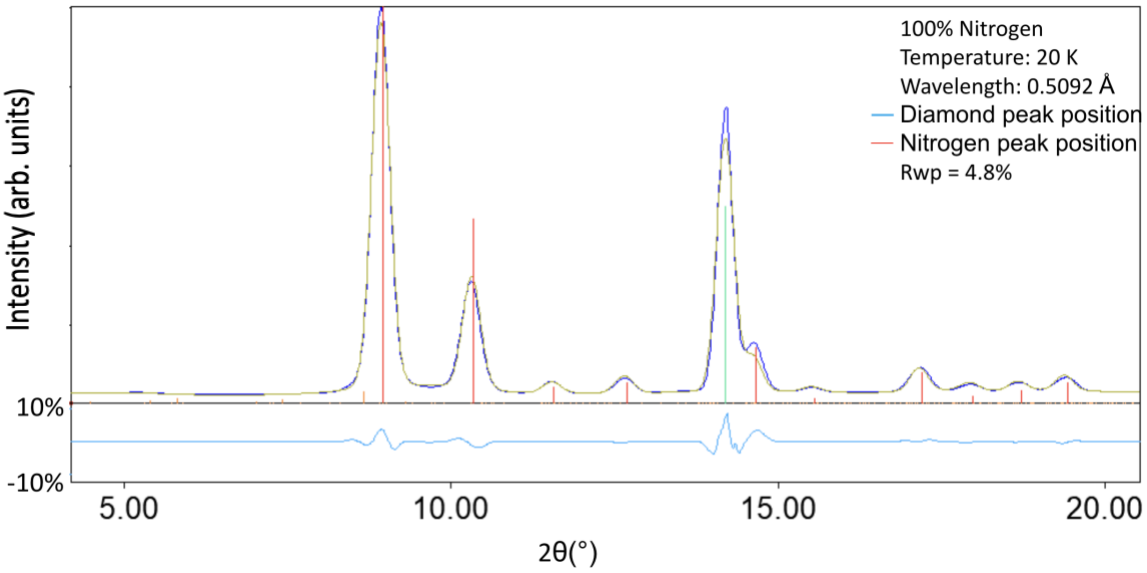

Figure 5.7. Rietveld analysis of pure N_2 at HXMA beamline at 20 K. The difference between the two patterns for pure N_2 at 20 K is less than 10%. The R_{wp} is 4.8%.

Rietveld analysis at 25 K

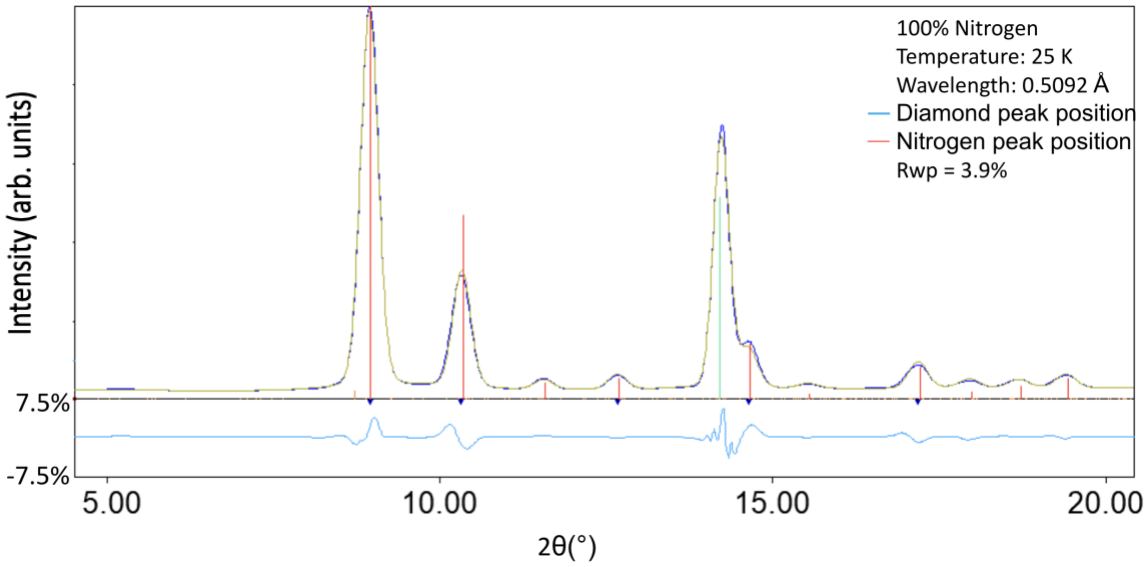

Figure 5.8. Rietveld analysis of pure N_2 at HXMA beamline at 25 K. The difference between the two patterns for pure N_2 at 25 K is less than 7.5%. The R_{wp} is 3.9%, which indicates that there is good agreement between the calculated and the experimental diffraction patterns.

As the sample is warmed from 10K to 25K, the peaks and profiles maintain their positions as observed in Figure 4.14 and 4.15. Once again, there is good agreement between the experimental and calculated profiles.

Rietveld analysis at 31 K

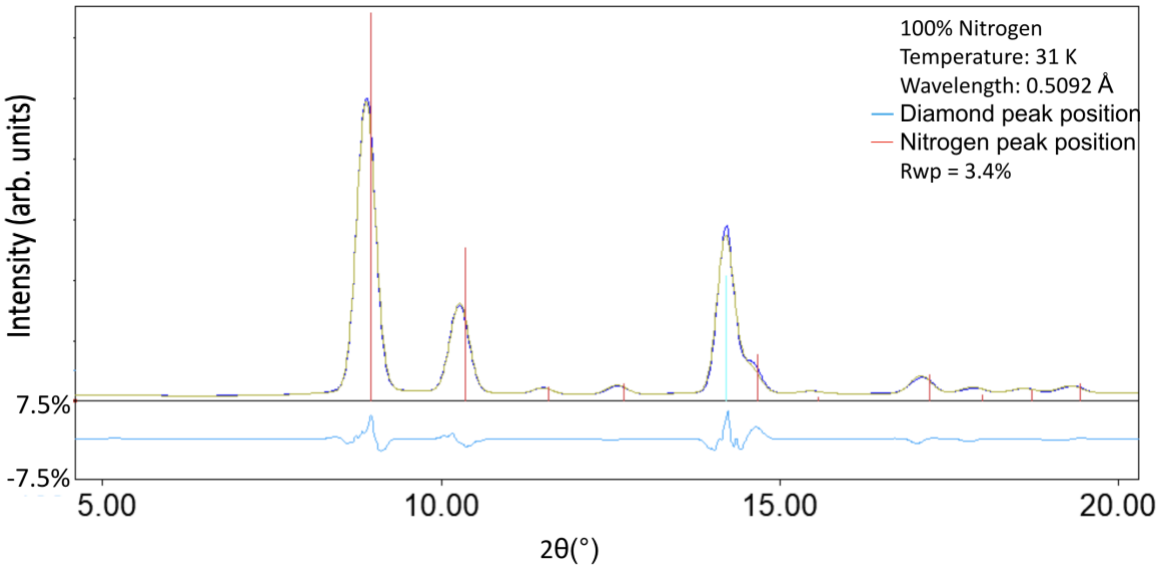

Figure 5.9. Rietveld analysis of pure N_2 at HXMA beamline at 31 K. The intensities of the peaks are lower than previous figures. The difference between the two patterns for pure N_2 at 31 K is less than 7.5%. The R_{wp} is 3.4%, which indicates that there is good agreement between the calculated and the experimental diffraction patterns.

As the temperature in the system continues to rise, now at 31 K, the relative intensities of the nitrogen peaks start to decrease but the positions remain unchanged.

Rietveld analysis at 35 K

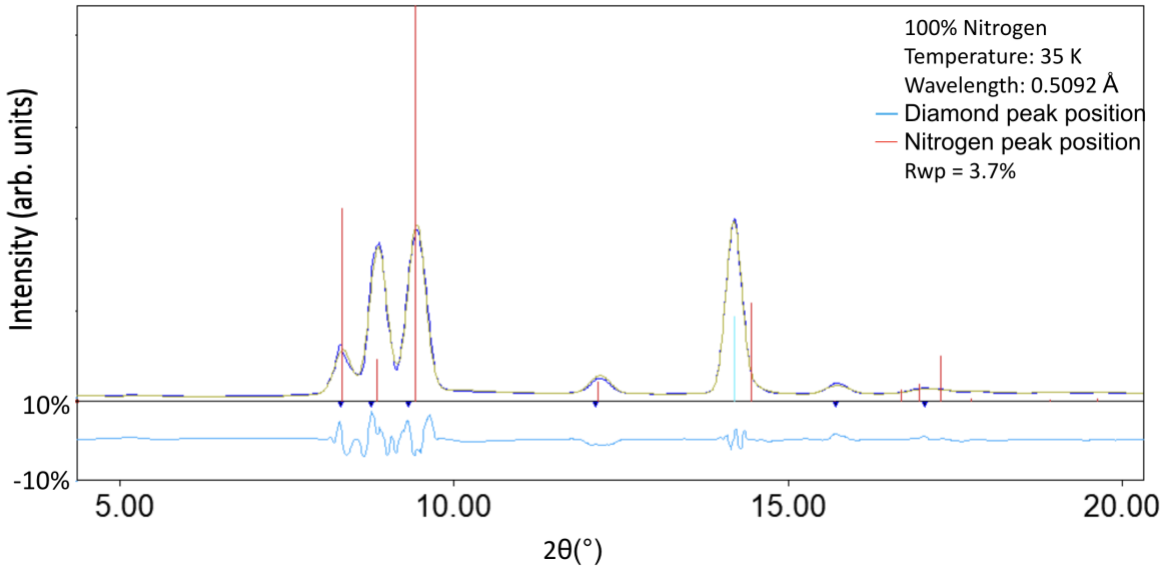

Figure 5.10. Rietveld analysis of pure N_2 at HXMA beamline at 35 K. There is a phase chance between 31 K and 35 K as the peak positions of N_2 are different from what they were between 10 K and 31 K, which means a new cif file was used as a reference diffraction pattern. The difference between the two patterns for pure N_2 at 35 K is less than 10%. The R_{wp} is 3.7%, which indicates that there is still good agreement between the calculated and the experimental diffraction patterns.

Figure 5.10 shows that at 35 K, there appears to be a structural changes in the sample. These are the same changes that were observed in Figure 5.9 and repeated in Table 5.1. These peaks are at 2θ (°) = 8.8°, 9.3°, 9.7°, 12.5°, 16.0°, and 17.4°. For this analysis, it is obvious that while the reference peaks used correspond to the experimental peaks, the expected intensities of those respective peaks are not a perfect match for the sample.

Rietveld analysis at 37 K

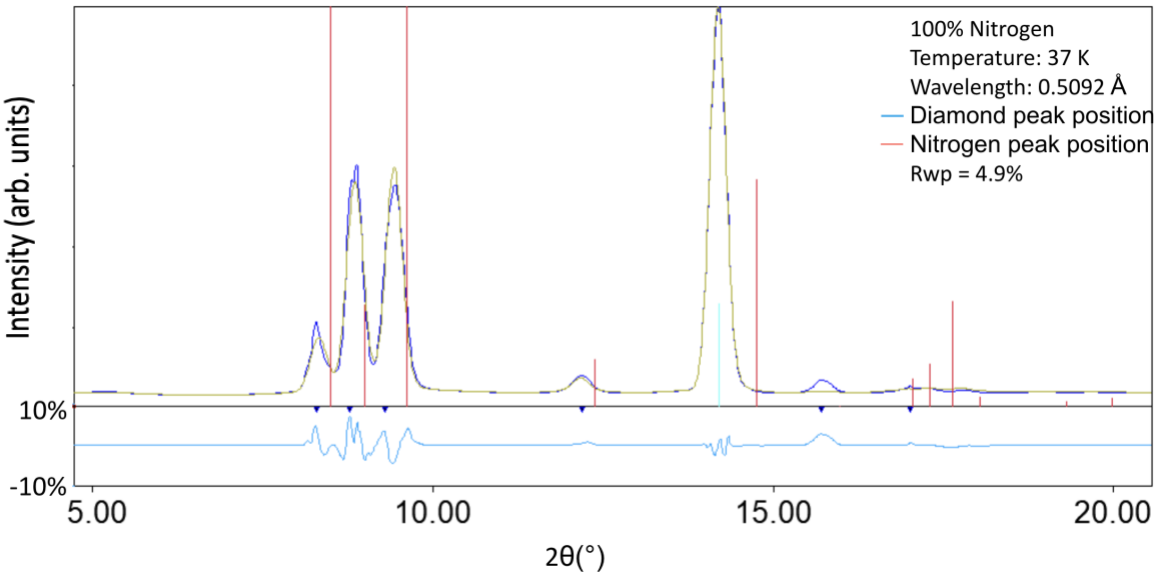

Figure 5.11. Rietveld analysis of pure N_2 at HXMA beamline at 37 K. The difference between the two patterns for pure N_2 at 37 K is less than 10%. The R_{wp} is 4.9%, which indicates that there is good agreement between the calculated and the experimental diffraction patterns.

Figure 5.11 has the same reference pattern and observed peaks in the pattern as Figure 5.10. supports the conclusion that there is an obvious these change in the structure of nitrogen at approximately 34 K, which agrees with the phase change observed in Figure 4.4.

Rietveld analysis at 40K

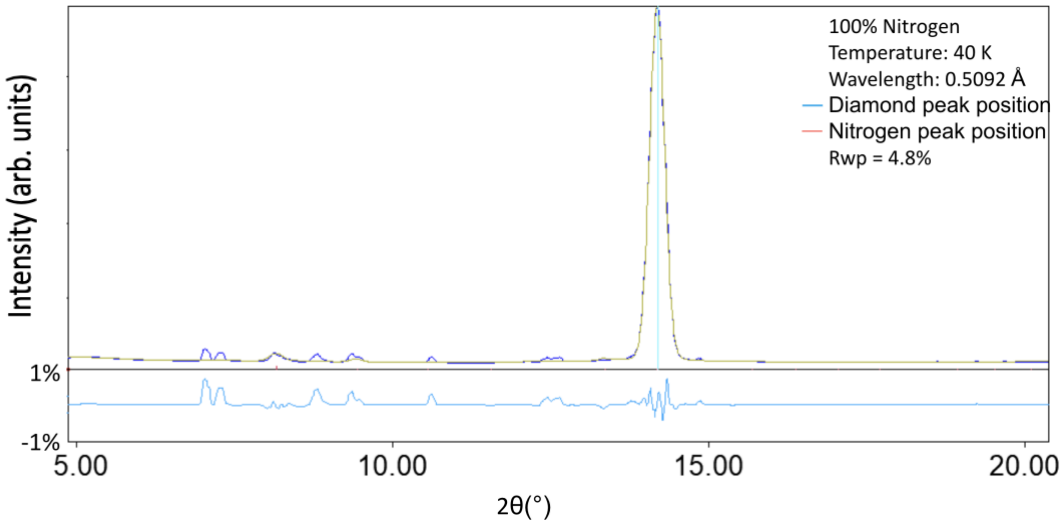

Figure 5.12. Rietveld analysis of pure N_2 at HXMA beamline at 40 K. N_2 reference peaks are no longer present. There appear to be some remnants of N_2 but not significant enough for the Match! Software to distinguish from background. Visibly, these peaks can be observed. The R_{wp} of 4.8% primarily represents a Rietveld analysis of the single diamond peak at 14.1°.

As the sample is warmed to 40K, the N_2 was pumped out of the system, meaning that it was no longer present in the diffraction pattern. Figure 5.12 shows a good example of this, where the diamond peak at 2θ (°) = 14.1° is still quite strong, while the other peaks corresponding to nitrogen have essentially disappeared.

5.1.3 Rietveld Refinement of Pure Nitrogen Measured at Brockhouse

Since there were some concerns regarding the quantitative ratio of the gas mixtures from the diffraction patterns at the HXMA beamline using the manual leak valve, the same experiments were repeated twice at the Brockhouse beamline in June and December of 2019. For the rest of the report, the focus will be on data analysis from the Brockhouse beamline as there was better quality control for the percentage of gas in the system using computer-controlled valves (described in Section 3.4.2)

The following section demonstrates Rietveld refinement on a pure nitrogen sample at the Brockhouse beamline when λ = 0.3455 Å (E = 35 keV) at increasing temperatures. The goal of this section is to determine if a similar crystal structure (Appendix C.1) from the data analysis as the HXMA beamline is obtained. This section will not demonstrate a systematic improvement of results but will only show refined diffraction pattern (to the best of my ability). Please note that for this section, the 2θ axis is limited to between 5° and 15° as it allows for better identification of the nitrogen peaks that are significantly smaller in terms of intensity compared to the strong diamond peak as described in previous sections. Figures 5.13 to 5.17 show the refinement results of pure N_2 at the Brockhouse beamline.

Table 5.2 summarizes the results of pure nitrogen at the Brockhouse beamline after the Rietveld refinement process.

Table 5.2. Summary of Rietveld refinement results for pure N2 at Brockhouse beamline.

Temperature (K)	a = b (Å)	c (Å)	α =β (°)	γ (°)	Volume (Å^3)	Crystal structure	Space Group
15	5.654(65)	5.654(65)	90	90	180.74	Cubic	P 2 3 (195)
25	5.663(22)	5.663(22)	90	90	181.85	Cubic	P 2 3 (195)

Table 5.3 shows a summary of some relevant results from Table 5.1 had previously shown the following results for pure N_2 at the HXMA beamline to compare with the results from Brockhouse.

Table 5.3. Summary of relevant results from Table 4.1 for pure N2 at the HXMA beamline.

Temperature (K)	a = b (Å)	c (Å)	α (°)	B (°)	γ (°)	Volume (Å^3)	Crystal structure	Space Group
15.8	5.652(22)	5.652(22)	90	90	90	180.582	Cubic	P 2 3 (195)
25.9	5.654(88)	5.654(88)	90	90	90	180.725	Cubic	P 2 3 (195)

Rietveld refinement at 15K

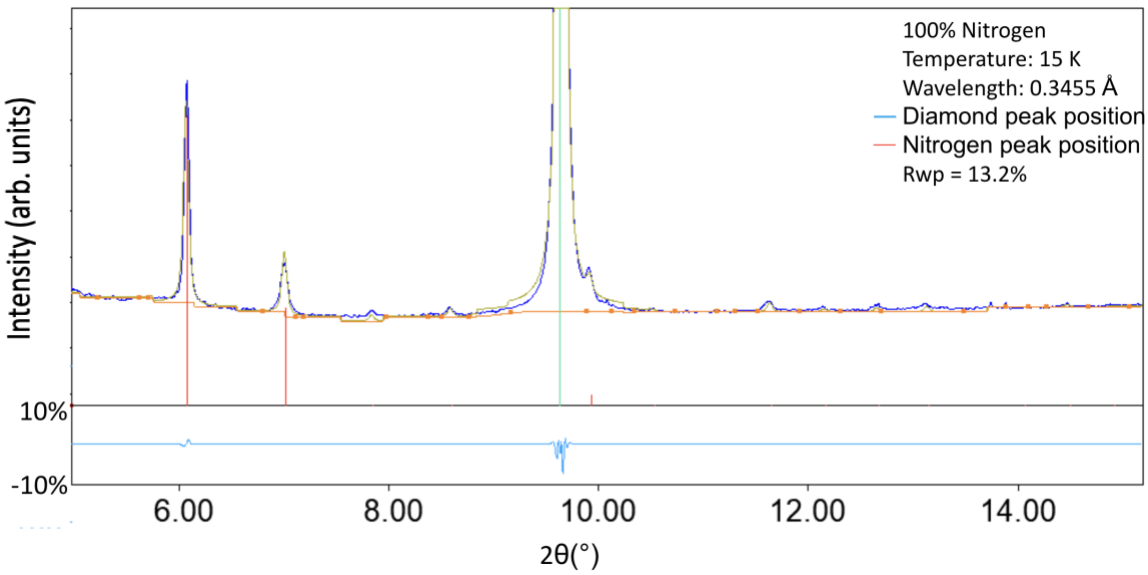

Figure 5.13. Rietveld refinement for pure nitrogen on the Brockhouse beamline at 15 K. The red sticks represent the peak positions for nitrogen. There are several peaks with smaller intensities that the Match! Software was unable to identify but can be visually noted. The green stick represents the peak for diamond at 9.6°. The dark blue diffraction pattern represents the experimental data, and the yellow diffraction pattern represents the calculated the diffraction pattern. The light blue graph represents the difference between the calculated and experimental diffraction pattern, which is less than 10%. The R_{wp} for this refinement is 13.2% which is an acceptable weighted Bragg R-factor but not ideal.

Figure 5.13 illustrates the Rietveld refinement for pure nitrogen at the Brockhouse beamline. This diffraction pattern and refinement shows that there is good agreement between the calculated and the experimental patterns. Although the weighted Bragg R-factor is 13.2%, the maximum deviation between the fitted and the observed intensity is 10%. The diamond peak is at 9.6° and has a relative intensity of 1000 arbitrary units compared the strongest nitrogen peak (6.0°) of ~ 30 units. As calculated previously for the Brockhouse beamline, the nitrogen diffraction pattern has a relative intensity of approximately 3% to the diamond pattern. It is clear from this diffraction pattern there are nitrogen peaks present but they are drowned out by the stronger intensity of the diamond peak. The nitrogen peaks are at 2θ (°) = 6.0°, 6.9°, 9.9°, 11.6°, 12.10°, 12.6°, and 13.1°.

Rietveld refinement at 25K

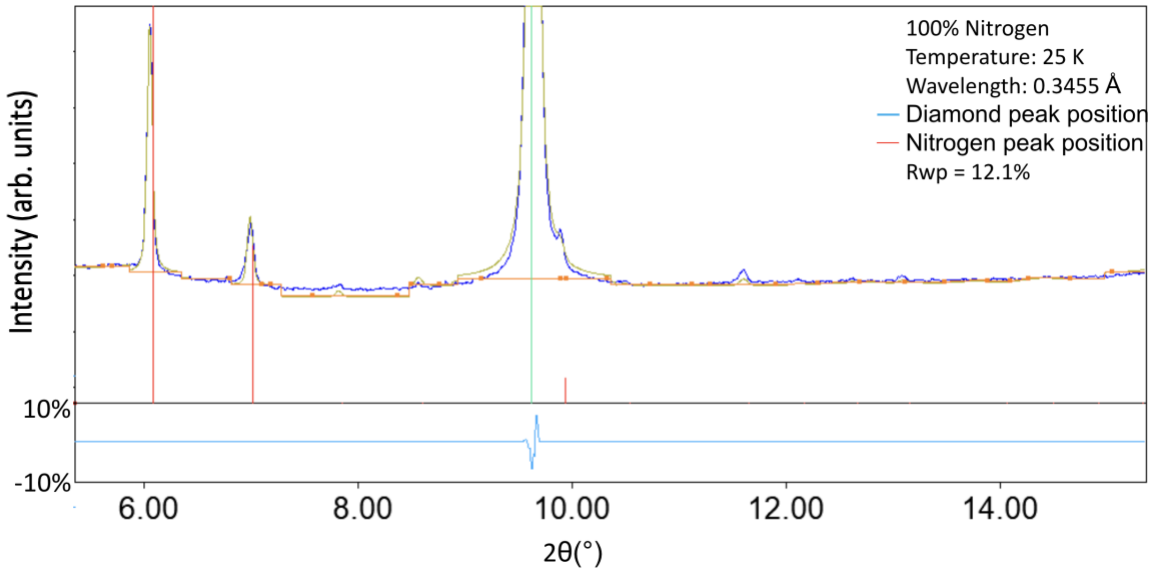

Figure 5.14. Rietveld refinement for pure nitrogen on the Brockhouse beamline at 25 K. The difference between the calculated (yellow) and experimental (dark blue) diffraction patterns is less than 10% and the R_{wp} for this refinement is 12.1% which is an improvement on the previous result but still not ideal.

Figure 5.14 shows the same diamond and nitrogen peaks as Figure 5.13. The 10 Kelvin increase in temperature did not result in any changes to the diffraction pattern. The relative intensity of the peaks at 7.9°, 8.4° and 11.3° are too weak to show in the stick plot but can be assigned to N_2 as previously summarized in Table 4.4.

Experimental diffraction pattern at 30K

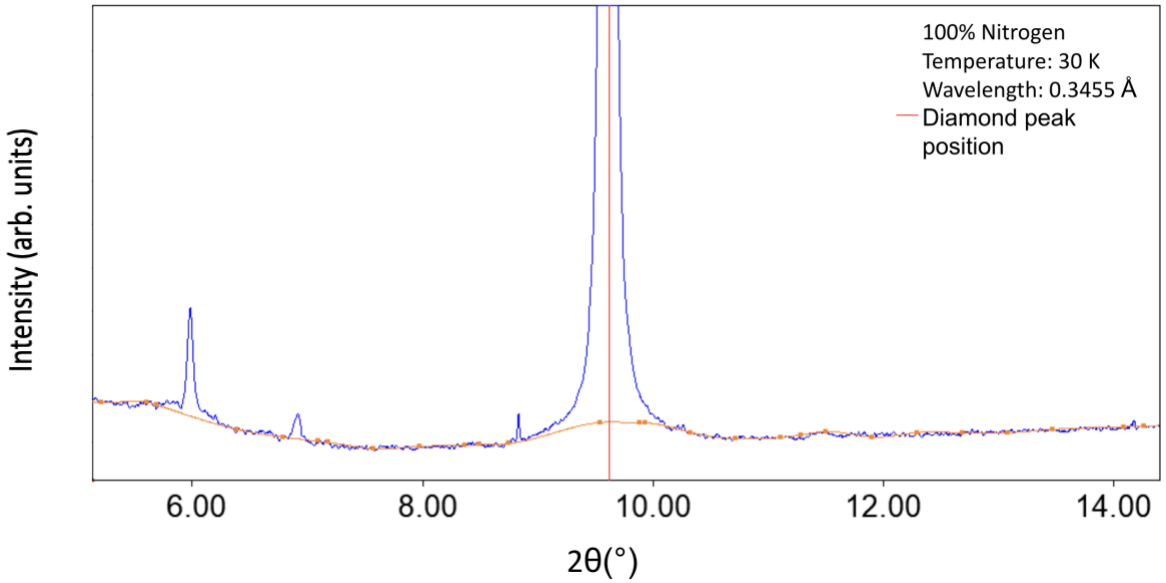

Figure 5.15. Diffraction pattern for pure nitrogen on the Brockhouse beamline at 30 K. The strongest nitrogen peak is only 2% of the intensity of the strongest diamond peak. The Match! Software was unable to calculate a diffraction pattern given the inability to match any of the low intensity nitrogen peaks.

As the sample is warmed, the intensity of the nitrogen peak starts to decrease. In Figure 5.15, the intensity of the strongest nitrogen peak (6.0°) is only 2 % of the strongest diamond peak (9.6°). As a result of this, the Match! Software failed to create a calculated profile for this set of data and Rietveld analysis was not possible for this sample at 30 K.

Experimental diffraction pattern at 35K

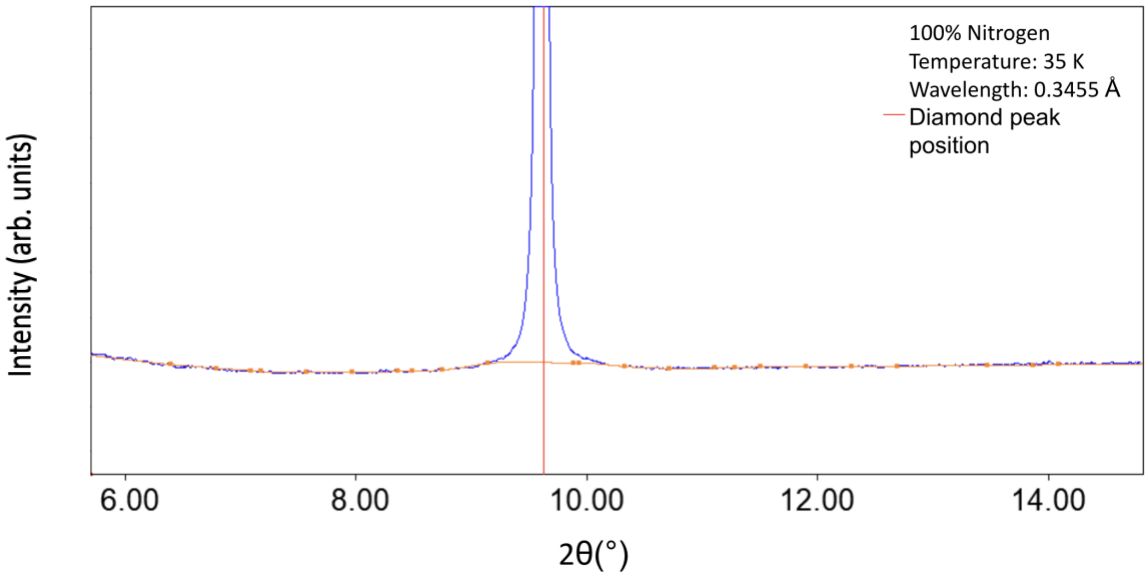

Figure 5.16. Diffraction pattern for pure nitrogen on the Brockhouse beamline at 35 K. There are no nitrogen peaks visible.

Figure 5.16 shows that as the temperature in the system continues to rise, the nitrogen peaks start to disappear. This is likely due to the low gas deposition resulting in the low intensity in the system. A summary plot of the patterns increasing with temperature is illustrated in Figure 5.17 below:

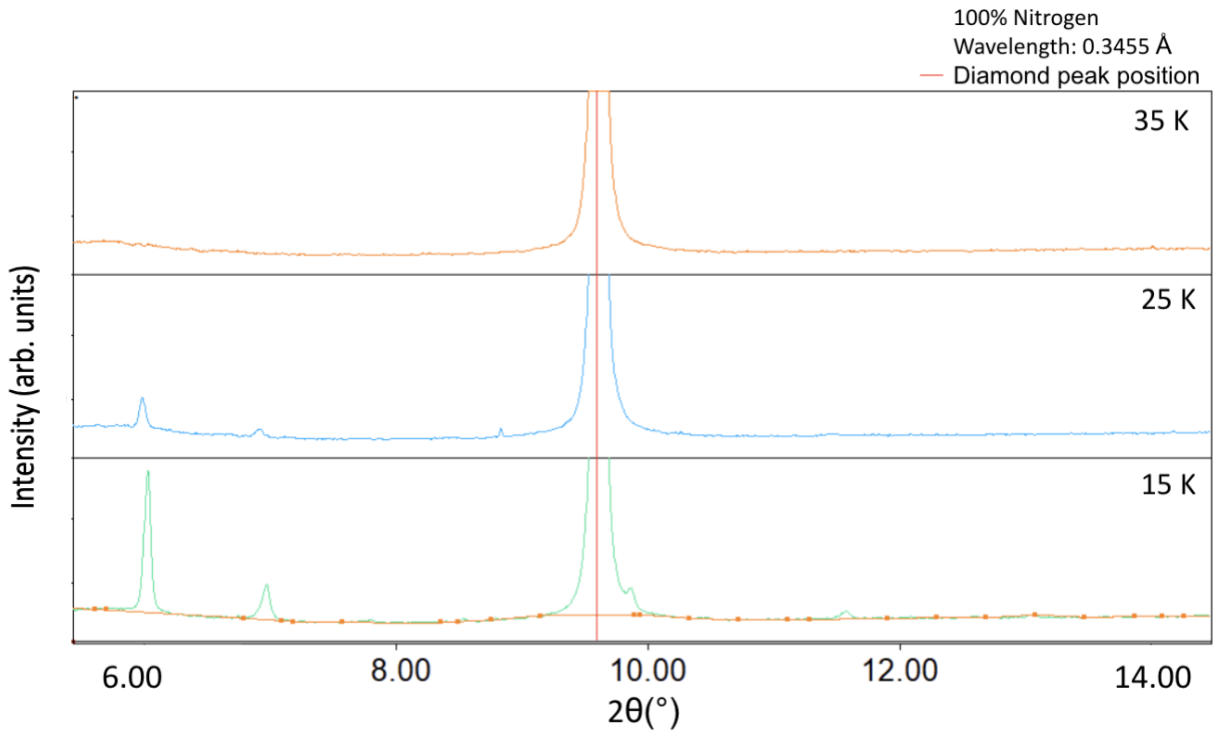

Figure 5.17. Diffraction patterns for pure nitrogen at the Brockhouse beamline between 15 and 35 K showing no crystal structure changes. The peak at 9.6° represents diamond, which remains constant throughout the warmup process.

5.2 Rietveld Analysis of Pure Methane

5.2.1 Rietveld Refinement of Pure Methane Measured at HXMA

This section reports Rietveld refinement on a pure methane sample obtained at the HXMA beamline with λ = 0.5092 Å (E = 24.5 keV) at 11 K. A series of plots shown below to illustrate the results of Rietveld refinement at each temperature. Table 5.4 summarizes the results of pure methane at the HXMA beamline following the Rietveld refinement process at each temperature.

Table 5.4. Summary of results for pure CH4 on HXMA the beamline

Temperature (K)	a = b (Å)	c (Å)	α =β (°)	γ (°)	Volume (Å^3)	Crystal structure	Space Group
10	5.905 (11)	5.905 (11)	90	90	205.9	Cubic	P 2 3 (195)
30	5.859 (06)	5.859 (06)	90	90	201.11	Cubic	P 2 3 (195)
59	5.676 (62)	11.270 (79)	90	90	363.04	Tetragonal	P 4 (75)
60	11.358 (15)	6.520 (24)	90	90	841.12	Tetragonal	P 4 (75)

Rietveld refinement at 10 K

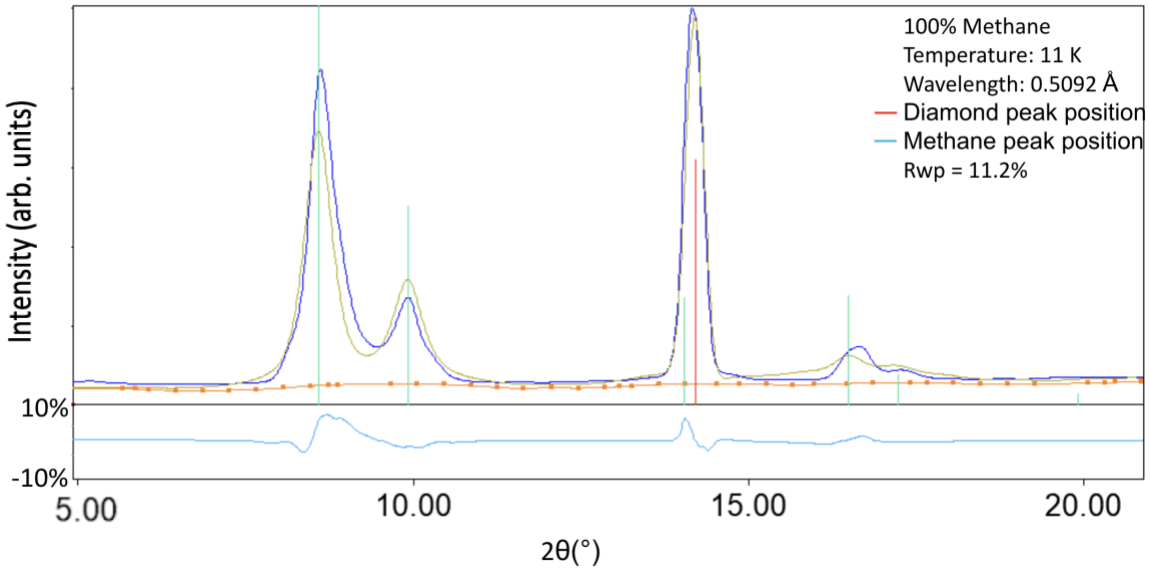

Figure 5.18. Rietveld analysis of pure CH_4 at HXMA beamline at 10 K. The light green sticks represent the methane peak positions, and the red stick represents the diamond peak. The dark blue diffraction pattern is the experimental diffraction pattern and the yellow represents the calculated pattern. The difference between the experimental and calculated patterns is less than 10%, shown by the light blue graph. The R_{wp} is 11.2%, which is acceptable but not ideal.

Figure 5.18 shows the diamond peak at 2θ (°) = 14.1°. CH_4 peaks can be observed by at 2θ (°) = 8.6°, 9.9°, 14.1°, 16.7°, and 17.2° as previously summarized in Table 4.3.

Rietveld refinement at 30 K

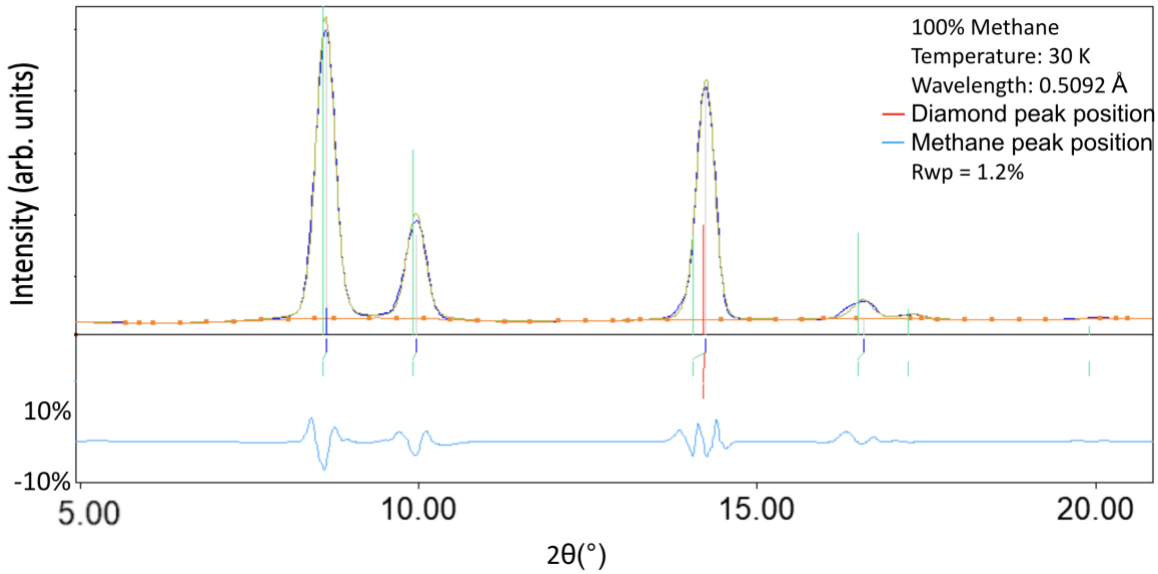

Figure 5.19. Rietveld analysis of pure CH_4 at HXMA beamline at 30 K. The difference between the patterns is still less than 10% and the R_{wp} is 1.2%, which represents a strong agreement between the patterns.

Figure 5.19 shows the same methane peaks as Figure 5.18. It is worth noting that with the increase in temperature, the intensity of the strongest methane peak relative to diamond has increased. From the waterfall plot in Figure 4.11, it is noted that at 37 K, there are changes noted in the diffraction pattern.

Rietveld refinement at 60 K

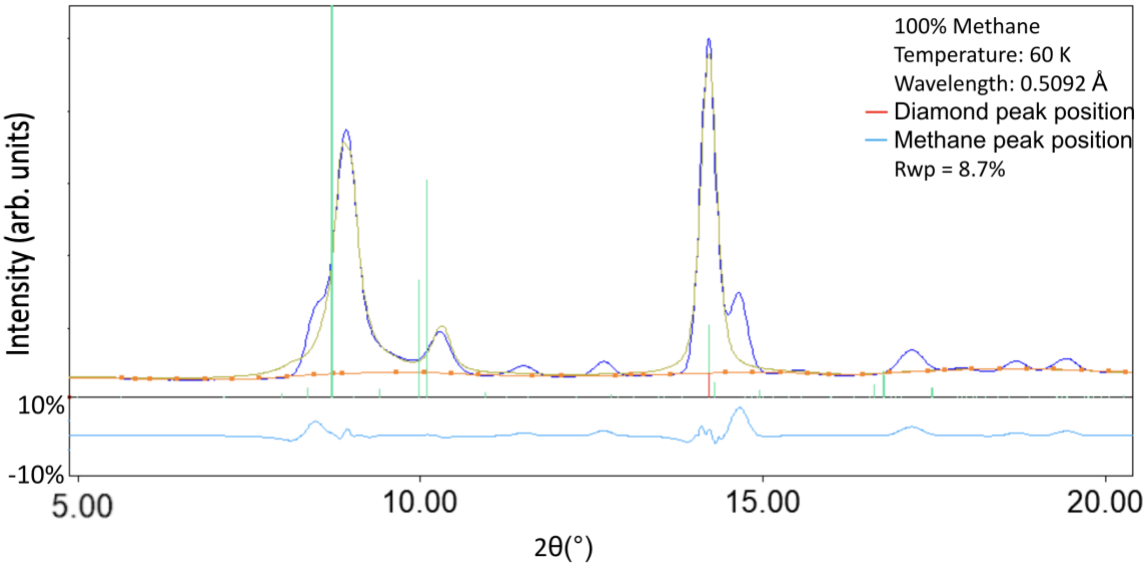

Figure 5.20. Rietveld analysis of pure CH_4 at HXMA beamline at 60 K. There are new peaks of methane that can be identified in this diffraction pattern. This was previously highlighted in Figure 4.13. The diamond peak remains unchanged from previous.

Figure 5.20 shows that there are changes in the diffraction pattern as temperature increases to 60 K. The methane peaks have shifted from the low temperature positions and are now observed at 2θ (°) = 8.9°, 10.9°, 11.5°, 12.7°, 14.7°, 17.3°, 18.7°, and 19.4°. It was not possible to find a known reference pattern for CH_4 at this temperature. The closest structure for this pattern is from the Crystal Structure of Methane Phase III paper[39]. Connelley et al.[4] noted that methane should remain in an fcc structure up until 91 K. However, this new phase change suggests that there is a phase change at 37 K.

Given the appearance of many new peaks, a more in-depth analysis of the diffraction pattern for methane were performed between 30 and 38 K.

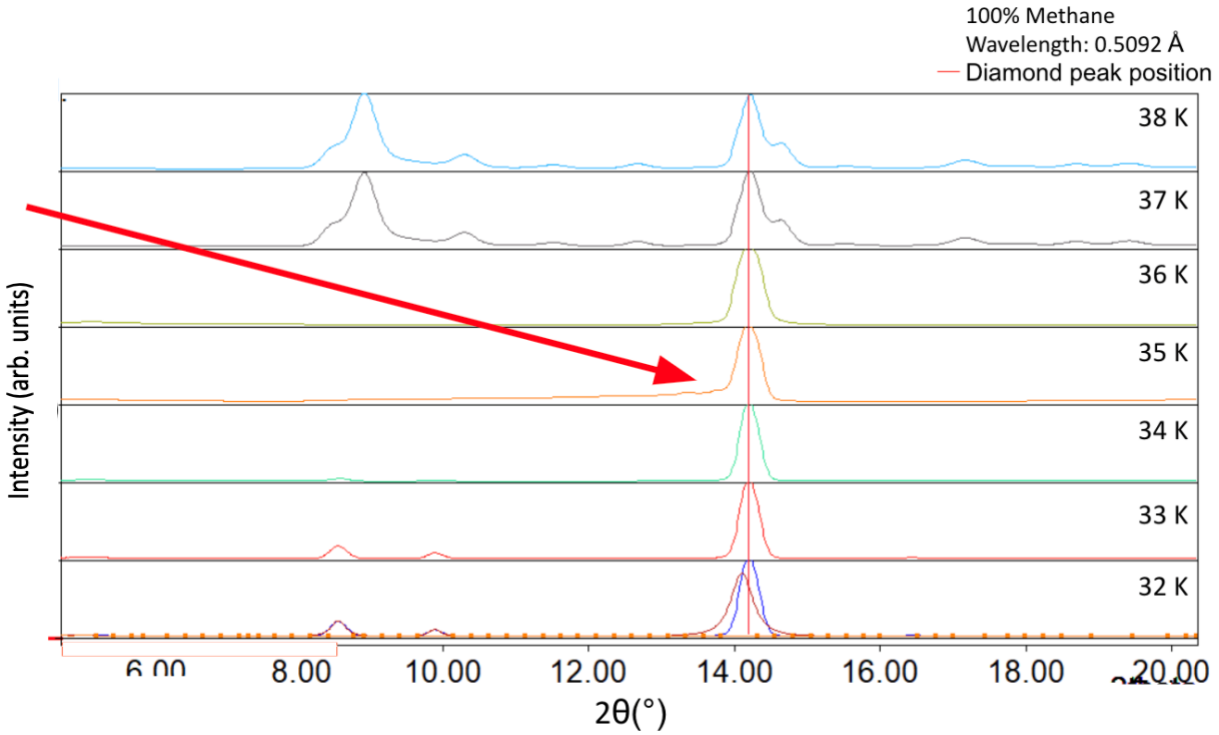

Figure 5.21. Diffraction patterns of pure methane at HXMA beamline between 32 and 38 K. The red arrow indicates a strange amorphous state that was identified as a shutter closure error identified on the raw diffraction pattern at 35 K.

To examine the phase change more carefully, Figure 5.21 shows the diffraction pattern collected between 32 and 38 K. The original 4 peaks disappear at 33 K as the sample is warmed. At 37 K, new peaks appear. Unfortunately, the experiment was terminated above 60 K, so it is difficult to assess the structural changes demonstrated above this temperature. This could perhaps be addressed at a later point as potential future research at this beamline. The raw diffraction pattern for pure methane at 35 K is shown in Figure 5.22 and 5.23 to illustrate that methane peaks were not visible at that temperature.

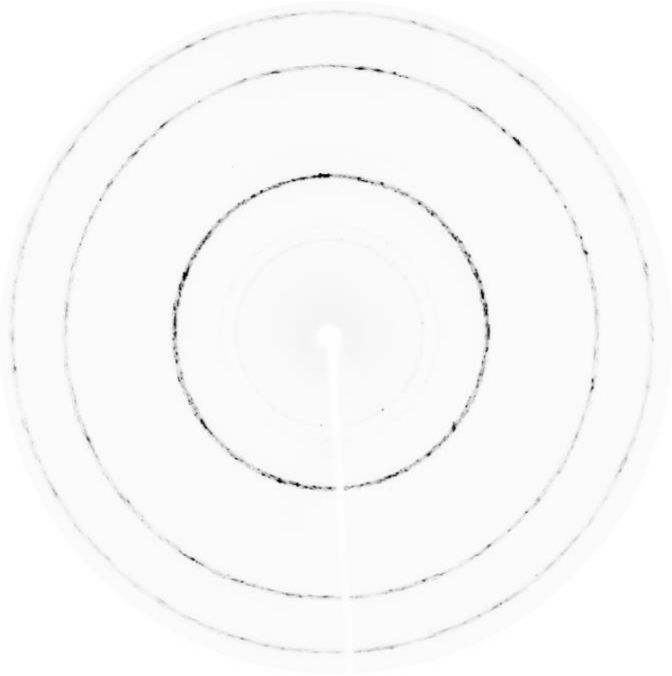

Figure 5.22. Dioptas diffraction pattern of pure methane at 34 K on the HXMA beamline shows that only the diamond diffraction rings are visible.

Figure 5.23. Dioptas pancake plot of the raw data for pure methane at 34 K on HXMA beamline.

The interesting observation made in this pure methane is between 36 K to 37 K. The 'new' methane structure appears quite suddenly. To explore this further, diffraction pattern just before the obvious appearance of these peaks at a lower intensity is studied, demonstrated in the Figure 5.24 below.

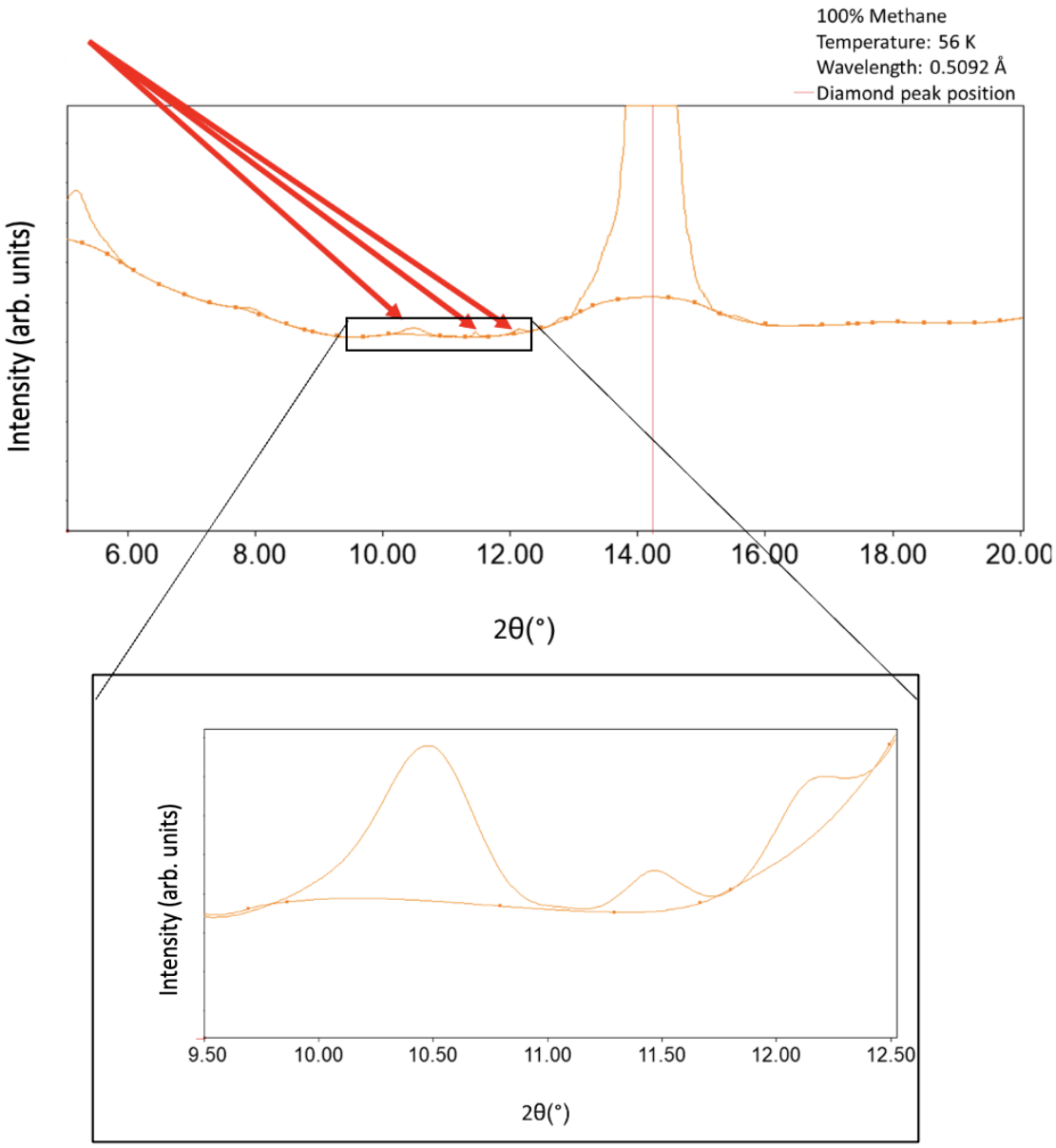

Figure 5.24. Detailed examination of pure CH_4 structural changes at 36 K at HXMA beamline to study if there were smaller peaks present in the diffraction pattern before the appearance of the stronger methane peaks at 37 K.

The red arrows in Figure 5.24 point towards the onset of a potentially new phase of methane. This figure also highlights how much detail can obtain using synchrotron radiation. In Figure 5.24, these

peaks can be identified distinctly at intensities of less than 10 arbitrary units from the background radiation.

The methane crystal structure at 37 K has been shown here in more detail.

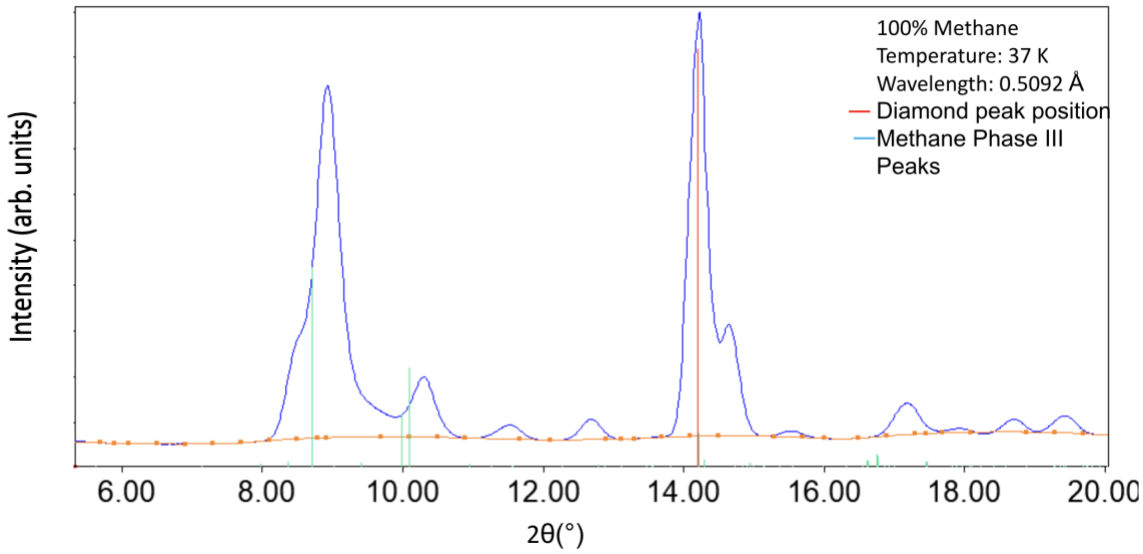

Figure 5.25. Rietveld refinement of pure methane at 37 K. The diamond peak is represented by the red stick and an attempt is made to match the new methane peaks to a known methane pattern.

The new methane peaks are found at 2θ (°) = 8.9, 10.3, 11.5, 12.7, 14., 17.2, 18.7, 19.4. For reference, the previous methane peaks were at 5.9, 6.8, 9.6, and 11.2.

From this analysis, the following lattice parameters are obtained and summarized in Table 5.5.

Table 5.5. This table summarizes the parameters from the Rietveld refinement of pure methane at the HXMA beamline

Number of peaks	a (Å)	b (Å)	c (Å)	α (°)	β (°)	γ (°)	Volume
8	5.676 (62)	5.676 (62)	11.270 (79)	90	90	90	363.04

The results show a tetragonal crystal system with a P 4 (75) space group. In comparison, the Crystal Structure of Methane Phase III[40] has lattice parameters a = 11.7079(1) Å, b = 8.1893(1) Å, c = 8.1842(1) Å at 18K.

5.2.2 Rietveld Refinement of Pure Methane Measured at Brockhouse

Table 5.6 summarizes results of the crystal structures of pure methane at the Brockhouse beamline followed by the Rietveld refinement patterns for increasing temperature.

Table 5.6. Summary of results for pure CH4 on the Brockhouse beamline.

Temperature (K)	a = b (Å)	c (Å)	α =β (°)	γ (°)	Volume (Å^3)	Crystal structure	Space Group
10	5.894(39)	5.895(39)	90	90	204.8	Cubic	P 2 3 (195)
22	5.897(35)	5.898(35)	90	90	205.15	Cubic	P 2 3 (195)
33	5.911(81)	5.911(81)	90	90	206.6	Cubic	P 2 3 (195)
43	5.928(13)	5.928(13)	90	90	208.3	Cubic	P 2 3 (195)
53	5.929(81)	5.929(81)	90	90	208.5	Cubic	P 2 3 (195)

Rietveld refinement at 10 K

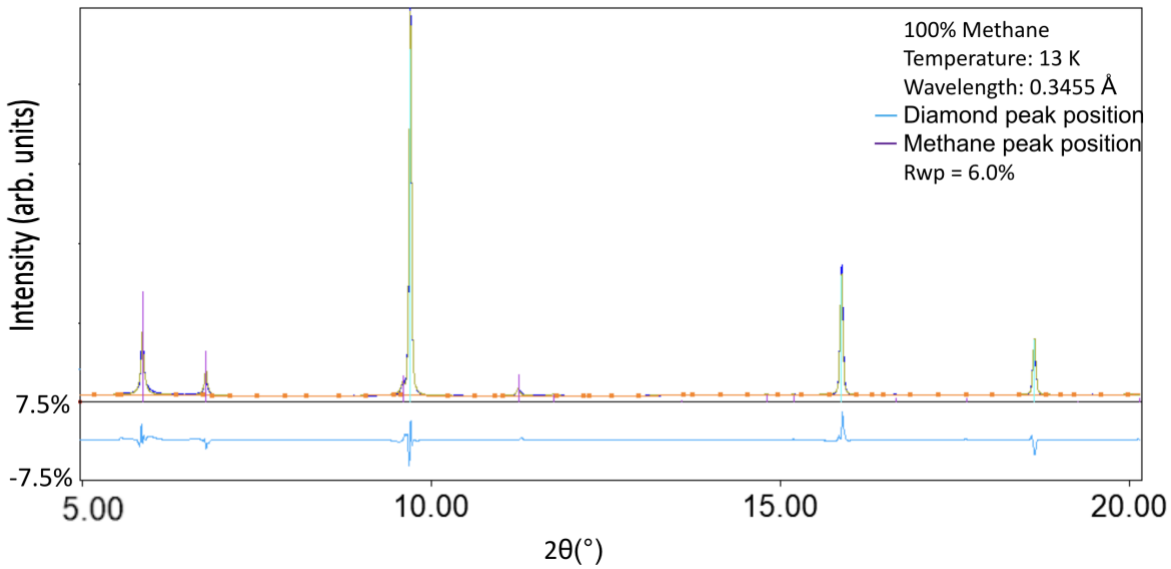

Figure 5.26. Rietveld refinement for pure CH_4 on the Brockhouse beamline at 10 K. The purple sticks represent the methane peak positions, and the light green stick represents the diamond peak. The dark blue diffraction pattern is the experimental diffraction pattern and the yellow represents the calculated pattern. The difference between the experimental and calculated patterns is less than 7.5%, shown by the light blue graph. The R_{wp} is 6.0%, reflecting a good fit for the data.

Figure 5.26 shows the Rietveld refinement of pure CH_4 on the Brockhouse beamline. Again, the diamond peaks are at 9.6°, 15.7°, and 18.5°. The methane peaks are at 2θ (°) = 5.8°, 6.8°, 9.6°, 11.2°, and 11.8°. The 2θ is limited between 5° and 20° to make comparison easier with the previous set of data of pure methane at the HXMA beamline. As can be noted in Figure 5.26, there is good

agreement between the experimental and the calculated patterns with a weighted Bragg R factor of 6.0%

Rietveld refinement at 22 K

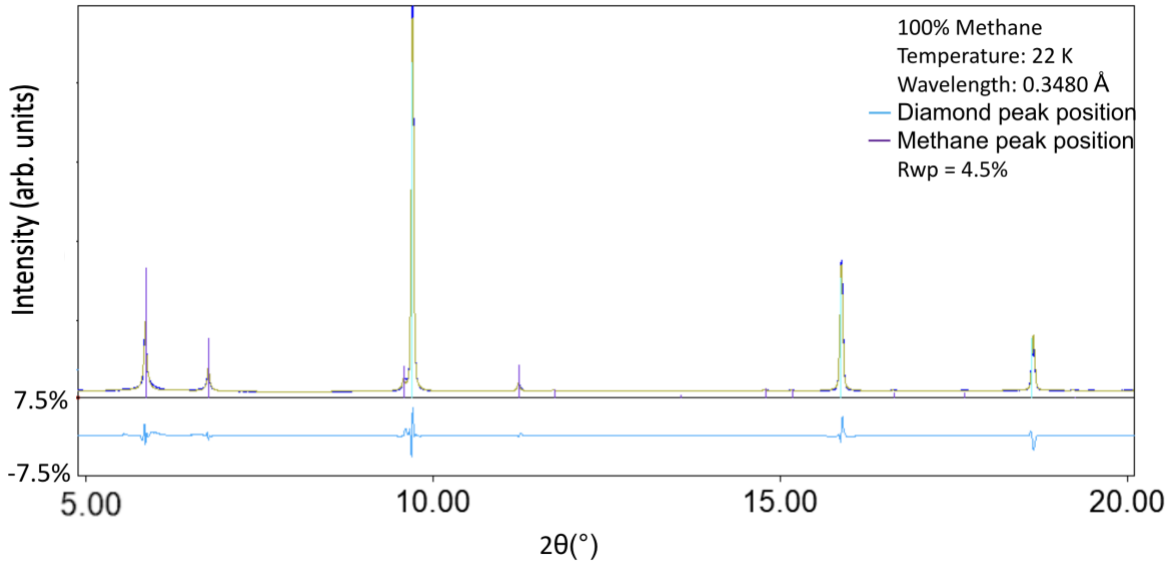

Figure 5.27. Rietveld refinement for pure CH_4 on the Brockhouse beamline at 22 K. The difference between the experimental and calculated patterns is less than 7.5%. The R_{wp} is 4.5%, reflecting a good fit for the data.

Figure 5.27 shows the same methane peaks as Figure 5.26, Which means with an increase of 10 Kelvin, there were no changes in diffraction pattern. Once again, there was good agreement between the experimental and calculated patterns as reflected by the R_{wp} of 4.5%.

Rietveld refinement at 33 K

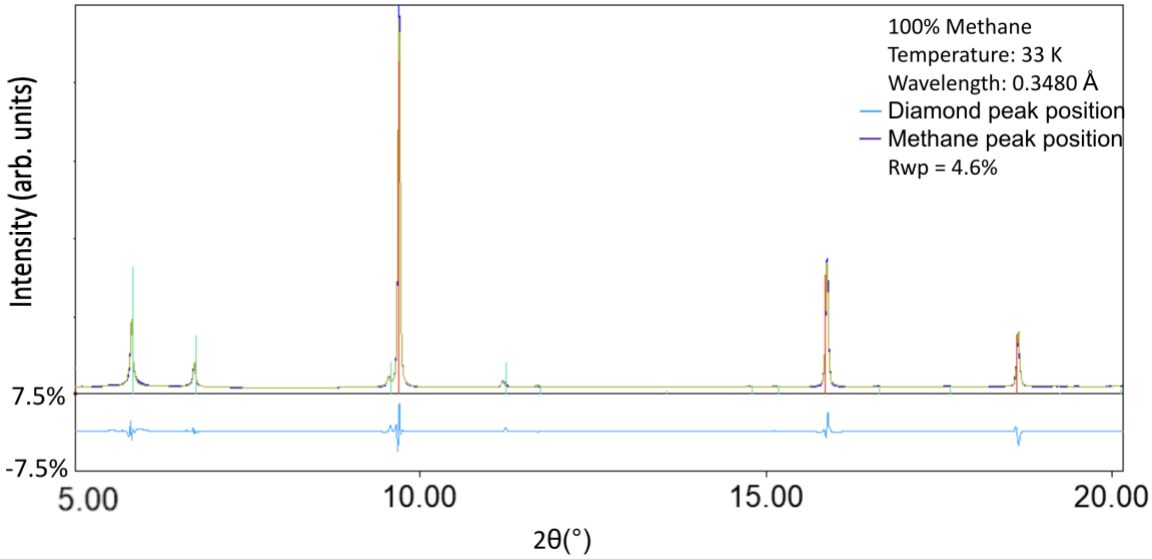

Figure 5.28. Rietveld refinement for pure CH_4 on the Brockhouse beamline at 33 K. The difference between the experimental and calculated patterns is less than 7.5%. The R_{wp} is 4.6%, reflecting a good fit for the data.

Figure 5.28 shows good congruence between the calculated and the experimental profiles, reflected by an R_{wp} of 4.6%. The peak positions have not changed.

Rietveld refinement at 43 K

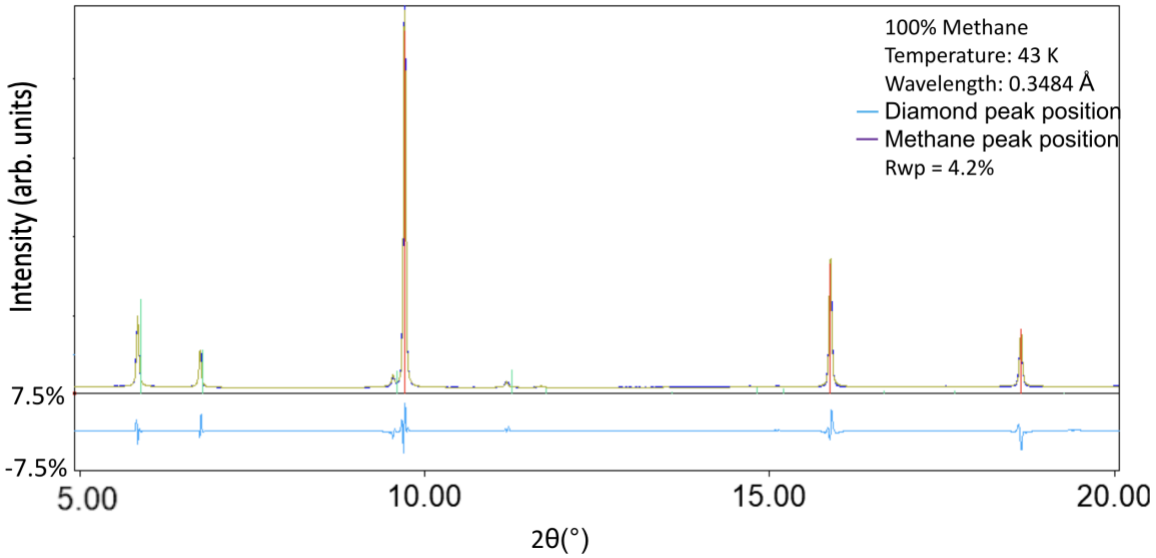

Figure 5.29. Rietveld refinement for pure CH_4 on the Brockhouse beamline at 43 K. The difference between the experimental and calculated patterns is less than 7.5%. The R_{wp} is 4.2%, reflecting a good fit for the data.

As the temperature continues to increase, the relative intensities of methane compared to the diamond peak starts to decrease. This means that methane is likely pumped out of the system.

Rietveld refinement at 53 K

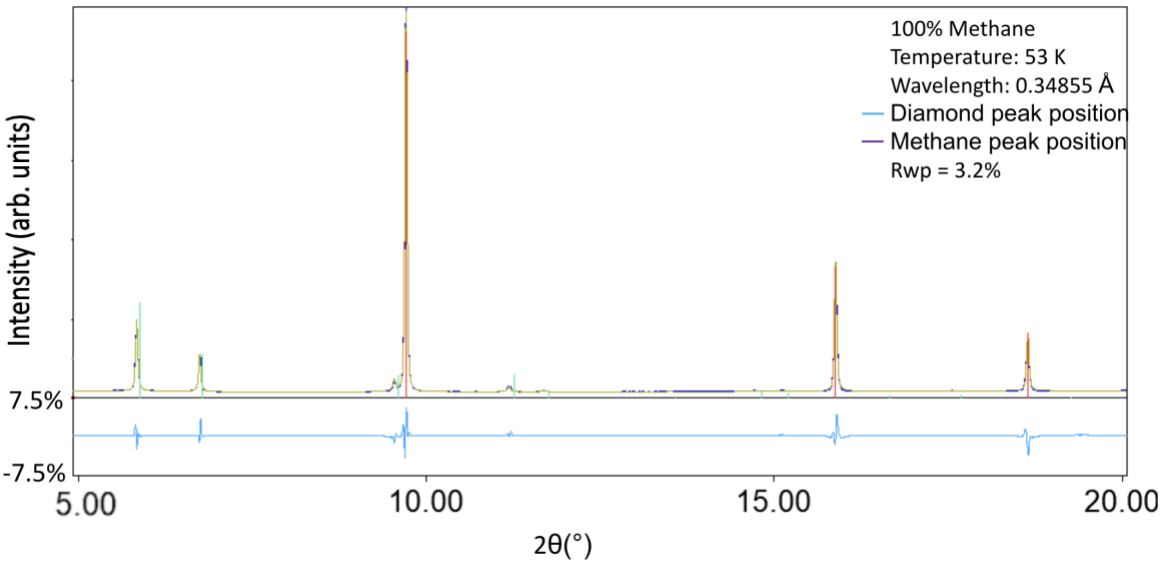

Figure 5.30. Rietveld refinement for pure CH_4 on the Brockhouse beamline at 53 K. The difference between the experimental and calculated patterns is less than 7.5%. The R_{wp} is 3.2%, reflecting a good fit for the data.

Figure 5.30 continues to show that the intensity of the methane peaks is decreasing.

Rietveld analysis at 63 K

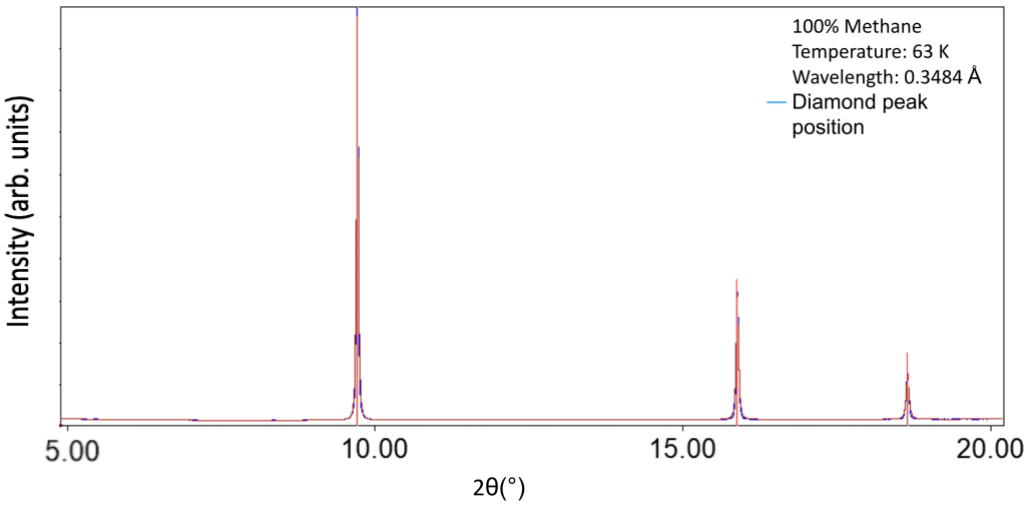

Figure 5.31 Rietveld refinement for pure CH_4 on the Brockhouse beamline at 63 K. The red sticks refer to the diamond peak positions. Since methane is no longer present in the system, Rietveld analysis has not been performed on this data set.

It is known that the melting point for methane is 63.15 K. Figure 5.31 shows the diffraction pattern above at 63 K and that there is no methane in the sample, only diamond peaks are still present.

5.3 Gases Co-deposition at Brockhouse

Unfortunately, quantitative data to illustrate the exact mixing ratios between different mixtures could not be obtained. However, it can be demonstrated from a qualitative point of view by inspection of diffraction patterns.

In summary, the following are the expected peaks for the composite system.

Diamond at 2θ (°) = 9.6° (this has been used mostly as a reference peak for the following diagrams).

Methane 2θ (°) = 5.8°, 6.8°, 9.6°, 11.2°

Nitrogen 2θ (°) = 6.0°, 6.9°

Mixture comparison at 13 K

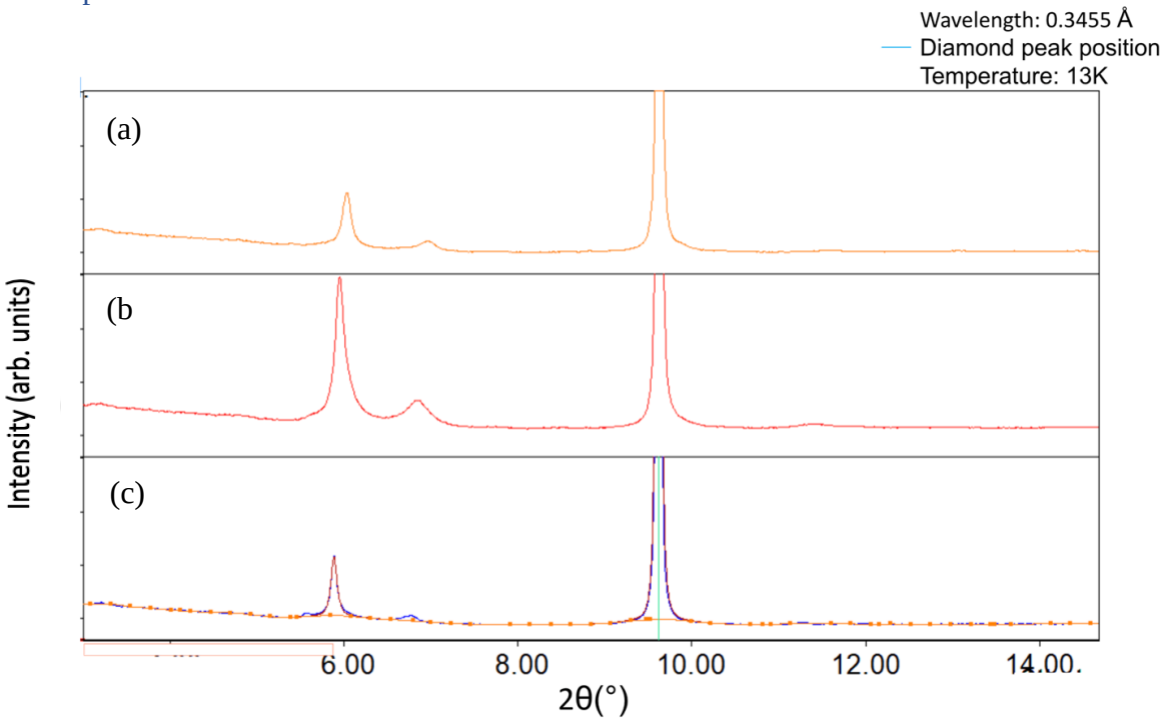

Figure 5.32. Diffraction patterns showing a summary of the mixture comparisons of CH_4 and N_2 at varying concentrations (a) 25% CH_4, 75% N_2, (b) 50% CH_4, 50% N_2, (c) is 75% CH_4, 25% N_2 at 13K. The diamond peak at 9.6° remains constant for each mixture set. The two main peaks observed in these data sets are at 5.9° and 6.8°.

Figure 5.32 illustrates all three methane and nitrogen mixtures between 5° and 15° to highlight the main area of interest in the diffraction profile. There are two main peaks observed at 5.9° and 6.8° in Figure 5.32. Given the raw data result from the pure methane and nitrogen crystal structures in Table 4.3 and 4.4, it is highly likely that the peak at 5.9° is a combination of methane (first peak

at 5.8°) and nitrogen (first peak at 6.0°). The peak at 6.8° is likely secondary to methane (pure methane peak is at 6.8°) but there may also be some contribution from the nitrogen peak at 6.9°. It is hard to discern other nitrogen peaks due to the extremely low intensity of these peaks on the Brockhouse beamline.

Mixture comparison at 20 K

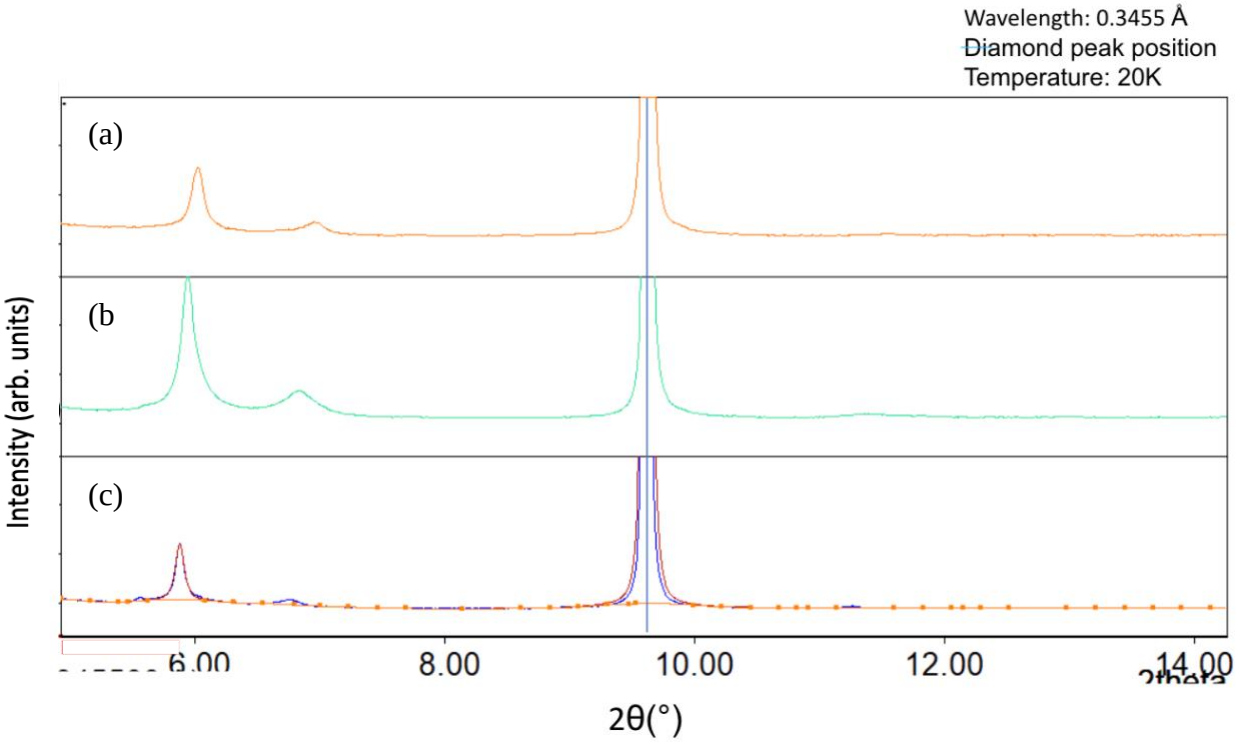

Figure 5.33. Diffraction patterns showing a summary of the mixture comparisons of CH_4 and N_2 at varying concentrations (a) 25% CH_4, 75% N_2, (b) 50% CH_4, 50% N_2, (c) is 75% CH_4 and 25% N_2% at 20K. The two main peaks observed in these diffraction patterns are at 5.9° and 6.8°.

Figure 5.33 shows the same two peaks as observed in Figure 5.32. There are other peaks at 7.8° and 8.2° but the intensity of these peaks is so low that the software is unable to identify them as separate from the background. It is possible that these two lower intensity peaks belong to nitrogen. Pure nitrogen has known diffraction peaks at 7.9° and 8.4°.

Mixture comparison at 30 K

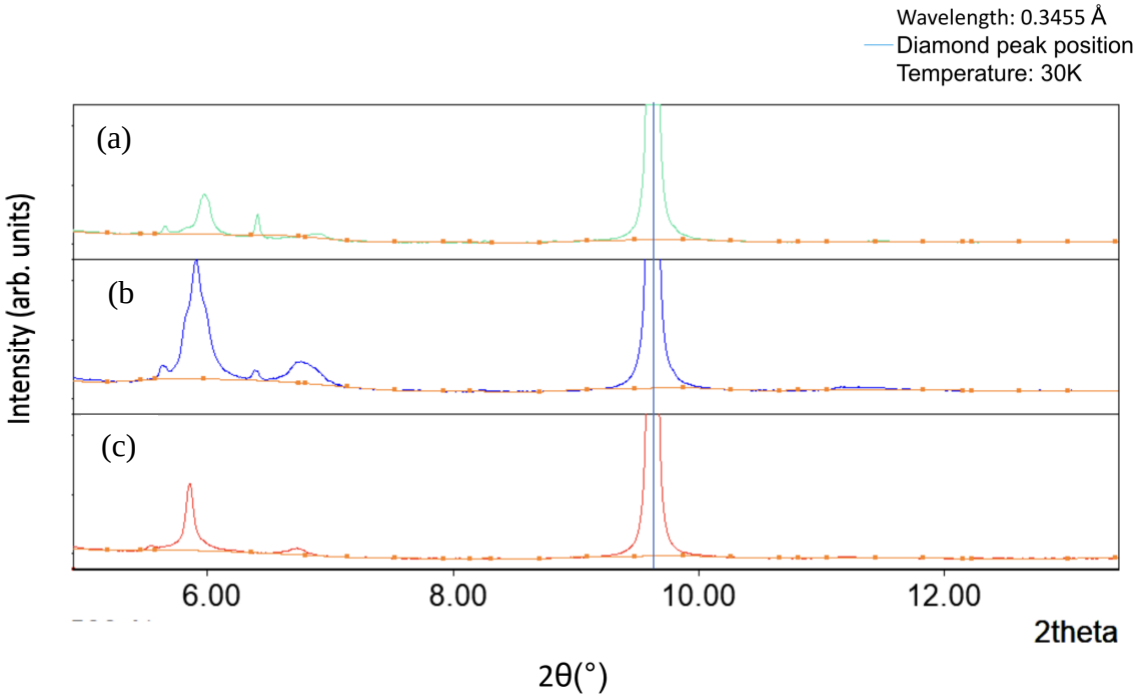

Figure 5.34. Diffraction patterns showing a summary of the mixture comparisons of CH_4 and N_2 at varying concentrations (a) is 25% CH_4, 75% N_2, (b) 50% CH_4, 50% N_2, (c) is 75% CH_4 and 25% N_2 at 30 K.

Figure 5.34 (a) shows that there is a change in the diffraction pattern at 30 K for the system that contains 25% methane and 75% nitrogen. It was previously noted that there were no phase changes for either pure methane or nitrogen at 30 K. For pure nitrogen, the sample was pumped out of the system by 32 K, and, for pure methane, there were no phase changes observed. However, on the HXMA beamline, a phase change was noted at 34 K for pure nitrogen. The phase change observed for Figure 5.34 (a) shows the emergence of new peaks at 5.8° and 6.5°. From this experiment, it is known that pure methane has peaks at 5.8° and 6.8° and pure nitrogen has peaks at 6.0° and 6.9°. Both these peaks may contribute to the two 'new' peaks observed in (a). However, it is interesting that they were not observed at the lower temperatures (13 K in Figure 5.32 and at 20 K in Figure 5.33). In (b) the sample that contains 50% methane and 50% nitrogen, similar diffraction pattern changes can also be observed at the same peak positions. There appears to be broadening of the peak that was at 6.8°. In (c) The sample that contains 75% methane and 25% nitrogen, the same diffraction pattern can also be observed but because of the significantly lower percentage of nitrogen in the system, the intensities of these peaks are much smaller.

Mixture comparison at 40 K

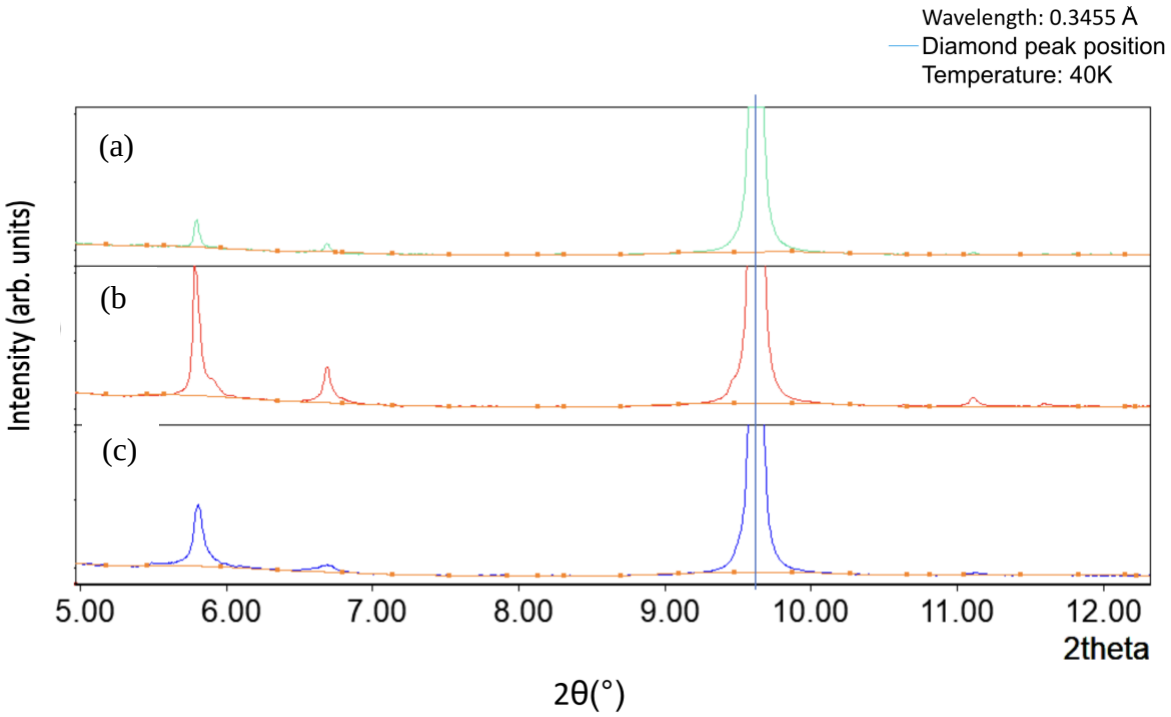

Figure 5.35. Diffraction patterns showing a summary of the mixture comparisons of CH_4 and N_2 at varying concentrations (a) is 25% CH_4, 75% N_2, (b) 50% CH_4, 50% N_2, (c) is 75% CH_4, 25% N_2 at 40 K.

In Figure 5.35, the intensity of the peak at 5.9° in (a) is significantly smaller. If it is assumed that nitrogen has been pumped out of the system at this temperature due to the low amount of sample present, it is possible that the peaks present represent only methane. The structural changes that were observed on Figure 5.34 can no longer be observed. In (b) The peak at 5.9° appears to have a widening at the base, this could once again reflect structural changes in the crystal system secondary to an increase in temperature.

Mixture comparison at 50 K

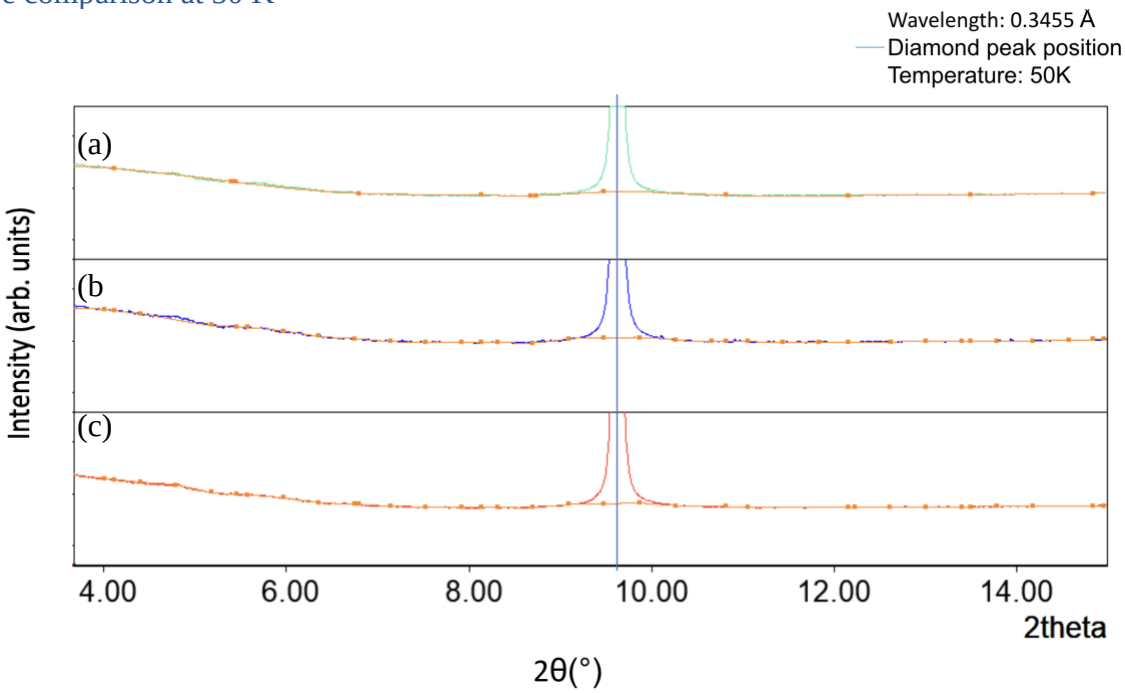

Figure 5.36. Diffraction patterns showing a summary of the mixture comparisons of CH_4 and N_2 at varying concentrations (a) is 25% CH_4, 75% N_2, (b) 50% CH_4, 50% N_2, (c) is 75% CH_4, 25% N_2 at 50K.

Finally, in Figure 5.36, as the temperature rises to 50K, the gases in the crystal system have been pumped out and are indiscernible from background radiation.

Table 5.7 summaries the expected relative intensities and actual relative intensities from the Brockhouse beamline.

Table 5.7. Summary of relative and expected intensities on Brockhouse beamline with varying concentrations of methane and nitrogen.

CH_4 (%)	N_2 (%)	CH_4:N_2
75	25	141:1
50	50	4:3
25	75	10:1

Table 5.7 illustrates that there are obvious differences in what the expected and relative intensities were. Out of all three mixtures, the 50% methane and 50% nitrogen seemed to have the best correlation between the expected and actual relative intensities. In Section 4.5, the mixture of 50% methane and 50% nitrogen showed new peaks at a temperature greater than 37 at

the HXMA beamline but these results were not observed on the Brockhouse beamline. Figure 5.37 below examines this more closely.

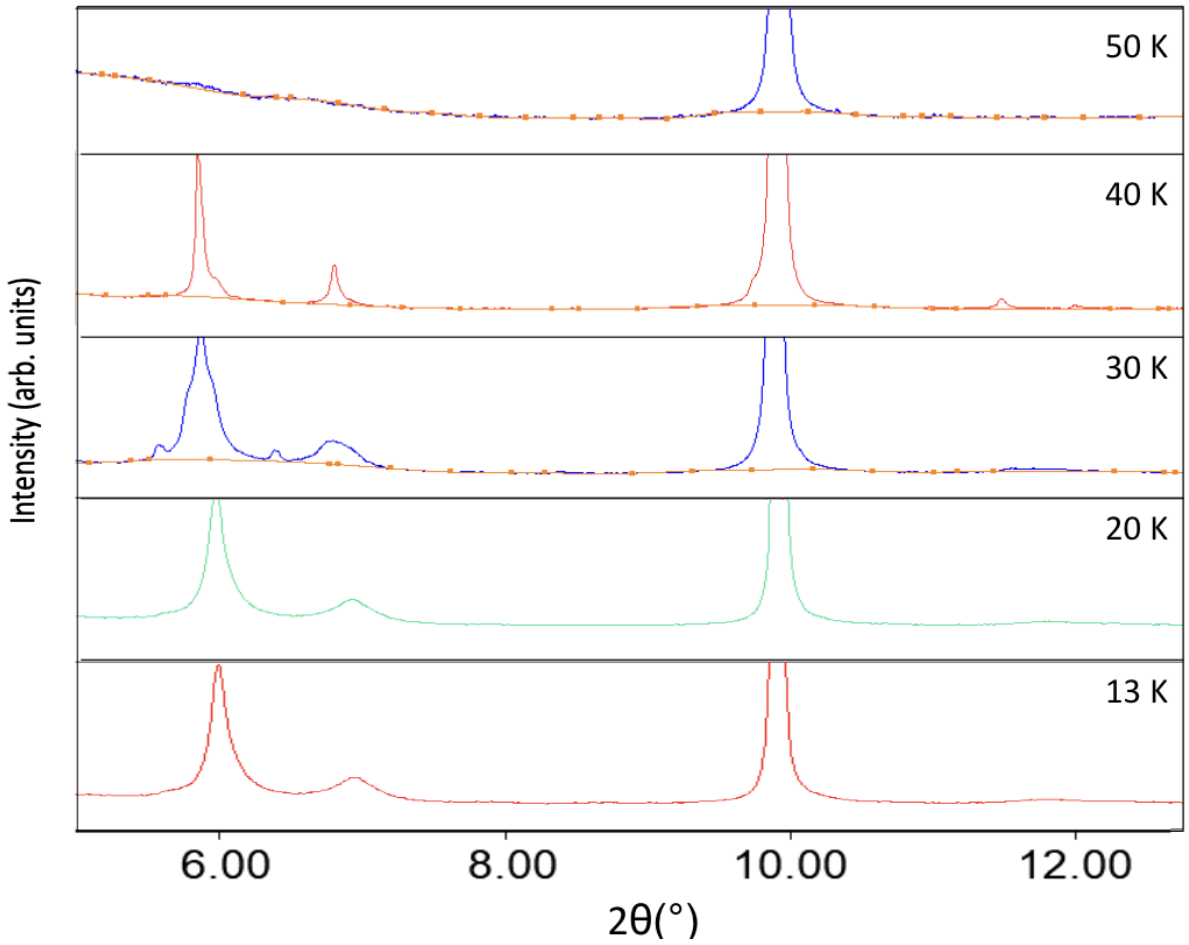

Figure 5.37. Diffraction patterns showing a summary of the mixture comparison of 50% CH_4 and 50% N_2 as temperature increases. The diamond peak remains constant at 9.6°. There is an obvious change in the diffraction pattern at approximately 30 K.

Figure 5.37 shows the diffraction pattern of the mixture of 50% methane and 50% nitrogen with increasing temperature. There is an obvious diffraction pattern change at 30 K. It is difficult to discern which has resulted in this structure change or if there is an entirely new structure at this temperature. It is known from previous results that methane does not have a phase change at temperatures less than 91.5 K, but nitrogen has a known phase change at 34 K. It is highly probably that this change is a result of nitrogen but without statistical analysis or quantitative data analysis using Rietveld refinement, it is difficult to confirm.

Overall, the results of these mixtures indicate that there are some interesting results at 30 K for each data set. Future work for this could include a quantitative analysis to identify how much of each substance is present in each data set but also attempt to isolate lattice parameters from Rietveld refinement to create a theoretical crystal structure.

CHAPTER 6: CONCLUSION AND OUTLOOK

There were several key findings from the experiments performed at the HXMA and Brockhouse beamlines. The following chapter will discuss the comparison of the leak valves used in the experiments, the quality of the diffraction patterns, the verification of the crystal structure of nitrogen at both beamlines, and the new crystal structure observed on the HXMA beamline at temperatures greater than 37 K.

6.1 Leak valve comparison

Section 3.4 discussed in detail the use of the manual leak valve on the HXMA beamline compared to the programed leak valve on the Brockhouse beamline. The assumption when the nitrogen and methane gases were leaked into system was that all the gas will deposit on the substrate. However, it is possible that they may have also deposited somewhere else in the cold head of the DISPLEX. The diffraction results from the HXMA beamline gave reasonable agreement by Rietveld refinement. The manual leak valves allowed the gases to deposit onto the substrate faster. For the computerized or programmed leak valve, the leak rate of the gases was controlled too tightly resulting in a slow leak rate of the gases. One of the indicators for this were the refined ratios of CH_4:N_2 (Table 5.7). Furthermore, mixing of the gases before deposition may not have been optimal due to the difference in vapor pressure and absorption properties of each of the gases on to the diamond substrate.

Overall, while the programmed leak valve offered better control of the flow rate, the manual valve allowed greater volume deposition of the gases on the diamond substrate. Since the manual leak valve required the user to physically turn the dial to control the rate at which the gases leaked into the deposition system, it was more prone to human error. In addition to this, to calculate the flow rate, the molecular mass was used to determine a ratio from which the deposition rate was extrapolated for other gases. For the purposes of this experiment, the manual leak valve proved to be more useful as it allowed fast release of the gases into the system, giving a better gas to diamond

intensity ratios for all sets of experiments on the HXMA beamline. As a result of this, changes in diffraction patterns for the pure and mixed samples were better studied on the HXMA beamline.

Future work on the Brockhouse beamline with these gases and valves would be to ensure that the leak valves are able to leak enough gases into the system to ensure adequate amount of sample has deposited on the substrate. This would ideally give reasonable relative intensities of the gases compared to the diamond diffraction peaks to allow a more accurate Rietveld analysis. The current experiment was limited by how much beam time users are allocated. One shift at the CLS is 8 hours. Users need to wait 1 hour for the beam to stabilize before using it for any experimental purpose. To conduct research, users are typically granted 7-8 shifts (which is approximately 3-4 days). The deposition time for each data set for the set of experiments in this thesis was approximately 2-3 hours. Consequently, 10 hours (for a total of 5 sets of experiments) were used primarily for gas deposition. If more deposition time was available for the programmed leak valve to deposit a greater amount of sample on to the substrate, the relative intensities for methane and nitrogen compared to diamond would have been significantly better, compared to 4% for nitrogen and 20% for methane. However, it would have been challenging, if not unreasonable, to allow 8 hours just to deposit enough sample for one set of diffraction data. The CLS is now running in top-up mode which means that the beamline is injected with the beam with the safety shutters open[35] (i.e., there are no electrons in the beamline during this time). This would ensure that beam time is not wasted on deposition. Alternatively, the flow rate of the computer-controlled leak valve could be increased but this the user would need to ensure that the flow rate between the two gases is equivalent to maintain accountability of how much of the gases are leaked into the system.

6.2 Quality of the Diffraction Pattern

The HXMA beamline used an x-ray with an energy of 24.5 keV ($\lambda = 0.5092$ Å) and the Brockhouse beamline used an x-ray with an energy of 35 keV ($\lambda = 0.3455$ Å). The quality of each diffraction pattern can be compared by examining the diffraction patterns produced by the diamond substrate on both beamlines. Reasonable results were obtained from Rietveld refinement for HXMA and Brockhouse. HXMA provided a better fit for the data with an R_{wp} (weighted Bragg R-factor) of 5.3% on HXMA and 9.8% on Brockhouse. Most of this difference was due to a poor profile shape

fit and line profile. Attempts were made to model the experimental data by using the pseudo-voigt function to use the properties of both the Lorentzian and Gaussian profile shapes. The line profile issues may have been secondary to the lack of precise focusing of the synchrotron beam. To obtain a narrower beam, slits were used. Unfortunately, this may have distorted the natural line width of the beam resulting in the inability to get a good fit for the wings of the diffraction pattern profiles. Improved focusing was needed to account for this issue. In addition to this, since more peaks were observed on Brockhouse due to the higher energy, it was more difficult to fit the low intensity, higher angle peaks. One of the advantages of using higher energy (and subsequently lower wavelength) was to reduce scatter. Interestingly, this was not reflected in how the calculated profiles fit the experimental patterns. For most of the Rietveld analyses performed for data obtained at the Brockhouse beamline, it is likely that the poor weighted Bragg R-factor was secondary to the strong diamond peaks rather than the appropriate fitting of the peaks. At the HXMA beamline, there was higher scatter but achieved a lower Bragg R-factor indicating better quality data.

Repeating these experiments with a longer deposition time would allow a better quantitative assessment of the diffraction peaks observed at each beamline as well as improved refinement.

6.3 Discussion of the Phase Changes

The results from the HXMA beamline are in good agreement with what previous data has shown with regards to structural refinement of nitrogen as well as the phase change at 34 K. The Brockhouse beamline crystal refinement for nitrogen was incomplete as the gas was pumped out of the system before it reached the temperature of the expected phase change at 32 K. In the future, it may be worth increasing the time of deposition for the gases if using the programmed leak valve or to repeat the experiment on the HXMA beamline.

Furthermore, for methane, the results were mostly reflective of previous work except the finding of the methane phase change. As observed in Figure 4.13 for pure methane on the HXMA beamline, there was evidence of a new phase of methane. The intensity of these peaks was too low for the Match! software to be able to identify them but the peaks have been clearly marked and next steps could potentially attempt to model this new structure using the lattice parameters obtained.

As a next step, this experiment can be repeated to measure data up to 90 K instead of the 60 K that it was stopped at.

6.4 Lattice Parameters

One goal of this thesis was to gain experience with Rietveld Refinement and data processing. Following that exposure, the results for pure methane and pure nitrogen were explored to determine the lattice parameters. The lattice parameters were then compared to those found in the literature.

Table 6.1. Comparison of the lattice parameters from the present experiment with literature values for pure nitrogen at 20 K.

Unit Cell Length (Å)	Space group	Source
5.654(71)	P 2 3	Experimental value on HXMA
5.685(44)	P 2 4	Experimental value on Brockhouse
5.660(20)	P a 3 or P 2 3	[14]
5.662(50)	P 2 3	[14]
5.649	P a 3	[15]

HXMA results show that up until 29 K, N_2 has a cubic crystal structure which corresponds to the finding in Connelley et al[2]. However, there is some discrepancy between the findings after 30 K with regards to the crystal structure formed by N_2 and the lattice parameters formed. Table 6.1 references two articles which have identified the unit cell length for N_2 at 20 K. These results agree well with the experimental findings discussed in Section 5.1.3. Further analysis of diffraction patterns may give more details regarding the structure of N_2 after 30 K.

The lattice parameters for methane still require some research as there is a lack of literature available for a pure methane crystal at 10 K. However, from literature, it is known that methane does not have any changes to its crystal structure below 91.K. There was one paper[39] that briefly discussed a phase change for methane at 20.4 K[43]. The results obtained from the HXMA and Brockhouse beamlines did not show any such phase changes.

Of note, the data for pure methane at the HXMA beamline did demonstrate a phase change at 37 K as noted in Figure 4.13 and 5.21. The lattice parameters for this are summarized in Table 5.4. The same results were not observed at the Brockhouse beamline.

In the future, higher quality of data should be obtained from the Brockhouse beamline to calculate lattice parameters for methane from both the HXMA and Brockhouse beamlines to verify this supposedly new phase of methane.

6.5 Methane and Nitrogen Co-deposition.

The relative intensities in Table 6.2 below demonstrate that the agreement between the amounts of nitrogen and methane that was deposited was not ideal at either beamline.

Table 6.2. Summary of the relative intensities in each gas co-deposition for both beamlines.

For HXMA		For Brockhouse	
Expected CH_4:N_2 ratio	Actual CH_4:N_2 ratio	Expected CH_4:N_2 ratio	Actual CH_4:N_2 ratio
1:3	Only N_2 observed	1:3	10:1
1:1	1:147	1:1	4:3
3:1	5:2	3:1	141:1

This was surprising as it was expected that the result of the relative intensities would be consistent with how much the valves were expected to deposit. It would be useful to confirm the percentages that were calculated from the diffraction patterns with in situ Raman. This data has been collected simultaneously when data for this thesis was collected on the Brockhouse beamline and will be analyzed in the near future.

It is clear that some of these experiments should be repeated but due to the Covid-19 pandemic and shut down of the Canadian Light Source, it was not possible.

REFERENCES

[1] Trafton, L. M. (2015). On the state of methane and nitrogen ice on Pluto and Triton: Implications of the binary phase diagram. Icarus, 246, 197–205. https://doi.org/10.1016/j.icarus.2014.05.022

[2] Connolley, D., Milbrodt, T., & Stoner, R. (1980). Preliminary solid–solid phase diagram for nitrogen–methane mixtures by x-ray diffraction. The Journal of Chemical Physics, 73(10), 5388–5390. https://doi.org/10.1063/1.439931

[3] Barrett, C. S., Meyer, L., & Wasserman, J. (1966). Argon—Oxygen Phase Diagram. The Journal of Chemical Physics, 44(3), 998–1000. https://doi.org/10.1063/1.1726856

[4] Pubchem. (2019). Nitrogen. Retrieved from Nih.gov website: https://pubchem.ncbi.nlm.nih.gov/compound/nitrogen

[5] DE-202. Retrieved from Advanced Research Systems website: https://www.arscryo.com/de-202

[6] Lloyd-Jones, G. (2016). Basics of X-ray Physics - X-ray production. Retrieved from Radiologymasterclass.co.uk website: https://www.radiologymasterclass.co.uk/tutorials/physics/x-ray_physics_production

[7] Yeung, J. (2022). Bremsstrahlung radiation | Radiology Reference Article | Radiopaedia.org. Retrieved from Radiopaedia website: https://radiopaedia.org/articles/bremsstrahlung-radiation

[8] Barnes, P., Jacques, S., & Vickers, M., Properties of Synchrotron Radiation. Retrieved from pd.chem.ucl.ac.uk website: http://pd.chem.ucl.ac.uk/pdnn/inst2/prop.htm

[9] Lawrence, W., & William Henry Bragg. (1966). The crystalline state; London, Bell.

[10] Dutrow, B., & Clark, C. (2022). X-ray Powder Diffraction (XRD). Retrieved from Methods website: https://serc.carleton.edu/msu_nanotech/methods/XRD.html

[11]Cockcroft, J. K., Choice of X-ray Target. Retrieved from img.chem.ucl.ac.uk website: http://img.chem.ucl.ac.uk/pdnn/inst1/anode.htm

[12] Mulder, M. (2016). Synthesis of LiNi0.5Mn1.5O4 nanofibers by electrospinning. Retrieved from essay.utwente.nl website: https://essay.utwente.nl/71370/

[13] Belford, R. (2016). 12.1: Crystal Lattices and Unit Cells. Retrieved from Chemistry LibreTexts website: https://chem.libretexts.org/Courses/University_of_Arkansas_Little_Rock/Chem_1403%3A_General_Chemistry_2/

[14] Hoffman, F. (2016). Chapter 2. Retrieved from The Fascination of Crystals and Symmetry website: https://crystalsymmetry.wordpress.com/chapter-1/

[15] Miller indices. Retrieved from clay.uga.edu website: http://clay.uga.edu/courses/8550/millerindices.html

[16] Structure factor - Online Dictionary of Crystallography. Retrieved from dictionary.iucr.org website: https://dictionary.iucr.org/Structure_factor

[17] Young, W.-S., (1993). Weighted norm inequalities for Vilenkin-Fourier series. Transactions of the American Mathematical Society, 340(1), 273–291. https://doi.org/10.1090/s0002-9947-1993-1124174-3

[18] Definition of Crystal Lattice - Chemistry Dictionary. (2017). Retrieved from Chemicool.com website: https://www.chemicool.com/definition/lattice_crystal.html

[19] Crystal Impact. (2021). Endeavour - Structure Solution from Powder Diffraction. Retrieved from www.crystalimpact.com website: https://www.crystalimpact.com/endeavour/

[20] Crystal Impact. (2022). Match! - Phase Analysis using Powder Diffraction. Retrieved from www.crystalimpact.com website: https://www.crystalimpact.com/match

[21] Rodríguez-Carvajal, J., Introduction to the Program FULLPROF: Refinement of Crystal and Magnetic Structures from Powder and Single Crystal Data. Retrieved from http://w3.esfm.ipn.mx/~fcruz/ADR/Cristalografia/Roisnel-Carvajal/fullprof_intro.pdf

[22] Jain, V., Biesinger, M. C., & Linford, M. R. (2018). The Gaussian-Lorentzian Sum, Product, and Convolution (Voigt) functions in the context of peak fitting X-ray photoelectron spectroscopy (XPS) narrow scans. Applied Surface Science, 447, 548–553. https://doi.org/10.1016/j.apsusc.2018.03.190

[23] Bharti, A., & Goyal, N. (2019). Fundamental of Synchrotron Radiations. Synchrotron Radiation - Useful and Interesting Applications. https://doi.org/10.5772/intechopen.82202

[24] HXMA - Canadian Light Source. Retrieved from www.lightsource.ca website: https://www.lightsource.ca/facilities/beamlines/cls/beamlines/hxma.php

[25] Gomez, A., Dina, G., & Kycia, S. (2018). The high-energy x-ray diffraction and scattering beamline at the Canadian Light Source. Review of Scientific Instruments, 89(6), 063301. https://doi.org/10.1063/1.5017613

[26] Granville Phillips 203 Variable Vacuum Leak Valve. https://www.machinedismantlers.org/East-Chicago-/Self-Propelled-/Foudation-Brakes-/Granville-phillips-203-variable-vacuum-leak-valve-uhv.shtml.

[27] von Kann, S. (2021). Bronkhorst. Retrieved from Bronkhorst website: https://www.bronkhorst.com/int/blog-1/flow-control-valve-which-valve-to-use-for-your-flow-meter/

[28]Bronkhorst. (2022). Retrieved from Bronkhorst website: https://www.bronkhorst.com/int/products/gas-flow/el-flow-select/f-201cv/

[29] Prescher, C., & Prakapenka, V. B. (2015). DIOPTAS: a program for reduction of two-dimensional X-ray diffraction data and data exploration. High Pressure Research, 35(3), 223–230. https://doi.org/10.1080/08957959.2015.1059835

[30] Paszkowicz, W., Knapp, M., Baehtz, C., Minikayev, R., Piszora, P., Jiang, J. Z., & Bacewicz, R. (2004). Synchrotron X-ray wavelength calibration using a diamond internal standard: application to low-temperature thermal-expansion studies. Journal of Alloys and Compounds, 382(1-2), 107–111. https://doi.org/10.1016/j.jallcom.2004.05.041

[31] Neumann, M. A., Press, W., Nöldeke, C., Asmussen, B., Prager, M., & Ibberson, R. M. (2003). The crystal structure of methane phase III. The Journal of Chemical Physics, 119(3), 1586–1589. https://doi.org/10.1063/1.1580809

[32] Momma, K., & Izumi, F. (2011). VESTA 3for three-dimensional visualization of crystal, volumetric and morphology data. Journal of Applied Crystallography, 44(6), 1272–1276. https://doi.org/10.1107/s0021889811038970

[33] McLennan, J. C., & Plummer, W. G. (1928). The Crystal Structure of Solid Methane. Nature, 122(3076), 571–572. https://doi.org/10.1038/122571c0

[34] Mooy, H. H. (1931). Crystal Structure of Methane. Nature, 127(3210), 707–707. https://doi.org/10.1038/127707c0

APPENDIX

A: Chronology of Data Collection

- November 2017: Introduction to experimental set up with Robert Bauer. Fast water deposition and Xe water experiments were done to gain a better understanding of the XRD and data analysis procedure.
- February 2018: The first set of CH_4 and N_2 mixture measurements were obtained at HXMA at CLS.
- June 2019: The second set of CH_4 and N_2 mixture measurements were obtained at HXMA at CLS.
- December 2019: The third set of CH_4 and N_2 mixture measurements were obtained at Brockhouse at CLS.

B: Crystal Structure of Nitrogen

The Endeavour software, designed by Crystal Impact, was used to import diffraction data from Match! to visualize a crystal structure and then create a cif file of the data. In this section, it has been demonstrated this for the nitrogen dataset. Nitrogen was used to represent this procedure as it is an easier gas to use, and it does not become as disordered as methane does as temperature increases. It is difficult to demonstrate the structure of methane between the two beamlines as the atom positions are not well known. The data is available if researchers in the future would like to model the crystal structure of methane or the data from the co-deposition mixtures.

C.1 100% Nitrogen HXMA at 13 K

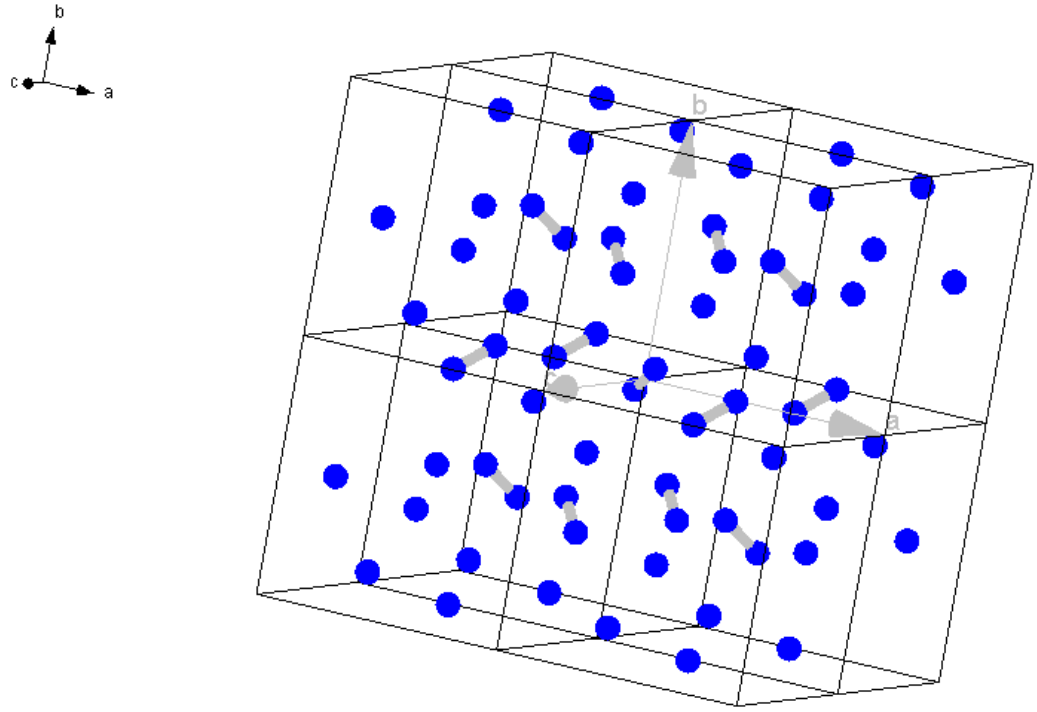

Figure C.1. Crystal Structure of 100% Nitrogen on HXMA beamline.

Crystal data

Formula sum	N_8
Formula weight	112.05
Crystal system	cubic
Space group	P a -3 (no. 205)
Unit cell dimensions	a =
Cell volume	179.79 $Å^3$
Density, calculated	1.035 g/cm^3
Pearson code	cP8
Formula type	N

Atomic coordinates and isotropic displacement parameters (in $Å^2$)

Atom	Ox.	Wyck.	x	y	z	B
N1	+0	8c	0.05404	0.05404	0.05404	1.0000

This attempt of structural analysis was done on the endeavor software. The goal was to assess whether it is possible to obtain the same crystal structures from both beamlines. From literature, it is known that nitrogen at 10 K has a unit cell dimension of 5.65 Å, cubic crystal system, and a space group of P 2 3 (195). From the structural refinement on the HXMA be mine, Figure C.1. shows a space group of P a -3.

Figure C.2. below shows the crystal structure of 100% Nitrogen from the Brockhouse beamline.

C.2 100% Nitrogen at Brockhouse at 13 K

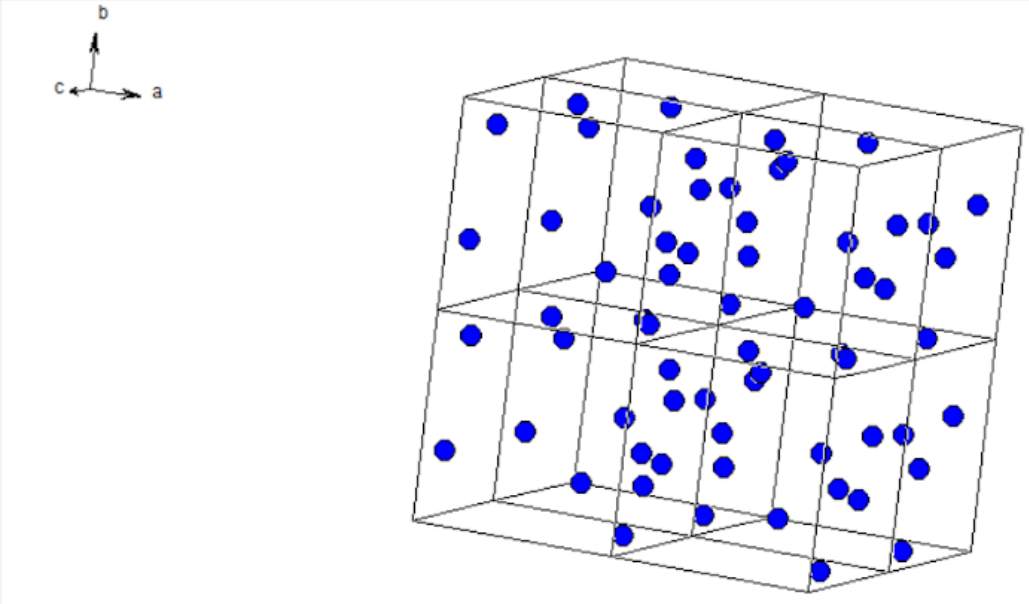

Figure C.2. Crystal Structure of 100% Nitrogen on Brockhouse beamline.

Crystal data
Formula sum N8
Formula weight 112.05
Crystal system triclinic
Space group
Unit cell dimensions a = 5.6842 Å
b = 5.6842 Å
c = 5.6842 Å
a = 90.00 °
b = 90.00 °
g = 90.00 °
Cell volume 183.66 Å3
Density, calculated 1.013 g/cm3
Pearson code aP8
Formula type N
Wyckoff sequence a8

Atomic coordinates and isotropic displacement parameters (in $Å^2$)

Atom	Ox.	Wyck.	x	y	z	B
N1	+0	1a	0.79613	0.56537	0.49978	0.0000

As can be observed in the result from the Endeavour software, the crystal system for nitrogen proposed on the Brockhouse beamline is more in keeping with what the expected results were. Due to limitations with the software, it was to perform a structural analysis for methane. However, this would be the next steps to identify the unique phase of methane on the HXMA beamline. The next step of this refinement would be to analyze the N_2 crystal structure as temperature increases and determine whether there are changes to the crystal structures.